NON-INVASIVE CANCER DETECTION: FROM BENCH TO BEDSIDE

GOKULA KRISHNAN.R

(B.Tech., Tamil Nadu Agricultural University, India)

A THESIS SUBMITTED

FOR THE DEGREE OF DOCTOR OF PHILOSOPHY

DEPARTMENT OF BIOMEDICAL ENGINEERING NATIONAL

UNIVERSITY OF SINGAPORE

2017

Supervisor:
Assistant Professor YEOW Chen Hua, Raye

Examiners:
Associate Professor Poh Chueh Loo
Assistant Professor Chen Chia-Hung
Professor Emeritus Terence H. Risby, The Johns Hopkins University

DECLARATION

I hereby declare that the thesis is my original work and it has been written by me in its entirety. I have duly acknowledged all the sources of information which have been used in the thesis. This thesis has also not been submitted for any degree in any university previously.

Gokula Krishnan. R
2017

Acknowledgement

I have my immense pleasure in placing on record my deep sense of gratitude and indebtness to my supervisor, ***Dr. Yeow Chen Hua,*** *Assistant Professor, Department of Biomedical Engineering, National University of Singapore, who never made me feel the difference between "Supervisor" and "Companion" during these four years. I will be always thankful to him for the guidance, inspiration, freedom and constant motivation in research and personal care. I truly consider it an honour to be his student*

I express my deepest gratitude to ***NUS Research Scholarship****, without which my Ph.D in National University of Singapore would not be possible.*

It is my pleasure to express my gratitude to ***Ministry of Education (MOE)*** *for the grants* ***MOE Academic research fund (AcRF) Tier-1 grant R397-000-143-133 and R397-000-204-133*** *for funding my four years of research.*

It is an honor to express my heartfelt thanks to ***Dr. Toh Siew Lok****, Associate Professor, Department of Biomedical Engineering, National University of Singapore, for allowing me to work in Tissue Repair Laboratory and his lab in-charge Mrs. Yee Wei for her untiring efforts to extend the best facility for research in the department.*

I express my heartiest thanks to ***Dr. Yong Wei Peng, Dr. So Bok Yan, Jimmy*** *and* ***all the co-ordinators*** *especially, Elya, Janelle, Amy and Teo Siok Chin for their untiring help in recruiting subjects and collecting breath samples for the clinical studies.*

My sincere gratitude is due to ***Dr. Neo Puay Yong*** *for teaching the techniques of human cell culture. My sincere thanks to* ***Dr Wu Ji'En*** *and* ***Ms. Han Yanhui*** *for helping me in using the Proton Nuclear Magnetic Resonance Spectrometer. My sincere thanks to* ***Dr. Liu Qiping*** *for training me in operating Gas Chromatography and Mass Spectrometry. I like express my deepest gratitude to* ***Prof. Thirumalai Venkatesan****, Provost Chair Professor, Director, NUSNNI-Nanocore, National University of Singapore, for permitting me to use Seleted Ion*

Flow-Tube Mass Spectrometry and his lab members for teaching me in operating the instrument. My sincere thanks to ***Chan Wai Kam Julee*** *for teaching me histology. I wish to express my gratitude to NUMI for suppling me all the consumables that I used in my research.*

My heartfelt thanks to ***my dearest lab mates*** *for all the valuable suggestions, motivation, support and sweetest memories that has helped me grow both personally and professionally.*

I thank ***my beloved friends Luis, Fanzhe, Shiva, Hareesh, Jin Huat, Cai Lin, May, Hong Kai, Sun Yi, Xin Quan and Tiana*** *for making these four years memorable and especially for all the tea time discussions and debates.*

I do not know how to express my gratitude ***to my dearest family*** *for their love, unflinching support and enormous sacrifices for my sake.*

Last but not the least, it is my pleasure to thanks ***all my failures*** *for moulding and sculpting me by their constant motivation and propulsion towards success.*

Gokula Krishnan.R

2017

Table of contents

Table of contents – Figures

Table of contents - Tables

Chapter 1

Introduction

1.1. Cancer

According to World Health Organization, cancer is one of the leading causes of death worldwide. In 2012 8.2 million people died due to cancer (WHO). More than 60% of the annual new cases occur in the underdeveloped and developing countries located in Africa, Asia, and South America. These countries bear more than 70% of the world's annual cancer deaths [1]. Uncontrolled proliferation of cells is called cancer. There are more than 200 types of cancer, but all of them results from the uncontrolled proliferation of abnormal cells. The unrepaired genetic aberrations often cause this abnormality.

According to the American Cancer Society report (2014) on the history of cancer, cancer was described throughout the recorded history. The oldest description of cancer came from the Edwin Smith Papyrus dates back to 3000BC [3]. Edwin Smith Papyrus describes 8 cases to tumors of the breast that were removed by a fire drill. Cancers were also found in mummified humans of ancient Egypt. Hippocrates (460-370 BC), who is considered as the Father of Medicine used the terms *carcinos* and *carcinoma* (Greek meaning crab) to describe tumors due to the finger-like projections observed in cancer tumors. Later, a Roman physician, Celsus (28-50 BC), translated the Greek term into Latin *cancer* (Latin meaning crab). Another Greek physician Galen (130-200 AD) used the term *oncos* (Greek meaning swelling) to describe tumors [4,5]. This term is now used to represent the study of cancer - oncology and to the people who study cancer – oncologists. In 1761, Giovanni Morgagni of Padua did autopsies to relate the patient's illness to pathologic findings, which laid the foundation for the scientific study of cancer [4]. Scottish surgeon John Hunter (1728-1793) made a statement that cancer can be cured by surgery. Rudolf Virchow, who is credited as the founder of cellular pathology, provided the scientific basis for the pathology of cancer.

1.2. Causes of cancer:

The pursuit for the identification of causes of cancer can be found as early as ancient Egyptians, who blamed cancers on gods. Hippocrates proposed the humoral theory, which states that there are four *humors* (body fluids) namely blood, phlegm, yellow bile and black bile. The key idea is that any imbalances in these four humors caused diseases. Cancers were believed to be caused by the excess of black bile. This theory was accepted and even taught by Galen. This theory remained unchallenged for over 1300 years. Lymph theory is one of the theories that replaced humoral theory. Stahl and Hoffman proposed that cancer was composed of fermenting and degenerating lymph that are varying in density, acidity and alkalinity. This theory was supported by John Hunter. In 1838, German pathologist Johannes Muller came to the conclusion that the cancer is made up of cells and lymph. However, he did not believe that cancer arose from the healthy cells and proposed that cancer developed from the budding elements called *blastemal* and existed between the normal tissues. This theory was proved wrong by Muller's student Rudolph Virchow, who demonstrated that all cells including cancer arise from other cells. Rudolph Virchow came up with the chronic irritation theory, where he theorized that cancer is caused by the chronic irritation but incorrectly conceived that cancer spread like liquid. In the 1860s, German surgeon Karl Thiersch disproved the liquid like spread notion of Virchow by showing that cancers spreads through malignant cells and not via a fluid. Trauma was also believed to be the cause of cancer from the late 1800s to 1920s. Two Holland doctors, Zacutus Lusitani (1575-1642) and Nicholas Tulp (1593-1674) proposed the contagion theory in 1649 and 1652 respectively based on their encounters with breast cancer in members of the same household [4,5]. They suggested that cancer is an infectious disease and cancer patients should be isolated. Now it has been proven that human cancer is not contagious but certain viruses, bacteria and parasites can make a person susceptible to develop cancer [2].

In 1761, London clinician John Hill recognized tobacco as a carcinogen, a substance that causes cancer. Tobacco has been rediscovered as the most lethal chemical carcinogen known. In 1915, Katsusaburo Yamagiwa and Koichi Ichikawa at Tokyo University induced cancer in rabbit by applying coal tar on its skin. Ionizing radiations from a variety of sources including the sun has to be proven to cause cancer [6]. In 1775, Percival Pott of Saint Bartholomew's Hospital in London observed occupational cancer of the scrotum in the people whose occupation is sweeping the chimney. He identified that this cancer is caused by the soot that is collected in the skin fold of the scrotum [6]. This study led to the public health measures to reduce the cancer risk at work by identifying and avoiding potential carcinogens in the work environment.

In 1911, Peyton Rous, at the Rockefeller Institute, described sarcoma in chickens for the first time, which eventually became Rous sarcoma virus and earned him a Nobel prize in 1968. Now we know several viruses that can cause cancer. Chronic infection with hepatitis B or C viruses can lead to liver cancer. Epstein-Barr virus had been linked with non-Hodgkins lymphomas and nasopharyngeal cancer. HIV (Human Immunodeficiency Virus) infection could increase the risk of developing various cancers, especially Kaposi sarcoma and non-Hodgkin lymphoma. Human Papillomavirus (HPVs) infection increases the cancer risk especially cancers of the cervix, vulva, vagina, anus, and pelvis. HPV infection can be prevented by vaccination [2,6].

The International Agency for Research on Cancer (IARC) has identified more than 100 chemicals, physical and biological carcinogens. Understanding of DNA and genes lead to the notion that DNA damage due to the chemicals and radiations, or introduction of new DNA sequences by viruses causes cancer. The cells with damaged DNA (mutated DNA) lead to the clones of abnormal cells. These abnormal clones become malignant clones by acquiring more

mutations. The fundamental difference between the normal tissues and cancer is that normal cells with damaged DNA dies but the cancer cells with damaged DNA do not die.

The 1970s saw the dramatic breakthrough in the cancer research. Researchers discovered two families of genes related to cancer: oncogenes and tumor suppressor genes. Oncogenes are responsible for the uncontrolled proliferation of cells. They arise from the mutations of the normal genes that control the cell division called proto-oncogenes. Tumor suppressor genes are involved in inhibiting the cell division, repair damaged DNA sequences and induce apoptosis (programmed cell death). Mutations in these genes could lead to uncontrolled proliferation of cells resulting in cancer. Inheritance of these mutated genes can cause cancer to the progeny [2,6].

1.3. Methods of cancer diagnosis:

Diagnosis of cancer at an early stage can prevent many cancer deaths. These data suggest that the people belong to the underdeveloped and developing nations, who did not have proper awareness and medical care is the worst hit by cancer. As the current cancer diagnostic procedures were laborious and expensive, many people around the world could not afford these procedures.

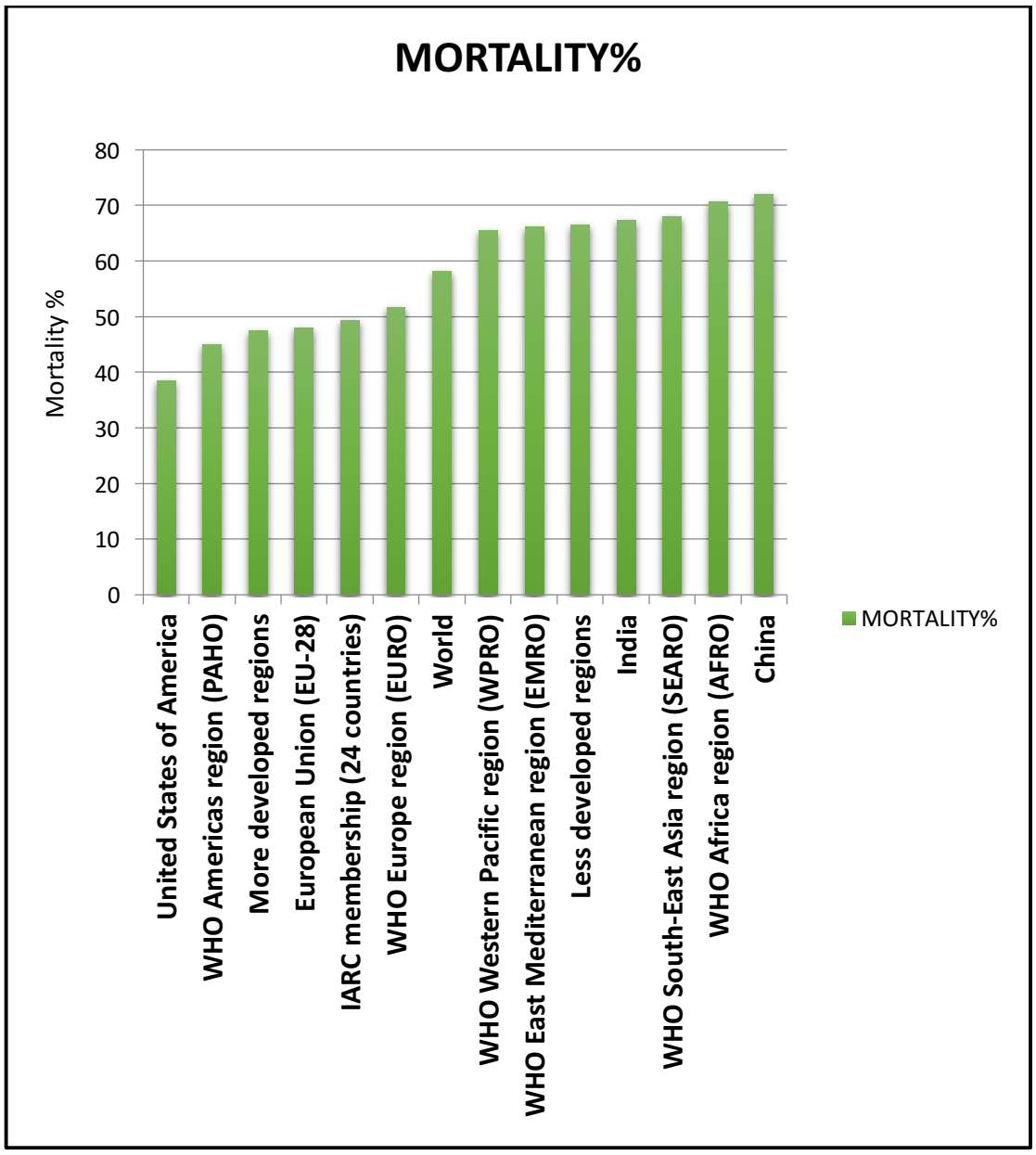

Data Source: WHO

Figure 1.1: Mortality rate of cancer in the world. Mortality rate = (total number of cancer deaths/ total number cancer cases reported) *100.

Current methods of cancer detection include computed tomography (CT) scans, mammograms, Pap (**Papanicolaou test**) and HPV testing, prostate specific antigen (PSA) tests, sentinel lymph node biopsy, tumor markers screening, endoscopy and other laboratory tests. CT scans are useful in screening lung cancer and colorectal cancer. CT scans are used to detect the abnormal growth, helps in guiding biopsy procedures and monitoring the cancer

treatment. Despite these advantages, CT scan works on passing the ionizing radiation into the body, which increases the risk of cancer, in particular for children. The risk of leukemia, brain cancer, and other cancers is very high for the children, who have undergone multiple CT scans below 15 years of age [7,8].

Mammography diagnosis cancer in the breast by using X-ray imaging technique. There are two types of mammograms: screening mammograms and diagnostic mammogram. Screening mammograms help to prevent breast cancer deaths by early detection. Diagnostic mammograms need a longer period of X-ray exposure, which is potentially undesired. Apart from the radiation exposure, the major limitations of screening mammography are high false positives and false negative results.

Pap and HPV testing are performed for the detection of cervical cancer in females. This test is based on the fact that, almost all types of cervical cancers are caused by the oncogenic human papillomavirus infection. Pap test is the cytological examination of the cells taken from the cervix for the detection of the abnormal cells. HPV test involves the detection of HPV DNA in the cervical swab samples. These cervical swabs were tested for the presence of the HPV 16 and HPV 18 DNA as these two types are highly dangerous in causing cervical cancer. Once this test is positive, it is followed by the further test for the detection of the HPV RNA. Although, Pap test and HPV test is less invasive; it is very discomfort for the patients.

PSA test is carried out for diagnosing prostate cancer. PSA is a protein produced by the prostate cancer cells, whose concentration in blood tends to increase. PSA test can be false positive or false negative as the there are many cases reported that men could have increased PSA level in the absence of prostate cancer and also not all prostate cancers are correlated with the increase in the PSA level in blood. It is noteworthy that prostate cancer can also be diagnosed by transrectal biopsy or transperineal biopsy followed by microscopic

examination. But this procedure is invasive and discomfort for the patient. Biopsy and biomarker identification is the gold standard method of diagnosis for most cancers.

1.4. Melanoma:

1.4.1. Causes of Melanoma:

This thesis focuses on two types of cancers namely melanoma and gastric cancer.

According to the National Cancer Institute, melanoma is a type of skin cancer, arise from melanocytes. The common risks of developing skin cancers include over exposure to sunlight. Sunlight is a major source of UV radiation. People who experienced blistering sunburn at least once and people sensitive to sun burn have increased the risk of developing any skin cancer including melanoma. The artificial sources of UV radiations including sunlamps and tanning booths cause severe DNA damage to the skin cells leading to cancer. People with fair skin have higher chances of developing skin cancers. Melanoma is very rare in people with dark skin. Other risk factors include *dysplastic nevus,* which is a type of mole, bigger than the normal mole. Its surface is smooth, scaly or pebbly with irregular borders. Dysplastic nevus has high chances of turning into a melanoma than an ordinary mole [9].

1.4.2. Diagnosing Melanoma:

The first sign of melanoma is the change in the shape, color, and size of the existing mole. Melanoma can be identified by looking for the few features abbreviated as "ABCDE." ‘A’ stands for the existence of asymmetry in the shape of the mole. ‘B’ stands for the irregular borders. ‘C’ stands for the uneven color complexion of the mole. ‘D’ stands for the increase in the diameter of the existing mole and finally ‘E’ stands for the continuous evolution of the mole over few weeks or months. The melanoma can be identified by closely looking for these “ABCDE” in the existing moles. The current standard for the diagnosis of melanoma is biopsy followed by the pathological examination. Excisional biopsy was performed for melanoma diagnosis, where the doctor excises the entire suspected growth along with some

tissues around it [9]. Especially for the melanoma, the doctor checks lymph nodes around the suspected region. If the lymph nodes are observed to be enlarged, the cells from the lymph node were removed using fine-needle aspiration biopsy and sent for the pathological examination. This method will help to identify whether the melanoma had already undergone metastases. If the melanoma is thick, the surgeons perform sentinel lymph node biopsy to remove the entire lymph node. This procedure is done because cancer cell tends to appear first in the sentinel lymph node before spreading to other lymph nodes [9].

1.5. Gastric Cancer:

1.5.1. Gastric Cancer and its Types:

Gastric cancer ranks third in the mortality rate (723,000 deaths/year) worldwide next to lung cancer (1.59 million deaths/year) and liver cancer (745 000 deaths/year) [1]. According to the American Cancer Society's report on stomach cancer (2014), stomach cancer is also known as gastric cancer, which is cancer arises from the stomach. Gastric cancers are slow growing cancer. Gastric cancer usually starts as a precancerous lesion in the inner lining (mucosa) of the stomach. These precancerous lesions were very hard to detect and often went undetected [10]. Gastric cancer can be categorized into different types as follows: adenocarcinoma, lymphoma, gastrointestinal stromal tumor (GIST), carcinoid tumor and other rare cancers like squamous cell carcinoma, small cell carcinoma, leiomyosarcoma, etc. Adenocarcinoma is the major type of gastric cancer; about 90-95% of gastric cancers were adenocarcinomas. These cancers arise from the mucosal cells. About 4% of gastric cancers are lymphomas. These are the cancers of immune system found in the wall of the stomach. GIST is a rare form of gastric cancer arising from the *interstitial cells of Cajal*. Carcinoid tumors arise from the hormone synthesizing cells of the stomach. About 3% of the gastric cancers are carcinoid tumors. Stomach cancer mostly affects the older adults, whereby the average age for developing gastric cancer is 69 years. About 6 of the ten people diagnosed with gastric cancer

were aged more than 65 years. Today, gastric cancer incidence is high in the less developed countries, where gastric cancer is the leading cause of cancer-related deaths [11].

1.5.2. Symptoms of Gastric Cancer:

In countries like Japan, which tops the gastric cancer incidence subject their people for the mass screening for gastric cancer. This mass screening initiative helped in identifying many people who were at the early or curable stages of gastric cancer reducing the gastric cancer deaths, but this is yet to be proved. Screening for gastric cancer is usually not done until the person experiences certain signs and symptoms of gastric cancer. Unfortunately, early stages of gastric cancer do not cause any symptoms, which is the principal bottleneck in detecting gastric cancer at early stages. The symptoms of gastric cancer include poor appetite, unexplainable weight loss, abdominal pain, discomfort in the abdominal region above the navel, a sense of fullness in the upper abdomen even after a small meal, indigestion or heartburn, nausea, vomiting with or without blood, swelling in the abdomen, anemia, etc. Since the symptoms of gastric are not caused by the advanced stages, only about 20% of the gastric cancers were diagnosed before metastasis in the USA. This discrepancy is the reason behind the high mortality rate of gastric cancer throughout the globe [10].

1.5.3. Diagnosing Gastric cancer:

If a person exhibits vague symptoms, such as indigestion, weight loss, nausea, and loss of appetite, screening tests may be recommended. Stomach cancer can be detected by various methods but the most commonly used methods or the following.

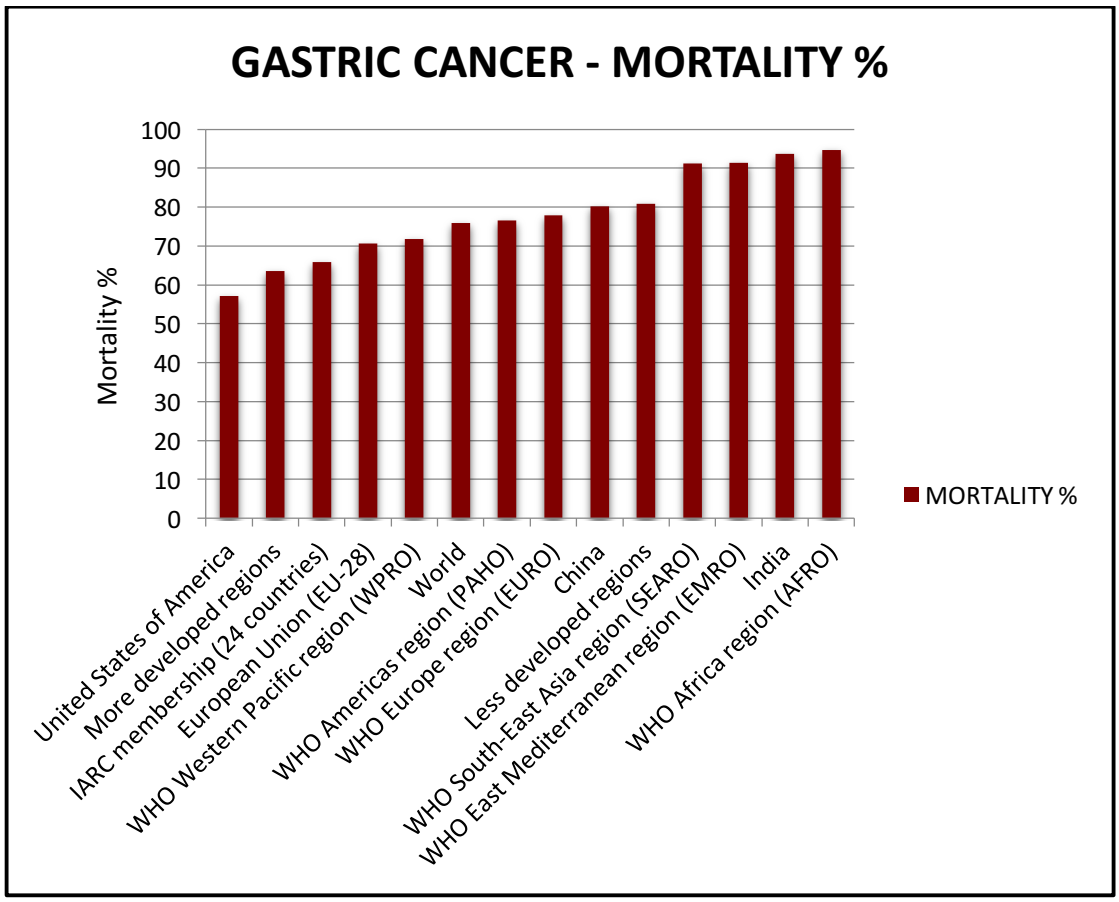

Data Source: WHO

Figure 1.2: Mortality rate of gastric cancer in the world. Mortality rate = (total number of gastric cancer deaths/ total number gastric cancer cases reported) *100.

1.5.3.1. Esophagogastroduodenoscopy and biopsy:

This test examines the esophagus and stomach using a thin, lighted tube called a gastroscope, which is passed through the mouth into the stomach. Through the gastroscope, the doctor can look directly at the inside of the stomach. If an abnormal area known as *linitis plastica* is found, the doctor will remove some tissue (biopsy) to be examined under a microscope. A biopsy is the only sure way to diagnose cancer. Gastroscopy and biopsy are the best methods of identifying stomach cancer. Hence this approach is the current gold standard method for the diagnosis of the stomach cancer. Even though this method, have high specificity and sensitivity, there are several disadvantages in using endoscopy as the first screening tool. It is

an invasive procedure with potential complications such as perforation and aspiration and is not a cost-effective screening tool for most of the countries. Unfortunately, stomach cancers in hereditary diffuse gastric cancer syndrome cannot be detected in endoscopy [10].

Endoscopy can also be used as part of an imaging test for gastric cancer, known as endoscopic ultrasound. In this method, a small transducer is placed at the tip of the endoscope. The patient needs to be sedated before this test. After sedation, the endoscope is passed into the stomach via throat. This procedure allows the doctor to visually access the spread of cancer in the stomach wall as well as the nearby lymph nodes. This approach also helps to guide the needle biopsy. Once the biopsy is taken it is sent to the pathologist, who observes the biopsies under microscope and look for the histological features of cancer. If the biopsy contains cancer cells, then the pathologist finds out the type of gastric cancer. If the sample is identified as adenocarcinoma, then it will be tested for the over-expression of the growth-promoting protein called HER2/neu. If it is positive, then these tumors are categorized as HER2 positive adenocarcinoma and treated accordingly [12].

1.5.3.2. Upper gastrointestinal (GI) series:

There are many imaging tests available for diagnosing gastric cancers which use different modalities like x-rays, magnetic fields, sound waves or radioactive substances. One such test is the upper gastrointestinal (GI) series. For this test, the patient is required to take barium as contrasting agent. The ingested barium coats the gastrointestinal wall. As X-rays cannot pass through the barium, the obtained X-ray pictures clearly show the abnormalities in the gastrointestinal wall. The main drawback of this method is the inability to get biopsies [10].

1.5.3.3. Computed Tomography (CT) scan:

Another X-ray based imaging test for gastric cancer is computed tomography scan (CT). For this test, the patients receive a contrast dye through intravenous injection line followed by the

CT scanning, which clearly confirms the location of cancer and also the spread of cancer. In this imaging modality, the contrast dye is not suitable for everyone. Although fatal complications are rare, a significant proportion of the people is allergic to this contrast dye [10].

1.5.3.4. Magnetic resonance imaging (MRI) scan:

Magnetic resonance imaging (MRI) scan is another imaging modality where radio waves were used instead of X-rays. The applied radio waves under a strong magnetic field are absorbed and released by the body parts, which is translated into detailed image of the body parts using a computer aided processing algorithm. MRI scans take longer time to scan when compared to other imaging modalities. Thus the patient has to lie in a narrow tube for more than an hour, which is very uncomfortable for the older adults [10].

1.5.3.5. Positron emission tomography (PET) scan:

Another imaging modality is the positron emission tomography (PET) scan, where radioactivity is employed to image cancer. A low dose of glucose-related radioactive substance called FDG is injected into the veins of the patient. As cancer cells consume sugar more than the normal cells, cancer cells tend to accumulate this radioactive glucose analog. Images from the PET scanner give the location and spread of cancer. This imaging modality is very useful to identify the location of the metastatic cancers as they scan for the radioactivity in the whole body. PET/CT hybrid scanners are available in the market and this hybrid machines are highly suitable for imaging gastric cancer. However, this procedure is expensive and not suitable for everyone [10].

1.5.3.6. Recent advances in gastric cancer biomarker identification:

Recently, certain serum biomarkers were identified for the diagnosis of gastric cancer, but these serum biomarkers were low in specificity and sensitivity. Chen et al. identified the

differential expression of certain metabolites by gas chromatography and mass spectrometry of the tumors isolated from the xenografted severe combined immunodeficiency (SCID) mice. They found 29 metabolites that are differentially expressed between the metastatic and non-metastatic gastric cancer tumors. Among which 20 are up-regulated, and nine are down-regulated [13]. Hao et al. isolated gastric cancer tissues and matched normal tissues from the 18 gastric cancer patients and identified 18 metabolites that are differentially expressed between cancerous and non-cancerous tissues using gas chromatography and mass spectrometry. These studies involve the identification of the metabolic biomarkers of the cancer tissues that needs the isolation of the cancer tissue that is invasive [14]. Jun et al. identified the differential expression of 10 metabolites between cancerous and non-cancerous group and seven metabolites between the metastatic and non-metastatic group by gas chromatography and mass spectrometry of the urine from the xenografted SCID (Severe combined immunodeficiency) mice [15]. However, the metabolic biomarkers identified were not- specific. Hence it is imperative to develop an inexpensive, easy to operate and non-invasive diagnostic tool for the diagnosis of gastric cancer.

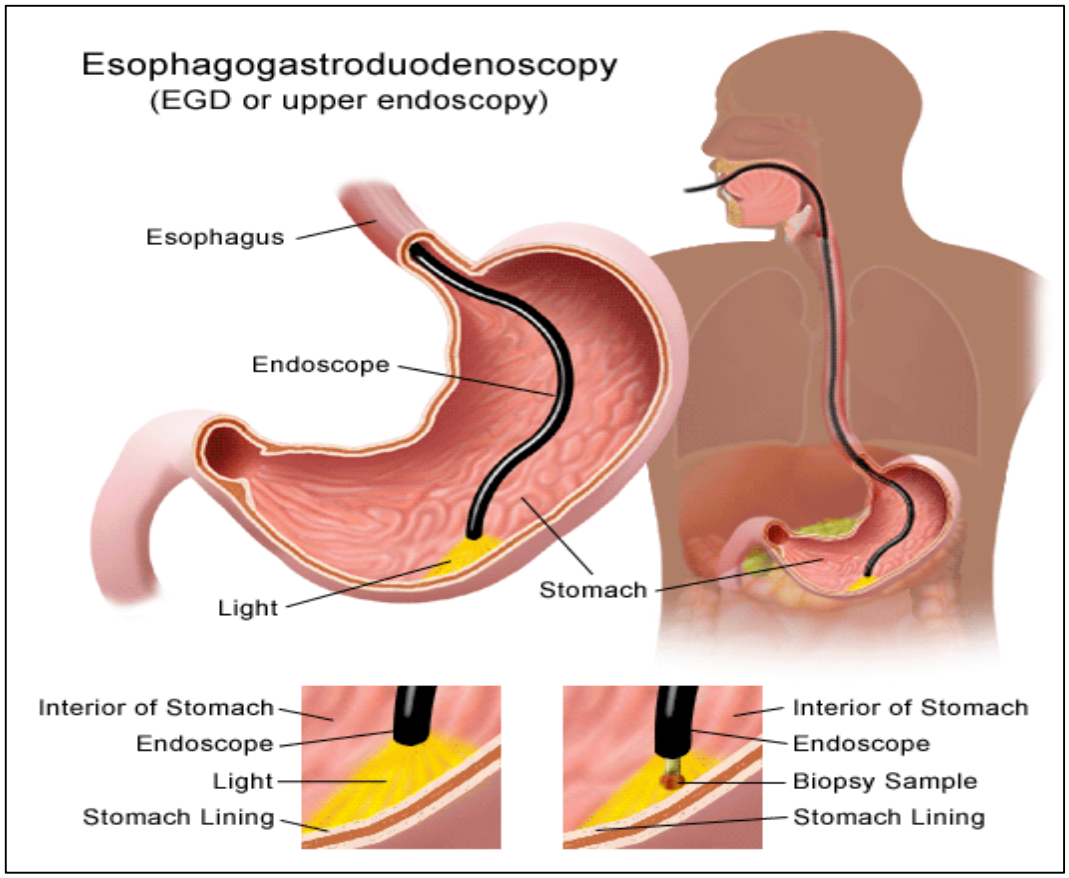

Figure 1.3. Illustration of Esophagogastroduodenoscopy
(Source: http://gisantamaria.com/egd/)

1.6. Metabolomics:

The metabolome is the ensemble of all the small molecules present in the cells, tissues, organs and biological fluids. The study of metabolome at global level is called metabolomics. Gene expression, protein expression, and the environmental cues play a vital role in synthesis, concentration, and flux of these metabolites. Any disease or syndrome can be traced back to any one or combination of the factors as mentioned above namely gene expression, protein expression, and environmental cues. Thus metabolite by itself or its concentration or its flux would be unique to the different pathological state. Hence metabolites could provide us the relevant information about the diseases and syndromes. In other words, metabolites could serve as the potential disease markers for the disease diagnosis.

The metabolites of the cells are known as cellular metabolites. Cellular metabolites can be grouped into three types as follows: (1) intracellular metabolites, (2) volatile metabolites and (3) surface metabolites. Intracellular metabolites are the metabolites that are synthesized or consumed by the cell and that are located within the cells. Volatile metabolites are the volatile organic compounds that are released by the cells into the environment as a product of metabolism. Surface metabolites are metabolites that are located on the surfaces or cell membrane. Intracellular metabolites can serve as potential biomarkers but for the detection of these biomarkers need invasive procedures like endoscopy. The intention of our study is to develop novel non-invasive biomarkers. Hence we concentrate on the volatile metabolites and cell surface metabolites, which are promising for the development of non-invasive biomarkers.

1.6.1. Volatile Metabolites:

Volatile organic compounds present in a person's exhaled breath can be an indicator of the pathological status of that person. The Roman physicians used the smell of the patient's breath for diagnosing the diseases. Some of the breath biomarkers used to them were as follows: sweet, acetone smell was used as an indicator for diabetes, liver failure was identified using the fish like smell, and renal failure is detected using the urine smell [16]. Hippocrates of Kos (460–370 BC) first described fetor oris and fetor hepaticus in his treatise on breath aroma and disease. In 1782-83, Antoine Lavoisier detected carbon dioxide (CO2) in the exhaled breath of guinea pigs, interpreted this as a product of combustion and paved the way for using CO_2 as a sign of life with its ubiquitous clinical use today [17]. In 1898, Johannes Müller performed the first quantitative investigations of acetone in exhaled breath [18]. Pauling, a noble laureate commenced the hunt for the volatile compounds in the breath. He could able to measure over 250 compounds in the human breath in 1971 by using Gas chromatography [19]. In 1999 Phillips estimated over 3000 compounds in the human breath.

Breath test for volatile markers of oxidative stress appeared to provide a sensitive and specific set of biomarkers for breast cancer [20]. Breath VOCs contained apparent biomarkers of active pulmonary tuberculosis comprising oxidative stress products (alkanes and alkane derivatives) and volatile metabolites of M. tuberculosis (cyclohexane and benzene derivatives) [21].

Exhaled breath contains thousands of volatile organic compounds (VOCs) of which the composition varies depending on health status (Table 1.1 and Table 1.2). Various metabolic processes within the body produce volatile products that are released into the blood and will be passed on to the airway once the blood reaches the lungs. Moreover, the occurrence of chronic inflammation and oxidative stress can result in the excretion of volatile compounds that generate unique VOC patterns [22].

S. No	Condition	Breath Markers
1	Lipid peroxidation	Alkanes and aldehydes.
2	Diabetes	Acetone, propan-2-ol and methyl nitrate.
3	Cancer	Alkanes, methylated alkanes, aromatic compounds, and aldehydes.
4	Heart transplant rejection	Alkanes and methylated alkanes.
5	Lung transplant rejection	Carbonyl sulfide.
6	Airway inflammation	Nitric oxide and halogenated amines.
7	Cholesterol-lowering therapy	Isoprene.
8	Liver disease	Sulfur compounds, carboxylic acids, ammonia, and ketones.
9	Kidney disease	Dimethylamine, trimethylamine, and ammonia.
10	Oral malodour	Sulfur compounds.
11	Trimethylaminuria	Trimethylamine.
12	Congestive heart failure	Acetone.

Table 1.1: List of physiological or pathological condition and its associated breath markers.

S. No.	Volatile organic compounds	Probable origin
1	Acetone	Fatty acid metabolism
2	Isoprene	Cholesterol synthesis
3	Methanol	Dietary sources
4	Propanol	Acetone metabolism
5	Acetaldehyde	Ethanol metabolism
6	Ammonia	Protein metabolism
7	Dimethyl sulphide	Methionine metabolism
8	Dimethyl disulphide	Methionine metabolism
9	Hydrogen sulphide	Methionine metabolism
10	Ethane	Lipid peroxidation
11	Ethene	Lipid peroxidation
12	Pentane	Lipid peroxidation
13	C1-C5 alkanes	Colonic bacteria
14	C1-C5 alcohols	Colonic bacteria
15	C1-C5 carboxylic acids	Colonic bacteria

Table 1.2: List of VOCs and their probable endogenous origin.

The compounds in the exhaled breath can be classified into three categories:

1. Inorganic compounds: this group includes carbon dioxide, oxygen, and nitric acid.
2. Non-volatile compounds: this category includes compounds like cytokines, leukotrienes, hydrogen peroxide, and isoprotanes.
3. Volatile organic compounds (VOC): this category is the largest of the three and contains organic compounds of different classes such as saturated hydrocarbons like ethane, pentane, aldehydes, etc., unsaturated hydrocarbons like isoprene, oxygen-containing organic compounds like acetone, sulfur-containing organic compounds like ethyl mercaptan, dimethyl sulfide, etc., nitrogen-containing organic compounds like dimethyl amine, ammonia, etc. The most commonly detected VOCs in the breath are isoprene, alcohols, and alkanes.

The VOC category is an important group of volatile compounds in this context. The VOCs of exhaled breath can be produced endogenously or exogenously. Endogenous in a sense as the end products of metabolic pathways for example isoprene, an unsaturated hydrocarbon formed during the mevalonic acid pathway of cholesterol synthesis, acetone

formed from the glucose metabolism and alkanes formed by the oxygen free radical-mediated lipid peroxidation in the cell membranes. Hence, alkanes are the key biomarkers of the oxidative stress. Exogenously the VOCs can be contaminants that are inhaled from the environment [23].

The relationship between volatile organic compounds (VOCs) in exhaled breath and local or general pathologies is a most exciting field of research. Different chemical signatures have been observed in breath from patients with lung, cardiovascular, gastrointestinal, liver, renal or mental diseases, diabetes, and different types of cancer or physiological conditions such as pregnancy. Prior studies suggest that depending on the affected tissue or organ, volatiles can have a specific profile. However, to date, information on the biochemical origin of this volatiles is rare [24].

1.7. Proton Nuclear Magnetic Resonance (NMR) Spectrometry:

Three instruments were used in these studies; they are proton nuclear magnetic spectrometry (NMR), Gas chromatography and mass spectrometry (GC-MS) and selected ion flow tube mass spectrometry (SPME-MS). Nuclear magnetic resonance (NMR) spectrometry identifies a unique chemical shift biomarker 1.28 ppm for the identification of the neural stem and progenitor cells (NPC). They could even identify the NPC in live mouse using this biomarker under proton magnetic resonance spectroscopy (1H-MRS). This achievement is possible as each type of cells has their unique surface receptor proteins and phospholipid composition. This study motivates us to look for the NMR-based biomarkers for melanoma and gastric cancer.

Nuclei are positively charged dense region located at the center of an atom. Nuclei tend to spin on an axis, which creates a small magnetic field and magnetic moment (μ).

$$\mu = \frac{\gamma h I}{2\pi}$$

γ - gyromagnetic ratio (^1H = 26,752)

h – Planck's constant

In the native state, the tiny magnetic fields around the nuclei are randomly oriented. But under the external applied magnetic field (B_0), these magnetic fields will either align or oppose the applied magnetic field. The energy difference between the aligned and opposed nuclear magnetic fields is small and depends on B_0.

$$\Delta E = h\nu$$

$$\Delta E = \frac{\gamma h B_0}{2\pi}$$

When the radio waves are applied to the nuclei under applied magnetic field, the nuclear spin-flip their orientation and the nuclei is said to be in resonance with B_0. Different nuclei absorb radio waves at different wavelength. Nuclei will resonate at different energies depending on their chemical and electronic environment. This resonance forms the NMR signals; the position referred as chemical shift and pattern called splitting, or multiplicity gives the information about the chemical environment of the nuclei [25].

The NMR machine has a provision for the placing the NMR sampling tubes containing the sample of interest. This arrangement is surrounded by a strong magnet and coils for applying radio waves. The strong magnetic field is first applied to the samples, which will align the nuclei in the samples to align or oppose the applied magnetic field

instantaneously. Then the radio frequency is passed to the samples at different wavelengths, and corresponding NMR signals will be acquired using a computer software application.

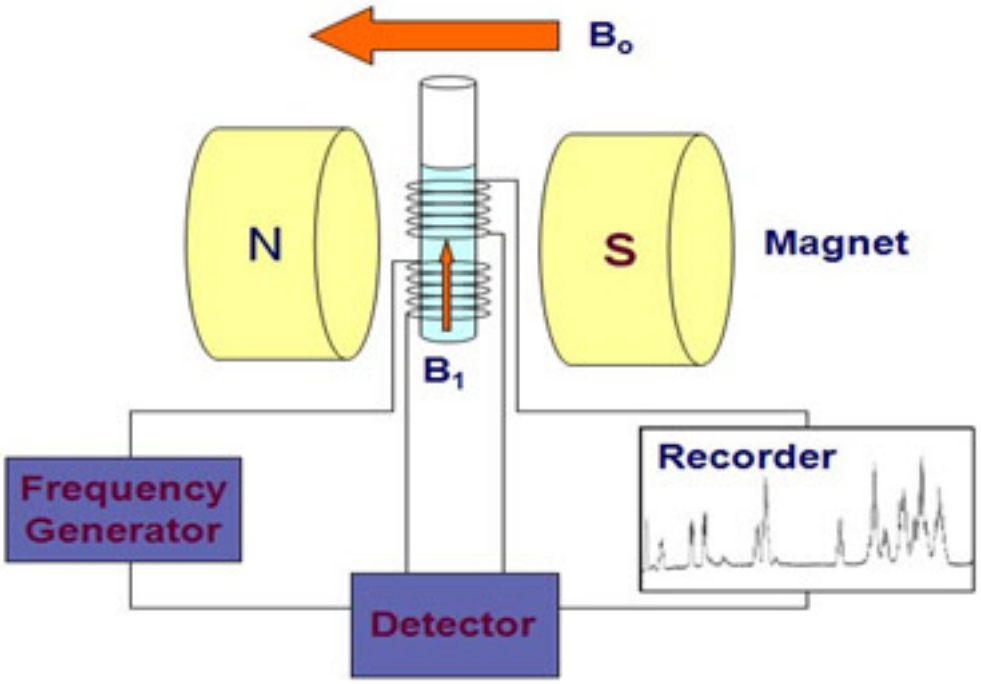

Figure 1.4: Working of Nuclear Magnetic Resonance Spectrometry. (Source: http://www.agilent.com/labs/images/figure2.jpg)

1.8. Solid-phase Microextraction and Gas Chromatography-Mass Spectrometry (SPME-GCMS):

Gas chromatography coupled with mass spectrometry is considered as the gold standard method for analyzing volatile organic compounds. The gas chromatography was invented by Martin and James in 1952 [26]. In GC, the sample to be analyzed is introduced to very high temperature (200-300° C) and mixed with a stream of carrier gas which is helium (He). This mixture is subsequently entered the chromatographic column made up of fused silica tubular capillary coated internally with a thin polymer film. Depending on the chemical structure, the analyte molecules are partitioned between the carrier gas stream (mobile phase) and the polymer coating (stationary phase). When the partitioned analyte

molecules reach the end of the stationary phase, they move to the detection system based on the thermal conductivity, ionization in a flame or electron capture is employed to produce an electrical signal that is proportional to the concentration of the analyte molecules. These electrical signals are plotted against time resulting in a gas chromatogram. The mass spectrometer is used to identify the compounds that were causing the electrical signals. The mass spectrometer generates a fingerprint of the compound using the charged fragments generated as a result of dissociation. This mass fingerprint is known as mass spectrum based on which the compounds can be identified. The GC-MS analysis gives retention times, chromatographic areas and mass spectra of each compound in a mixture that is obtained as a result of ionization of electron impact at standard energy of 70 eV.

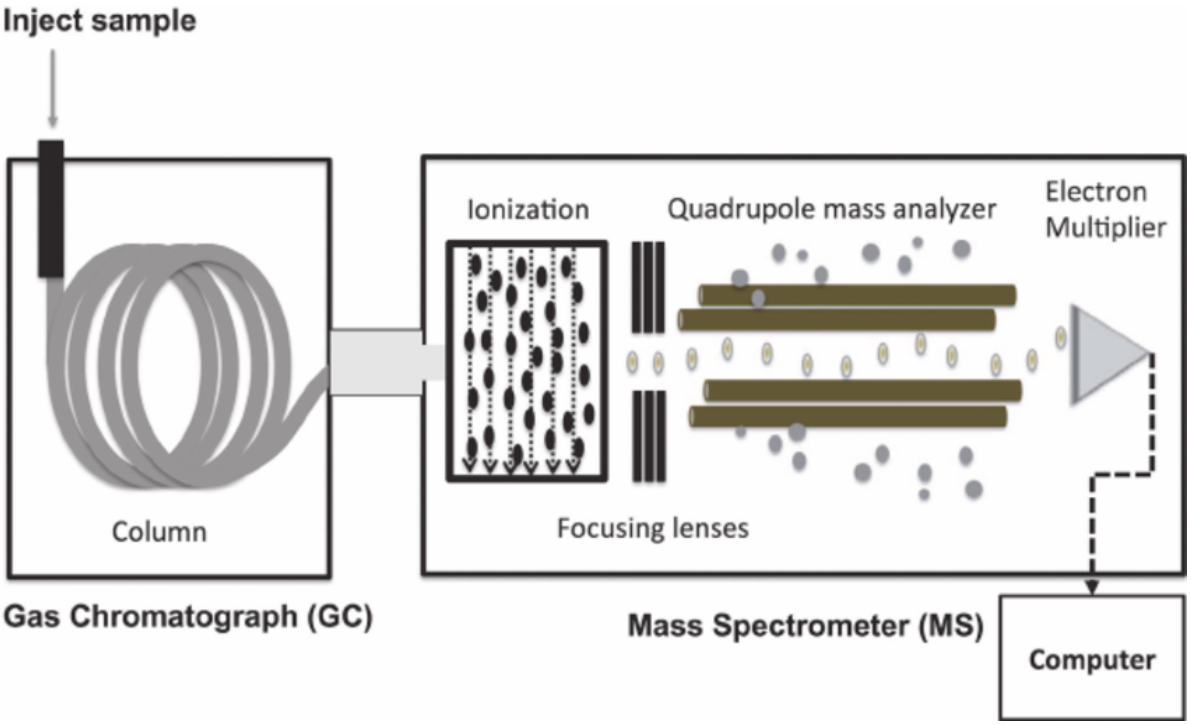

Figure 1.5: Working of Gas Chromatography and Mass Spectrometry (Source: Kim, I., Suh, S., Lee, I., & Wolfe, R. R. (2016). Applications of stable, nonradioactive isotope tracers in vivo human metabolic research. *Experimental & Molecular Medicine*, *48*(12).

Even though GCMS is a very traditional method for the VOCs analysis, this approach has certain weakness such as matrix effects. It requires accurate sample preparation before the actual analysis. It is not real time and needs 10-60 mins to analyze single sample. Thus limiting its use in the researches where a large number of samples to be analyzed on the same day. Pre-concentration of the samples is a must for the biological specimens, and it is mostly done using solid phase micro-extraction procedure (SPME) followed by thermal desorption (TD) before GC [27]. SPME is a very successful solvent free method of sample preparation for GC. It was invented by Pawliszyn et al. in 1989. It is a simple device looks like a syringe consisting a fiber holder which is needle and a fiber assembly. This fiber is made up of fused silica optical fiber coated with the VOC adsorbing polymer film such as polydimethylsiloxane (PDMS), carbowax, etc. This polymer coating adsorbs the VOCs when exposed to the environment which is known as headspace sampling. Once the sampling is done the fiber is retracted into the fiber holder and transferred to the inject port of the GC which is at 250-280° C. when the fiber is exposed to the injection port, the VOCs adsorbed to the fiber will be desorbed due to the high temperature of the port [28]. This procedure is called thermal desorption (TD).

1.9. Selected Ion Flow-Tube Mass Spectrometry:

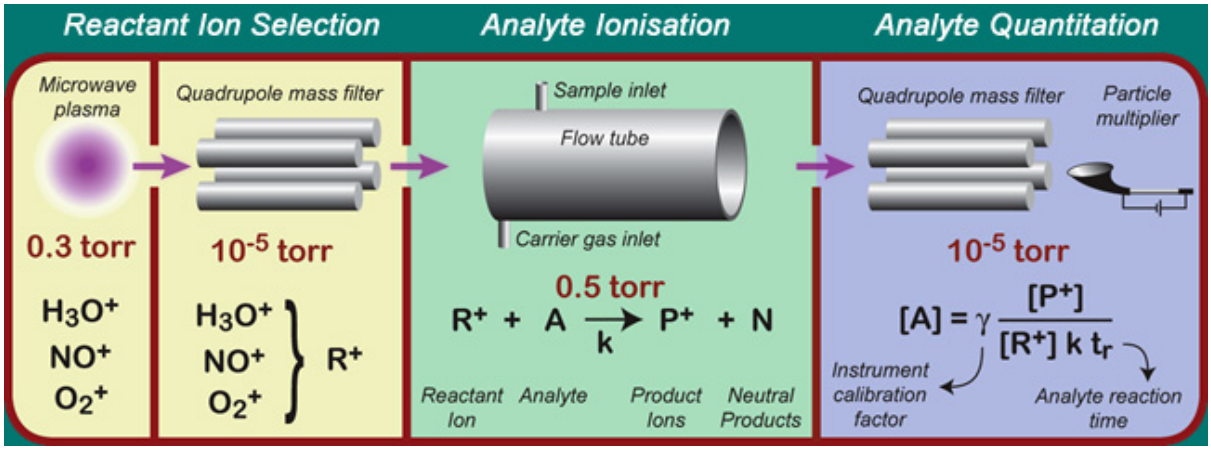

Figure 1.6: Selected Ion Flow-Tube Mass Spectrometry (Source: http://www.kgn-measurement.nl/images/sift-ms.jpg).

The SIFT-MS is derived from the selected ion flow tube (SIFT) method developed by N.G. Adams and D. Smith in 1976 [29]. It was initially developed for studying the kinetics of gas phase reactions between ions and molecules. Later in 1995, D.Smith and P. Spanel developed SIFT-MS method for the analysis of trace gases. In 1997, transportable SIFT was constructed at Keele University, and the current portable version of SIFT-MS was built in 2006. The principle of SIFT-MS is the chemical ionization, where the neutral molecules were ionized using the selected precursor ions. Chemical ionization minimizes the number of fragmented product ions, thus simplifying the resulting mass spectrum [30]. In this dissertation, the precursor ions were used namely H_3O^+, NO^+ and O_2^+. These three precursor ions are ideal as they unreactive to the major components of the ambient air, thus facilitating the analysis of the trace compounds [31-33]. This multiple precursor ion strategy is the real strength of SIFT-MS method.

The precursor ions are generated in a microwave glow discharge ion source from a mixture of steam and air, maintained at 0.3 mbar [34]. From these generated ions, the selected precursor ions were filtered out by a mass filter. A current of these selected precursor ions is injected into a fast flowing helium carrier gas. These precursor ions along with the carrier gas enter the flow tube, where the sample to be analyzed is introduced. The volume of the sample injected can be controlled using the flow meter connected to the sampling inlet. The precursor ions react with the gases in the injected sample. Theses reactions resulted in the generation of the product ions. These product ions where detect and identified using the quadrupole mass spectrometer and counted by the channeltron multiplier/pulse counting system. The computer software application generates an output plot of product ion M/Z ratios vs. counts per second (C/S). SIFT-MS can be operated in two modes: 1. Full scan mode (FS)

and 2. Multiple ion monitoring mode (MIM) [35]. In FS mode the mass spectrum of all the product ion M/Z within the selected range will be detected. This method is particularly useful when there is no information about the sample is known. In MIM mode only the count rates of the selected product ions were monitored. This mode is used to quantify the VOCs that are known to present in the sample. In this dissertation, FS mode is used as there is no prior information is available regarding the composition of the VOCs in our samples.

1.10. Thesis objectives:

The primary objectives of this thesis is as follows:

1. To explore the possible ways of identifying non-invasive biomarkers for cancers.
2. To identify and confirm the reliability of the non-invasive cancer biomarkers using *in-vitro* 3D cancer models.
3. To carry out a clinical study focused on discovering novel non-invasive cancer biomarkers.
4. To develop a low-cost, reusable, portable, easy to operate and novel diagnostic tool for detecting the non-invasive cancer biomarkers identified in the clinical study.

All the studies in this thesis are performed to achieve all the objectives mentioned above.

Chapter 2

Proton NMR characterization of intact primary and metastatic melanoma cells in 2D & 3D cultures

2.1. Background:

14.1 million new cancer cases are reported every year with 8.2 million annual deaths [1]. As cancer is very heterogeneous, it is indispensable to have a better characterization procedure for its diagnosis and treatment. One non-destructive way of characterizing cancer cells is by employing nuclear magnetic resonance. In this study, we intend to access the specificity of the proton NMR method using the two closely associated melanoma cell lines. Cancer cells contain higher levels of phospholipids than normal cells, which was responsible for enhanced cell proliferation and signal transduction. The alteration of phospholipid composition aids the cancer cells in the invasion, metastasis, and expression of growth factor receptors [36,37]. Past studies concluded that 1H MRS could be used to diagnose cancer and also to monitor treatment responses [38-41]. It had been reported in the gene expression studies that 576 genes were differentially expressed between primary melanoma and metastatic melanoma among which most of the genes showed decreased expression in metastatic melanoma when compared to primary melanoma [42]. These genes were found to be involved in cell adhesion, tumor suppression, cell cycle regulation and apoptosis. It is noteworthy that two proteins namely MAGEC1 (Melanoma antigen family c1) and FCRL1 (Fc receptor-like 1), which were known for melanoma progression were up-regulated in metastatic melanoma [42]. Another study showed that in primary melanoma SPRR1A/B, KRT16/17, CD24, LOR, GATA3, MUC15, and TMPRSS4 were up-regulated whereas, MAGE, GPR19, BCL2A1, MMP14, SOX5, BUB1, RGS20 were up-regulated in metastatic melanoma [43].

Coherent anti-Stokes Raman Scattering imaging revealed that free fatty acids (FFA) induced lipid accumulation in the cancer cells. FFA accumulation could adversely affect the cell-cell contact and promotes tissue invasion. FFA accumulation was positively correlated with the extent of metastasis [44]. The blocking of the lipogenesis either by pharmacological drugs or using antisense shRNA resulted in the inhibition of tumor growth and metastasis after anti-angiogenic treatment [45, 46].

The higher levels of the choline related compounds were not only due to the biosynthetic pathways but also due to oncogene-induced activation of phosphatidyl choline and phosphatidyl ethanolamine-specific phospholipases resulting in the accumulation of choline related compounds in tumorous or actively proliferating cells [47]. Differences in the concentration of choline-containing compounds could be considered as an indicator for accessing the clinical response of cancer to chemotherapy. The outcome of the chemotherapy could be considered as positive if the choline-containing compounds decrease after the chemotherapy [48]. It was already reported that metastatic melanoma of lymph node can be detected using proton NMR spectroscopy with the sensitivity of 92.9% and specificity of 90.3% [49]. Proton NMR chemical shifts of choline could alone separate the melanoma biopsies from non-melanoma biopsy with 69% accuracy [50]. Another study reported elevated levels of choline, taurine, lactate and amino acids like alanine, lysine, glutamine and glutamate in the biopsies could be the potential biomarkers for the identification of both primary and secondary melanoma cells [51]. From these studies, it was evident that proton NMR spectroscopy is capable enough in discriminating melanoma cells from non-melanoma cells.

The biomarkers identified by the MRI coupled with 1H-MRS and proton nuclear magnetic resonance spectrometry (1H-NMR) could be correlated, as both these methods evolve from the same principle where the former was the addition of imaging to the later [52]. In a recent

study, Proton Nuclear Magnetic resonance spectrometry identifies a unique chemical shift biomarker 1.28 ppm for the identification of the neural stem and progenitor cells (NPC). This method was used to determine the NPC in the live mouse using the same biomarker under proton magnetic resonance spectroscopy (1H-MRS) [53]. From the previous studies, it is clear that magnetic resonance can be employed for cancer diagnosis using the lipid signals, but the specificity of the magnetic resonance method for detecting cancerous tissues is still not well established.

The objective of this study is to access the specificity of proton NMR spectrometry in characterizing cell lines. We hypothesize that the differences between these biologically very close cancer cells can be deduced by proton NMR. To test this hypothesis, we explore the specificity of proton NMR method by characterizing the primary and metastatic melanoma cells that were extracted from a single donor. The specimens we selected for this study were WM 115 (Primary melanoma) and WM 266 (Metastatic melanoma) cell lines. These cells are closely associated to one another as they are excised from the same donor and vary only in the stages of cancer. We also explored the differences in these cells grown as adherent cells and as multi-cellular tumor spheroids using proton NMR. If our hypothesis is correct, then it is evident that proton NMR shows high specificity and suitable for cellular level characterization.

2.2. Methods and materials:

2.2.1 Cell culture:

WM-115 (Human primary melanoma) and WM-266 (Human metastatic melanoma) cells were purchased from American Type Culture Collection (ATCC), USA. These cells were cultured in Eagle's modified essential medium (EMEM) with 10% fetal bovine serum (FBS).

For the comparison of different cell lines in-vitro by nuclear magnetic resonance (NMR), it is necessary that the cells should have the same histologic origin and same growth medium [38]. All the experiments were carried out in triplicates for both the cell lines.

2.2.2 Extraction of the intact cells:

The cells were cultured until they reached 90-95% confluence. The cells were washed twice with DPBS and harvested by trypsinization. The viability of the cells was checked by hemocytometer using bromophenol blue dye exclusion as a criterion for distinguishing live and dead cells. The samples with over 95% of viable cells were assumed to be suitable for the NMR spectrometry. The cells were diluted so that each sample has 1 x 10^7 cells.

2.2.3 Formation of cellular spheroids:

For the spheroids formation, the cells were grown under 2D culture condition and harvested using trypsinization. The harvested cells were checked for viability as described above. These cells were diluted to 2.5 x 10^6 cells/mL, and each sample is an aliquot of 4 mL containing 1 x 10^7 cells. The diluted cell samples were drawn into 20µL droplets on the lid of the petri dish. The petri dish was filled with 10mL of DPBS which forms the hydration chamber. The petri dish lid was gently inverted and placed in the incubator for the spheroid formation. The petri dish was then incubated for three days. After three days, the spheroids could be observed by the naked eye as white spheres. The spheroids were harvested, and 600µL of D_2O was poured gently on the harvested spheroids and carefully poured into the NMR tubes (Figure 2.1).

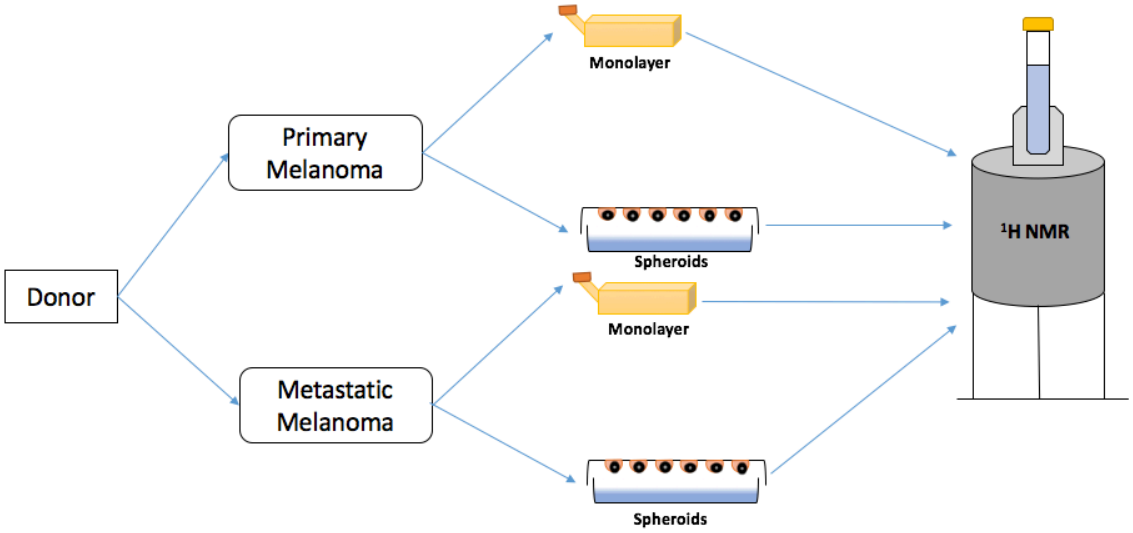

Figure 2.1: Experimental design

2.2.4 Nuclear magnetic resonance (NMR) spectrometry:

We performed one-dimensional ^{1}H NMR spectroscopy (DRX500, Bruker USA) on the collected samples and matched controls using deuterated water (D_20) as the proton NMR solvent. The acquired proton NMR spectral data was Fourier-transformed followed by phase and baseline correction using the Bruker XWinNMR software version 3.5. All the spectrums were aligned using the Mnova 11 software. The peak lists were extracted for the metabolite identification. The peak list was given as input to the MetaboAnalyst 3.0 online statistical software (http://www.metaboanalyst.ca, Canada) for statistical analysis [54].

2.3. Results:

2.3.1 NMR spectrum of the melanoma cells from monolayer culture and spheroid culture:

The peaks were binned together by the moving window of 0.03 ppm and a step of 0.015 ppm, which results in a group of 131 chemical shifts. The binned data was then normalized using generalized log transformation and auto scaling.

2.3.2 Chemical shift markers identified using Proton NMR analysis:

One-way ANOVA was performed for the identification of the statistically significant chemical shifts (p-value <0.05). We focus only on the qualitative markers as they are more relevant for the clinical translation of this study. In the monolayer culture, the 1H NMR spectrum of the primary and metastatic melanoma cells were almost similar and varied only in their intensity (quantitative markers) expect the chemical shift at 5.86 ppm.

In the spheroid culture, we had observed several qualitative chemical shift markers for both primary and metastatic melanoma spheroids. Eight (3.58 ppm, 3.60 ppm, 3.67 ppm, 3.75 ppm, 4.12 ppm, 4.39 ppm, 6.16 ppm, 8.07 ppm) chemical shift markers were observed in the primary melanoma spheroids and one marker namely 8.25 ppm for metastatic melanoma spheroids (Figure 2.2, Table 2.1).

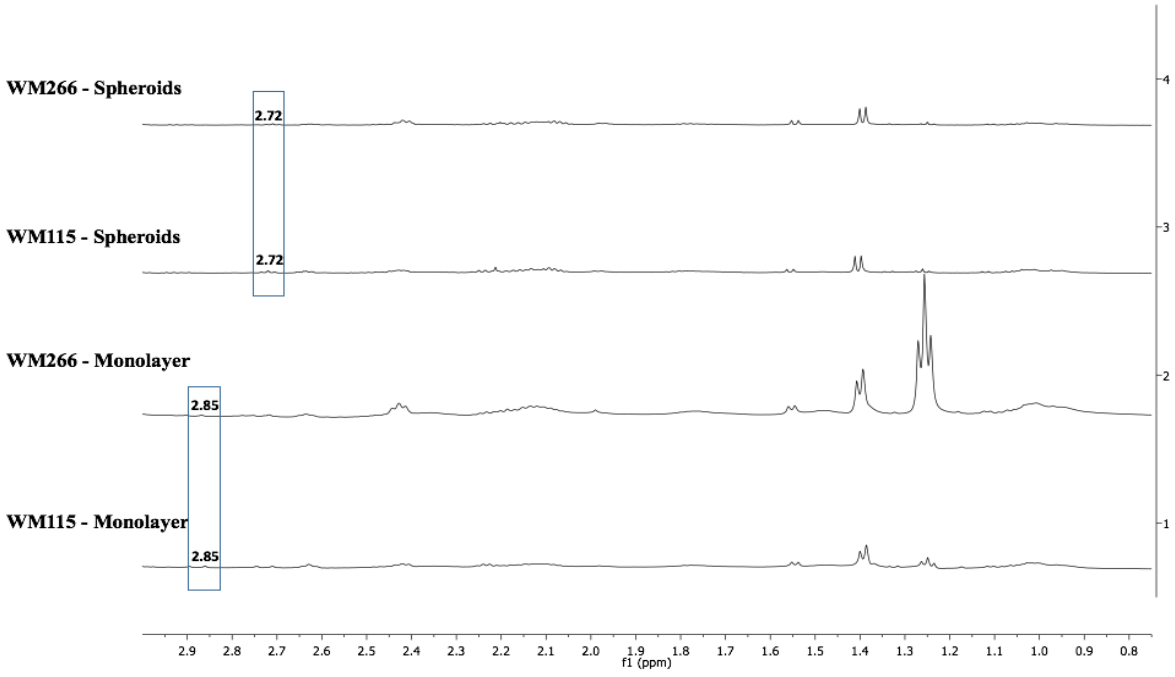

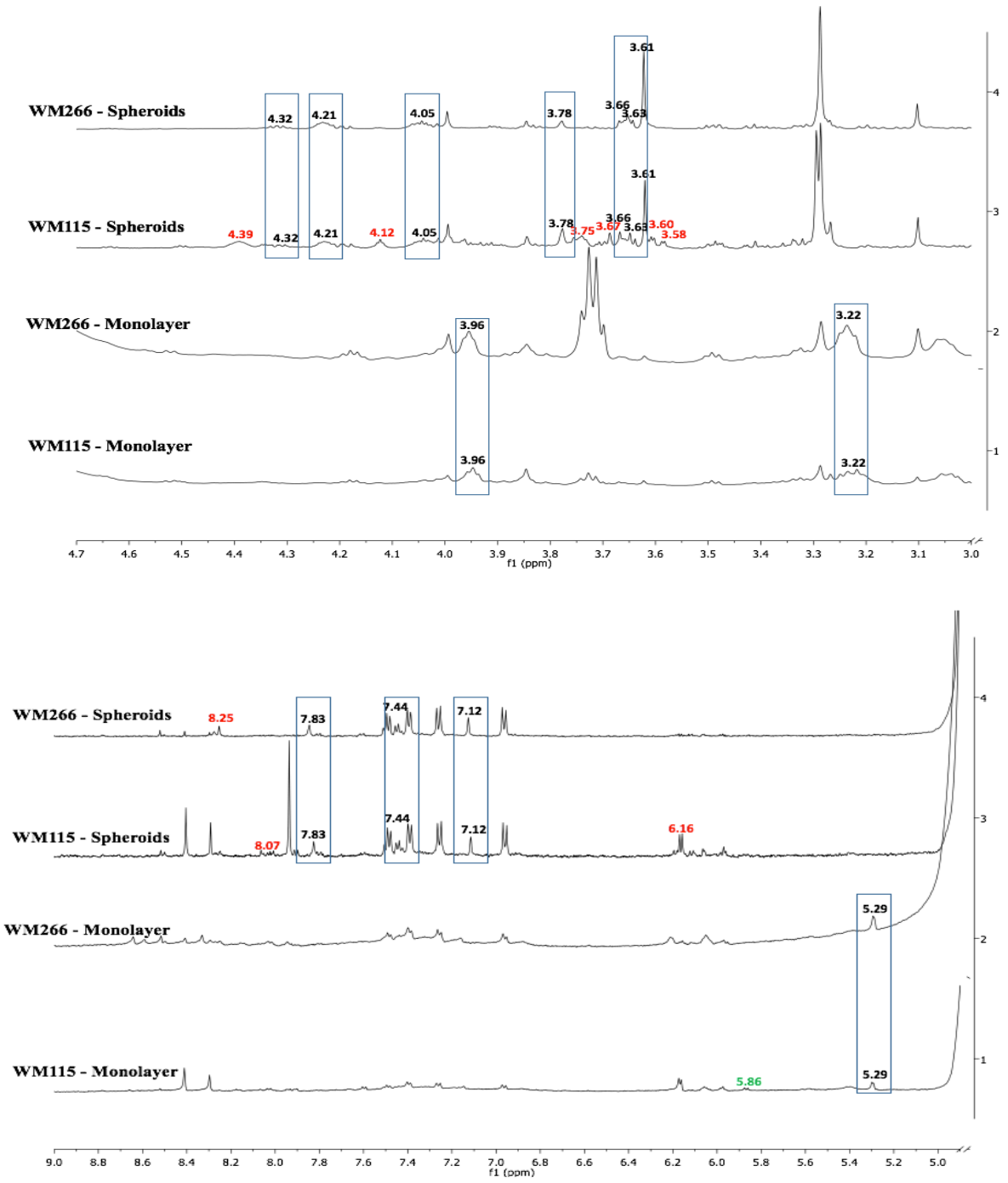

Figure 2.2: 1D 1H NMR spectra showing the qualitative chemical shift markers; **Red font:** Qualitative chemical shift markers between WM115 spheroids and WM266 spheroids; **Green font:** Qualitative chemical shift markers between WM115 monolayer and WM266 monolayer; **Black Font – Boxed:** Qualitative chemical shift markers between monolayers and spheroids irrespective of the type of cell lines.

Melanoma cells were observed to behave differently with different cell culture methods. In this analysis, we are reporting the chemical shifts that were unique to the cell line by

excluding the chemical shifts that were specific to the cell culture method, irrespective of the cell lines. Comparison of primary melanoma cells cultured as monolayer and as spheroid yields 5 chemical shift markers (1.16 ppm, 2.71 ppm, 2.74 ppm, 3.04 ppm, 3.25 ppm) for primary melanoma cells cultured as monolayer and 10 chemical shift markers (2.19 ppm, 2.72 ppm, 2.93 ppm, 3.58 ppm, 3.61 ppm, 4.02 ppm, 4.12 ppm, 4.39 ppm, 6.07 ppm, 6.17 ppm) for primary melanoma cells cultured as spheroids (Figure 2.3).

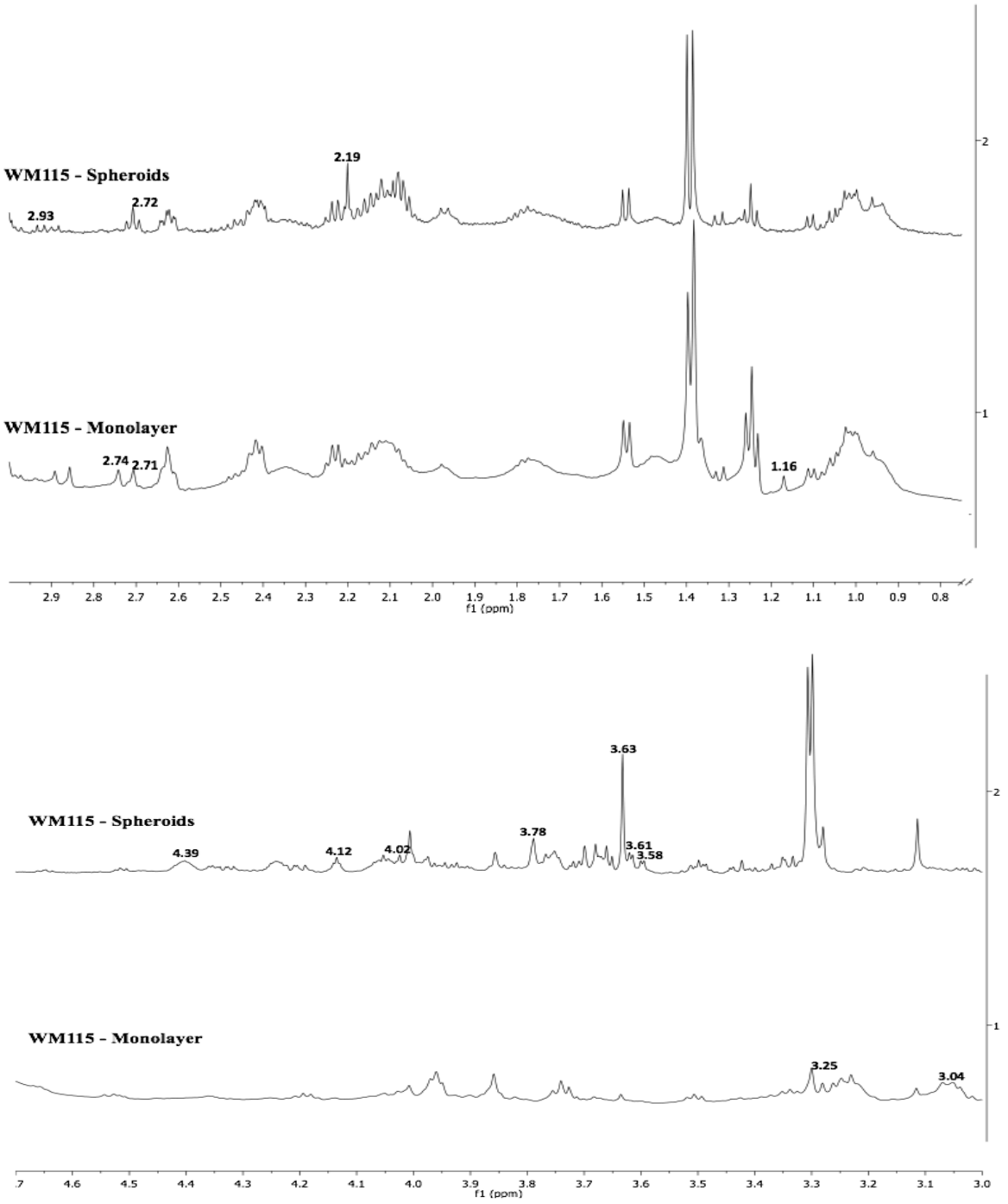

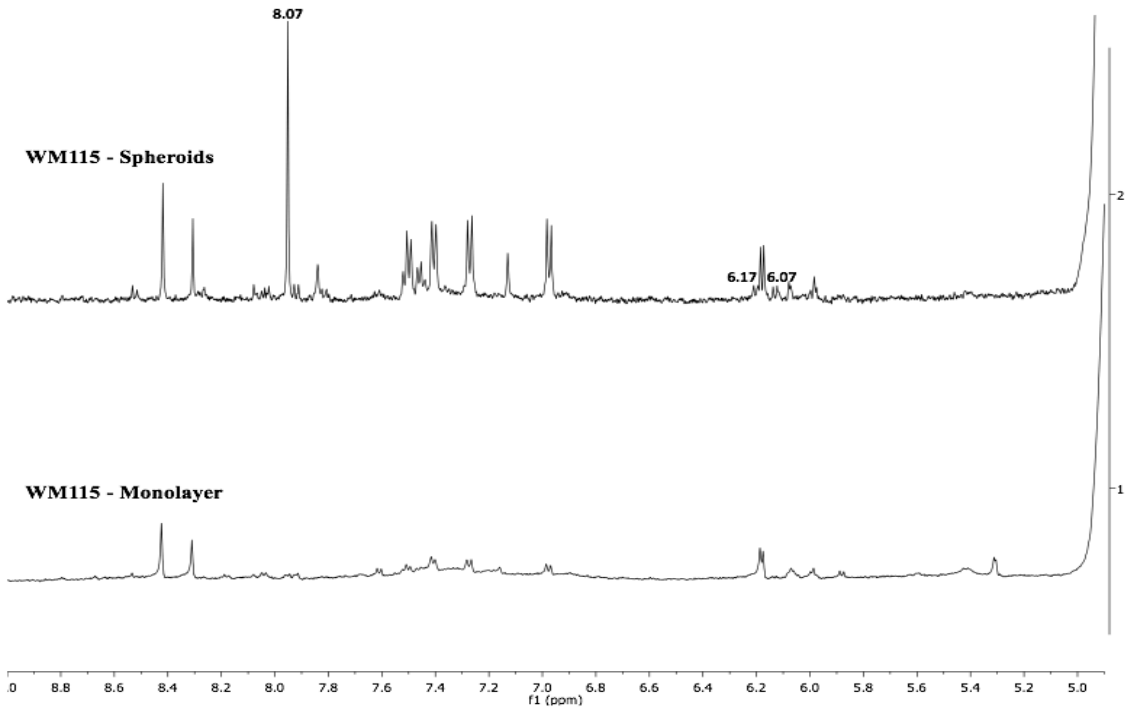

Figure 2.3: 1D 1H NMR spectra showing the qualitative chemical shift markers between WM115 monolayer and WM115 spheroids.

Similarly, in the case of metastatic melanoma cells, 3 chemical shift markers (3.08 ppm, 3.72-3.75 ppm, 3.90 ppm) were observed for metastatic melanoma cells cultured as monolayer and 2 (3.19 ppm and 3.48 ppm) chemical shift markers were found in metastatic melanoma cells cultured as spheroids (Figure 2.4, Table 2.1).

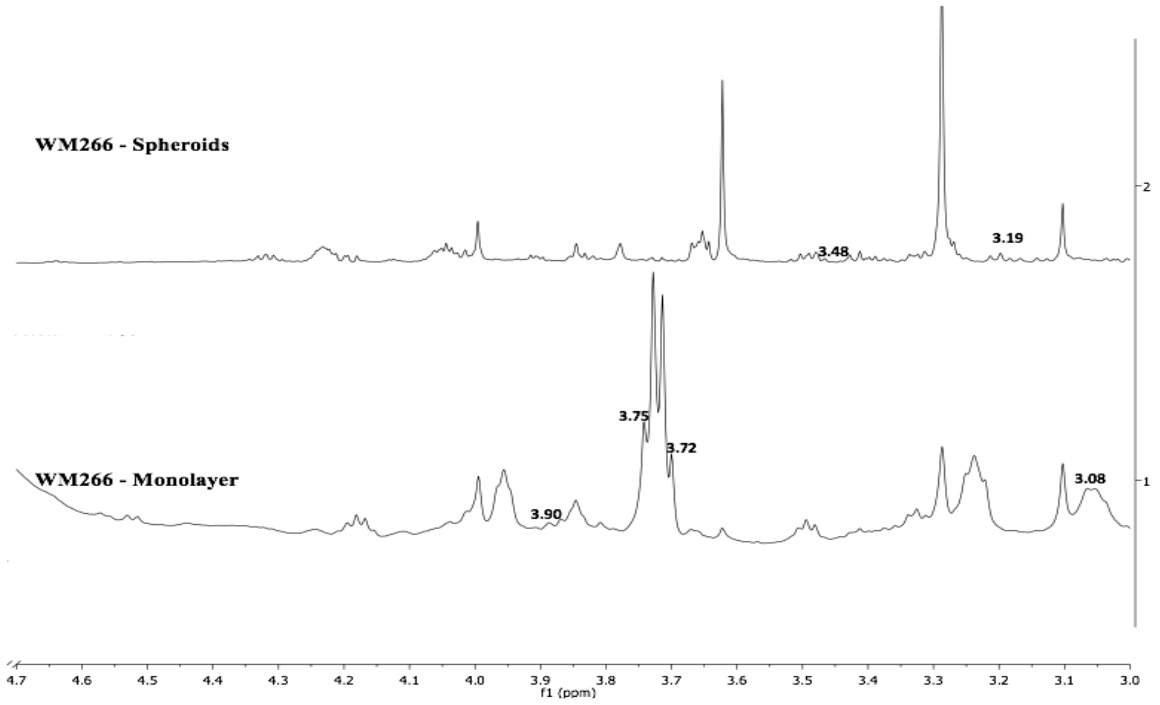

Figure 2.4: 1D 1H NMR spectra showing the qualitative chemical shift markers between WM266 monolayer and WM266 spheroids.

In this study, we also intend to identify chemical shift markers with respect to the culturing method irrespective of the type of cell line. We were able to determine 4 chemical shift markers (2.85 ppm, 3.22 ppm, 3.96 ppm, 5.29 ppm) found only in the cells grown as monolayer and 10 chemical shift markers (2.72 ppm, 3.63 ppm, 3.66 ppm, 3.78 ppm, 4.05 ppm, 4.21 ppm, 4.32 ppm, 7.12 ppm, 7.44 ppm, 7.83 ppm) found specific to the cells grown as spheroids (Table 2.1).

S. No	Cell Line/Culture Type		^{1}H NMR Markers (ppm)	Assignment	Reference
1	2D	Primary Melanoma	5.86 (d)	Guanosine	[55]
2		Metastatic Melanoma	-	-	-
3	3D	Primary Melanoma	3.58 (d)	Threonine	[56] [57]
			3.60 (d)	Threonine	[58]
			3.67 (s)	Glucose	[57]
			3.75	Glutamine	

			4.12 (t)	Glycerophospoethanolamine	[59] [60]
			4.39 (s)	N-acetylgalactosaminitol	[61]
			6.16 (d)	Glucose	[62]
			8.07 (s)	Nh2	[63]
4		Metastatic Melanoma	8.25 (s)	ATP	[64]
5	Primary Melanoma	2D	1.16 (s)	Lipids	[65]
			2.71 (s)	Dimethylamine	[66]
			2.74 (s)	Dimethylamine	[67]
			3.04	Creatine/phosphocreatine	[59] [68] [69]
			3.25 (s)	Choline head groups of phospholipids	[70]
6		3D	2.19 (s)	Adipate	[71]
			2.72 (t)	Unassigned	
			2.93 (s)	Dimethylglycine	[60]
			3.58 (d)	Threonine	[57]
			3.61 (d)	Glycerol	[72]
			4.02 (s)	2 hydroxyglutarate	[73] [74]
			4.12 (t)	Glycerophosphoethanolamine	[72]
			4.39 (s)	N-acetylgalactosaminitol	[61]
			6.07 (d)	Unassigned	
			6.17 (s)	Unassigned	
7	Metastatic Melanoma	2D	3.08	Methyl-lysine	[74] [75]
			3.72-3.75 (q)	Unassigned	
			3.90 (s)	Glucose	[76]
8		3D	3.19 (s)	O-acetylcarnitine	[71]
			3.48 (s)	Unassigned	
9	2D		2.85 (s)	Asparagine	[77]
			3.22	Choline	[59]
			3.96 (t)	β-Cyclodextrin	[78]
			5.29 (s)	Hc−ch (l, ch)	[75]
10	3D		2.72 (t)	Unassigned	
			3.63 (s)	Glycerol	[72]
			3.66	Glycerol/inositol	[72] [79]
			3.78	Phosphoinositol	[79]
			4.05 (t)	Ethanolamine	[79]
			4.21	Phosphocholine	[72]
			4.32	Glycerophosphocholine	[65]

		7.12 (s)	Ar-H	[65]
		7.44 (d)	Unassigned	
		7.83 (s)	Amide (-NH)	[71]

Table 2.1: List of qualitative chemical shift markers and its chemical shift assignment.

Partial least square - discriminant analysis (PLS-DA) and clustering analysis performed between the primary and metastatic cells showed that culturing method had a more dominant influence over their 1H NMR spectrum than the cell line differences (Figure 2.5 and 2.6).

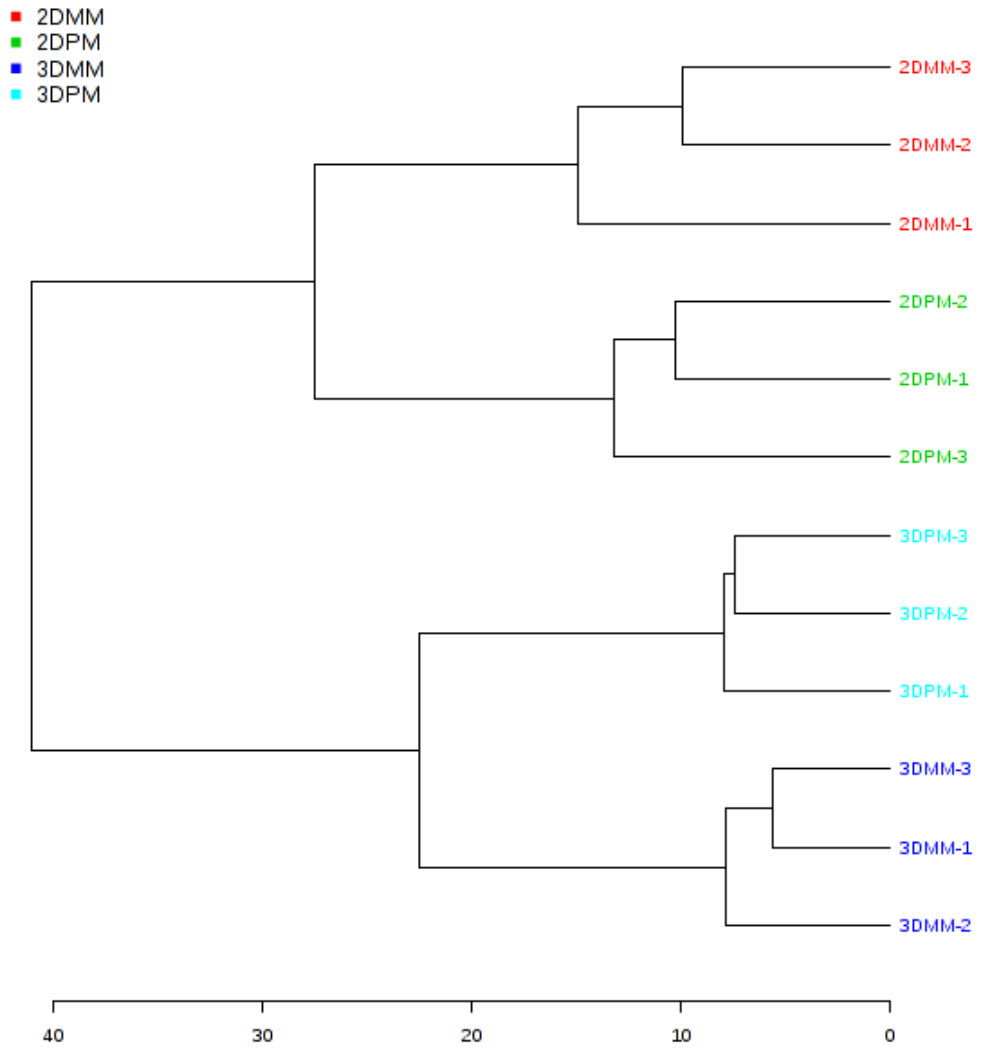

Figure 2.5: Dendrogram showing distinct clusters of primary and metastatic melanoma cells cultured as monolayer and spheroids. This shows the impact of the cell culturing method.

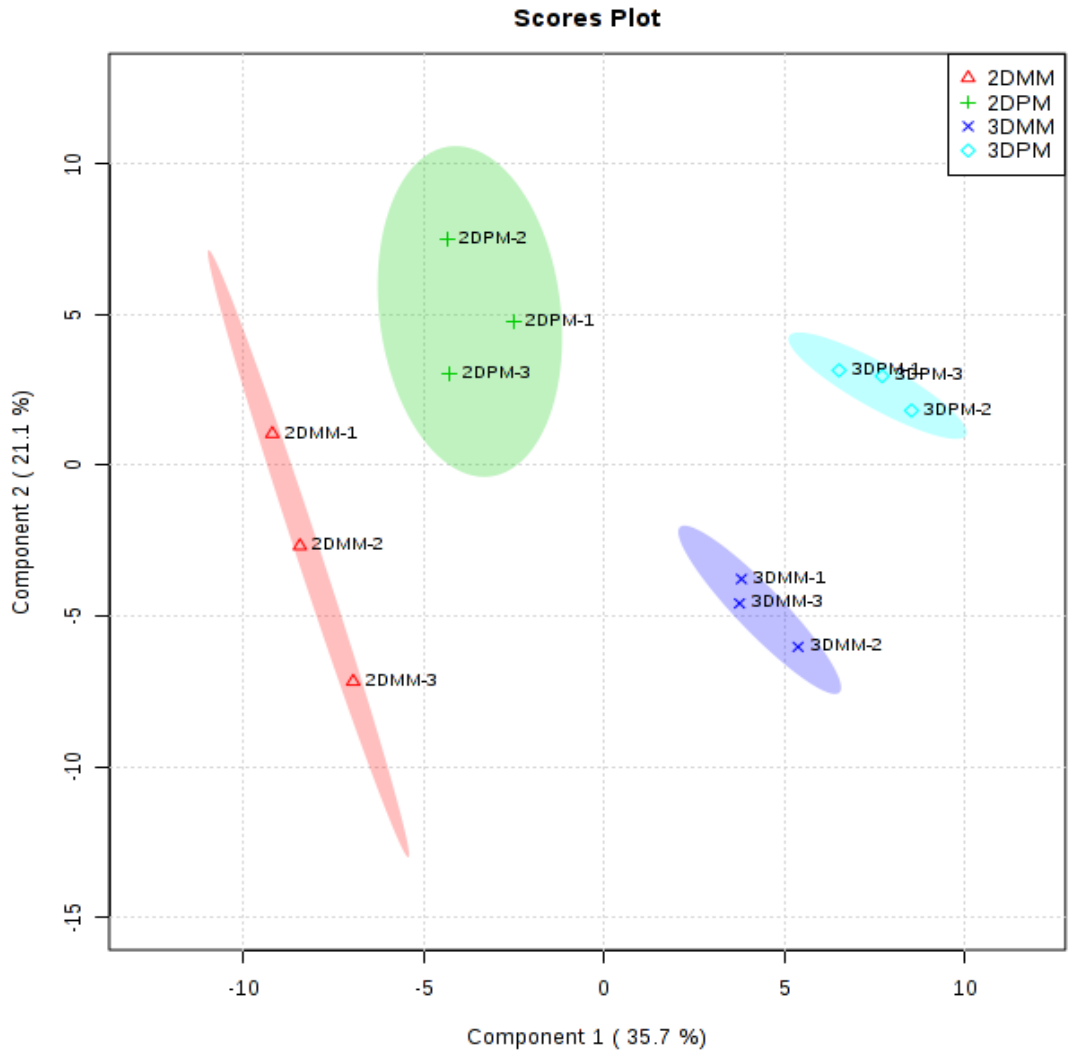

Figure 2.6: PLS-DA plot showing the variance between the primary (PM) and metastatic melanoma (MM) cells cultured as monolayer and spheroids.

2.4. Discussions:

2.4.1 Guanosine as the biomarker for primary melanoma in monolayer culture:

This chemical shift 5.86, which was unique to the primary melanoma cells cultured as monolayer was assigned to guanosine, which is an integral part of the cGMP, an important second messenger in various intra-cellular signal transduction pathways. This observation suggested that in monolayer culture, primary melanoma (WM115) and metastatic melanoma (WM226) vary only in the guanosine related pathways.

2.4.2 Primary melanoma spheroids and metastatic spheroids vary in glucose accumulation and phospholipid composition:

The identified chemical shift markers of primary melanoma spheroids were assigned to threonine (3.58 ppm, 3.60 ppm), glucose (3.67 ppm, 6.16 ppm), glycerol-phosphoethanolamine (4.12 ppm) N-acetyl-galactosaminitol (4.39 ppm) and NH_2 proton (8.07 ppm) (Table 2.1). The chemical shift marker of the metastatic melanoma spheroids was assigned to ATP (8.25 ppm). The primary melanoma spheroids suggest the presence of amino acid threonine which could indicate the presence of a membrane protein that was rich in threonine. Threonine had been reported in the literature as a biomarker for ER (Endocrine hormone receptor) positive breast cancer [57]. Interestingly primary melanoma spheroids had been found to have glucose, a key energy source that was not detected in metastatic melanoma spheroids. It had been shown that during the detachment of cells from the extracellular matrix, the cancer cells stopped the glucose consumption that resulted in energetic stress. In melanoma, it was shown that the ROS levels increase dramatically during metastasis, which could be attributed to the cessation in the glucose uptake. When the glucose consumption was stopped the ATP production would cease but we observed ATP as the biomarker for metastatic melanoma, this is because once the ATP level starts to decline AMP –activated protein kinase (AMPK) will be activated and inhibits fatty acid synthesis and activate fatty acid oxidation pathway. This shift in the fatty acid metabolism resulted in the generation of NADPH and promoted the production of α-ketoglutaric acid from isocitric acid, which also increased the NADPH. This NADPH which is generated by the AMPK activation could enter into electron transport chain resulting in the synthesis of ATP [80]. N-acetylgalactosaminitol, observed in the primary melanoma spheroids, forms an integral part of cancer associated glycoproteins [84].

2.4.3. Differences in the cell culturing method is primarily reflected in the phospholipid composition:

The comparison of the chemical shifts of the cells cultured as monolayers and cells cultured as spheroids irrespective of the cell line differences we could observe chemical shift signatures for both monolayer cultures as well as the spheroid cultures. The chemical shift signatures of the monolayer cultures were assigned to Asparagine (2.85 ppm), choline compounds (3.22 ppm), β-Cyclodextrin (3.96 ppm), and lipids (5.29 ppm). From our data, the presence of lipids and choline compounds, which formed the plasma membrane were evident in the monolayer cultures as the more cellular surface area had been exposed compared to the cells in the spheroid culture. The triplet at 3.96 is assigned to β-Cyclodextrin, but the biological origin of this compound is unclear. They have a very interesting property of forming inclusion complexes with various lipophilic compounds [78].

On the other hand, the chemical shift signatures of the spheroids were assigned to glycerol (3.63 ppm and 3.66 ppm), inositol (3.66 ppm), phosphoinositol (3.78 ppm), ethanolamine (4.05 ppm), phosphocholine (4.21 ppm), glycerophosphocholine (4.32 ppm) and amide group (-NH) (7.83 ppm). The presence of glycerol, inositol, ethanolamine, phosphocholine and glycerophosphocholine shows the existence of the glycerophospholipids, the key component of cell membrane suggests that the multicellular spheroids closely resembles the cells *in-vivo*.

2.4.4: Differences in the culturing method is reflected in the phospholipid of primary melanoma cells:

Primary melanoma cells showed differences in their behavior with respect to the culturing method. The markers of primary melanoma cultured as monolayer were assigned to lipids (1.16 ppm, 5.29 ppm), dimethylamine (2.71 ppm, 2.74 ppm), phosphocreatine (3.04 ppm)

and choline head groups of phospholipids (3.25 ppm). Thus primary melanoma cells in monolayer produce certain standard cell membrane components like choline and lipids. They also contain phosphocreatine a key reserve for the high energy phosphates, which could be utilized for the formation of ATP. Dimethylamine could be the result of L-citrulline formation from asymmetric dimethylarginine (ADMA) [82].

On the other hand, when these same primary melanoma cells were cultured as spheroids they produce some unique chemical shift signatures that could be assigned to adipate (2.19 ppm), dimethylglycine (2.93 ppm), threonine (3.58 ppm), glycerol (3.61 ppm), 2-hydroxy glutarate (4.02 ppm), glycerophosphoethanolamine (4.12 ppm), N-acetylgalactosaminitol (4.39 ppm). Adipate is an acidity regulator, which plays a vital role in maintaining the acidity balance in the cellular microenvironment. This acidity regulation is necessary as the cells would produce lactate as a result of their metabolic activity. Glycerol and glycerophosphoethanolamine were the integral components of the phospholipids in the cell membrane. These observations suggested that the 3D architecture of the multicellular spheroids of the metastatic melanoma cells vary from their monolayer counterpart primarily in the plasma membrane composition. 2-hydroxy glutarate (2-HG) is a well known as oncometabolite which will usually accumulate in malignant cells due to the gain of function mutation of the isocitric dehydrogenases (IDH). Accumulation of the 2-HG inhibited the 2- oxoglutarate-dependent oxygenases which in turn inhibits histone lysine demethylases thus impairing the epigenetic modifications of histones [83,84]. These findings proved the closeness of the 3D spheroids with the *in-vivo* tissues. Previous studies on the rectal adenocarcinoma had shown that N-acetylgalactosaminitol forms an integral part in all the four oligosaccharides isolated from the mucin-like glycoprotein of rectal adenocarcinoma. Apparently, N-acetylgalactosaminitol involves the formation of cancer associated glycoproteins [81].

2.4.5: Glucose accumulation and O-acetyl carnitine mark the differences between the metastatic melanoma cells cultured as monolayer and as spheroids:

The chemicals shifts of the monolayer cultured cells suggested the presence of Methyl-lysine (3.08 ppm), glucose (3.90 ppm), and whereas the chemical shifts of metastatic melanoma spheroids revealed the presence of O-acetyl carnitine (3.19 ppm). This data showed that methyl-lysine and glucose resonating at 3.08ppm and 3.90 ppm were the qualitative markers for the metastatic melanoma cells cultured as monolayer but the same cell line when cultured as spheroids they do not produce chemical shift peaks at 3.08 ppm and 3.90 ppm instead they produce a chemical shift at 3.19 which is assigned to O-acetyl carnitine. It is also previously reported that 3.08 ppm chemical shift manifested the presence of the SH_2 group in taurine [85, 86]. In these studies, the 3.08 ppm chemical shift has appeared as a triplet, but in our data, the 3.08 ppm shift appeared as a singlet. In a previous report, where the chromatin core particles where analyzed using proton nuclear magnetic resonance spectrometry encountered the 3.08 ppm chemical shift as a singlet, and it was assigned to the CH_2 group proton of the methyl lysine [75]. Hence, chemical shift at 3.08 ppm is attributed to proton from the CH_2 group of the methyl lysine. Methylated amino acids especially methyl-lysine and methyl-arginine in the chromatin plays a vital role in recruiting proteins that induce structural changes in chromatin thus influencing gene expression and repression [87].

2.4.6. Clinical projections of this study:

In this study, we used the 3D spheroids, to minimize the limitations in its clinical translation. Flat monolayer cultures were the simple cancer models, having a physiologically uniform environment and lacked cell to cell attachment, which is not the case in the actual tumor environment. In in vivo tumors, there exists cell to cell attachment, oxygen gradient, nutrition

gradient and waste gradient. This in vivo tumor environment could be reproduced in the 3D spheroids with ease. This behavior can be reproduced by culturing cells as 3D spheroids [88]. 2D flat monolayer cultured cells showed apical-basal polarity and lacks in the histological differentiation of the in vivo tumors whereas one could obtain the histological morphology similar to that of the in vivo tumor in 3D spheroids [89, 90]. The cells *in-vivo* tumor exhibits phenotypic heterogeneity in the cell proliferation rate, gene expression, and differentiation which led to the heterogeneity in the function and morphology and 3D spheroids could capture all this phenotypic heterogeneity [91]. Few cells exhibited the stem cell-like characteristics such as self-renewal and undifferentiated multipotent phenotype called cancer stem cells (CSCs) [92]. These CSCs were observed in both *in vitro* 3D tumor spheroids and *in vivo* tumors [93] and these stem-ness related genes were found to be upregulated in 3D spheroids compared to the 2D monolayers [94]. All the above studies showed the cells grown as 3D spheroids resemble closely to the cells in the in vivo tumors. Thus, we expect there will not be any potential limitations in the clinical translation of the results of this study and of course an actual clinical translational study is necessary to corroborate this statement.

2.5. Conclusion:

In this study, we showed that the two closely associated cell lines, which were obtained from the same donor and differed only in the stages of melanoma could be identified as different cell lines by employing 1D 1H NMR spectrometry. Our study suggests that the glucose accumulation and phospholipid composition vary significantly between the primary and metastatic cells lines that were obtained from single donor and also with the cell culturing methods. These results encourage further researches on understanding the effects of phospholipid and glucose accumulation in cancer development, progression, and invasion. This study also showed that the method of cell culture would drastically affect the

phospholipid composition of the cells and also depicts that the cells in spheroid culture closely resembled the cells *in-vivo*.

2.6. Summary:

Primary melanoma cells (WM 115) and metastatic melanoma cells (WM 266) extracted from single donor were cultured in 2D as well as 3D cultures. These cells were characterized using proton NMR spectrometry and the qualitative chemical shifts markers were identified and discussed. In monolayer culture (2D), one qualitative chemical shift marker for primary melanoma cells is observed. In spheroid cultures (3D), nine significant chemical shifts, of which eight markers were specific for primary melanoma spheroids, whereas one marker was specific to metastatic melanoma spheroids were observed. This study suggests that the glucose accumulation and phospholipid composition vary significantly between the primary and metastatic cells lines that are obtained from single donor and also with the cell culturing methods. 14 qualitative chemical shift markers were obtained in the comparison between monolayer culture and spheroids cultures irrespective of the differences in the cell lines. Among which four were unique to monolayer cultures whereas ten chemical shifts were specific to the spheroid cultures. This study also shows that the method of cell culture would drastically affect the phospholipid composition of the cells and also depicts that the cells in spheroid culture closely resembles the cells *in-vivo*. This study shows the high specificity of proton NMR spectrometry in characterizing cancer cell lines and also lists the variations in the glucose accumulation and phospholipid composition between the primary and metastatic melanoma cell lines from the same donor. Differences in the cell culture method play a significant role in phospholipid composition of the cells.

Chapter 3

Identification of Gastric Cancer Biomarkers Using ^{1}H Nuclear Magnetic Resonance Spectrometry.

3.1. Background:

According to World Health Organization, gastric cancer (0.72 million deaths) ranks third in causing cancer death worldwide in 2012, with the highest incidence in the Asia-Pacific region especially in Japan, gastric cancer is much more prevalent than other countries. The prognosis of gastric cancer is destitute especially for the one that occurs in the cardiac region. Given the high global incidence rate, early detection of gastric cancer appears to improve survival rates. Mass screening of gastric cancer in Japan has considerably decreased the mortality rate. Usually, the gastric cancer is often diagnosed at the metastatic stage which is tough to treat [95,96]. The gastric cancer incidence is higher in developed countries whereas the mortality is high in developing countries, which is attributed to the lack of early detection, environmental changes, and lifestyle changes. Hence, the economic burden regarding morbidity and mortality cost will be higher in the developing countries [97]. The gold standard for the diagnosis of gastric cancer is esophagogastroduodenoscopy (EGD) and biopsy. When a doctor identifies an abnormal tissue area through EGD, a biopsy will be performed followed by the routine procedure for the confirmation. Even though this method has high specificity and sensitivity, there are several disadvantages in using endoscopy as the first screening tool; to mention a few, it is an invasive procedure with potential complications such as perforation and aspiration and is not a cost-effective screening tool for most of the countries. Hence, this test is out of reach for most of the people in Asia, Africa, and South America. This method is invasive and creates significant discomfort for the patients especially children and elderly.

One promising non-invasive way of detecting and locating cancer is by employing nuclear magnetic resonance as this method safe as it is non-ionizing. Cancer cells contain higher levels of phospholipids than normal cells, which plays a significant role in membrane formation to cope up enhanced cell proliferation and signal transduction. The alteration of phospholipid composition also plays a pivotal role in cancer invasion, metastasis, and expression of growth factor receptors [36, 37]. Various prior studies concluded that 1H MRS could be used to diagnose cancer and also to monitor responses to the cancer treatment [38-41]. Magnetic resonance imaging and magnetic resonance spectrometry in combination can diagnose of prostate cancer. Prior studies have suggested that combined MRI and MRS could serve as a useful test for the low-risk patients. Martin et al. also recommend larger studies for the confirmation of this statement [98]. The lipid composition was significantly altered in the extracts of benign (chronic cholecystitis), intermediate (xanthogranulomatous cholecystitis) and malignant gallbladder tissue. This study provided proof that the lipid composition of cancer tissues and normal tissues vary significantly and which can be detected using magnetic resonance [99]. Mobile lipid resonances profiled using 1H MRS can be used to distinguish cervical cancer tissues, low-grade intraepithelial neoplasia, and non-cancerous tissues [100]. This study serves as the proof for the diagnosis of cancer using lipid signals from 1H magnetic resonance. These studies provide an insight that there is a possibility for the presence of a particular mechanism in the cancer cells that alter the phospholipids composition.

In-vivo 1H magnetic resonance spectrometry can be used to quantify choline compounds in the breast; it is observed that the choline-containing compounds were significantly higher in malignancies than benign abnormalities and normal breast tissue. Sensitivity, positive predictive value, and accuracy of the cancer diagnosis can be enhanced when 1H MRS and

biopsy are employed together. This study also proves that 1H MRS has better sensitivity, positive predictive value, and accuracy that biopsy [101]. 1H MRS is a potential procedure for detecting cancerous breast lesions that are 15mm or larger in diameter without the need of invasive endoscopy procedure [102].

Magnetic resonance method identifies not only lipid biomarkers but also metabolic biomarkers. In human prostate tissues, 1H MRS signals of citrate, creatine, and choline compounds were observed. The citrate to choline ratio can be used for the cancer diagnosis. This ratio is lower for the cancerous tissues in comparison with the noncancerous normal tissues. 1H MRS is a promising method for the detection and treatment follow-up for prostate cancer [103]. Few studies reported that the *in vitro* 1H magnetic resonance spectrometry (MRS) of the perchloric acid extracts of the breast tissue showed resonance at 3.2 ppm, which was significantly high for the breast carcinoma when compared to the normal and benign breast tissue.

The higher levels of the choline related compounds may be primarily attributed to the oncogene-induced activation of phosphatidyl choline and phosphatidyl ethanolamine-specific phospholipases. This phenomenon resulted in the accumulation of choline related compounds in tumorous or actively proliferating cells [104]. Differences in the concentration of choline-containing compounds can be considered as an indicator for accessing the clinical response of cancer to chemotherapy. The outcome of the chemotherapy can be regarded as positive if the choline-containing compounds decrease after the chemotherapy [48].

The biomarkers identified by the 1H-MRS and Nuclear magnetic resonance spectrometry (NMR) could be the same as both these methods employ the same principle. Nuclear magnetic resonance spectrometry identifies a unique chemical shift biomarker 1.28 ppm for the identification of the neural stem and progenitor cells (NPC). They could even identify the

NPC in the live mouse using this biomarker under proton magnetic resonance spectroscopy (1H-MRS) in xenografted mice [105]. This observation is possible as each cell type has unique cell surface receptor proteins and phospholipid composition. From the previous studies, it is clear that magnetic resonance can be employed for cancer diagnosis using the lipid signals.

We hypothesize that one dimensional H^1 Nuclear Magnetic Resonance (NMR) can distinguish between the in-vitro 3D models of the normal gastric cells and gastric cancer cells with reliable NMR chemical shift markers. In this study, we are using the *in-vitro* 3D models (spheroids) of the normal gastric cell line and gastric cancer cell lines to decipher the magnetic resonance based gastric cancer markers. The rationale for using spheroids is that it shows similar characteristics of the *in-vivo* tissues. *In-vivo* cells are interconnected to each other as well as to the extracellular matrix (ECM). Further *in-vivo* cells show many inherent properties like polarization, intercellular communication, developing the extracellular matrix and so on. All these unique features can be replicated in in-vitro spheroids, and these are not possible in 2D culture [106,107].

3.2. Methods and Materials:

3.2.1. Cell culture

For this study, a set of twelve gastric cancer cell lines namely SNU484, MKN28, MKN7, SCH, AGS, IST1, KATO3, YCC10, YCC11, N87, NUGC3 and NUGC4 and a normal gastric cancer cell line HS738. The Gastric cancer cells were cultured in RPMI medium with 10% fetal bovine serum (FBS), and the normal gastric cell line was cultured in Dulbecco's modified essential medium (DMEM) with 10% fetal bovine serum (FBS). All the

experiments were carried out in triplicates for all the cell lines along with the spent medium, which serves as background control.

3.2.2. Formation of cellular spheroids:

For the spheroids formation, the cells were grown under 2D culture condition and harvested using trypsinization. The harvested cells were checked for the viability using bromophenol blue dye. The samples with required viability (95%) were diluted into $2.5x10^6$ cells/mL, and each sample will contain $1X10^7$ cells i.e. 4 mL of the diluted cell suspension. The diluted cell samples were drawn into drops of 20µL on the lid of the sterile petri dish. The petri dish was filled with 10mL of DPBS for hydrating the drops. The petri dish lid was gently inverted and placed in the petri dish and placed in the incubator for the spheroid formation [53]. The petri dish was then incubated for three days. After three days, the spheroids could be observed by the naked eye as white spheres. The spheroids were harvested, washed twice with DPBS and gently suspended in 600µL of D_2O. As a final step, the suspended spheroids were then carefully poured into the NMR tubes.

3.2.3. Nuclear magnetic resonance (NMR) spectrometry

We performed one-dimensional ^1H NMR spectroscopy (DRX500, Bruker USA) on the collected samples and matched controls using deuterated water (D_20) we used as the solvent (Figure 3.1). The acquired NMR spectral data was Fourier-transformed followed by phase and baseline correction using the Bruker XWinNMR software version 3.5. The peak lists were extracted for the metabolite identification. The peak list was given as input to the MetaboAnalyst 3.0 online statistical software (www.Metaboanalyst.ca/, Canada) for statistical analysis [54].

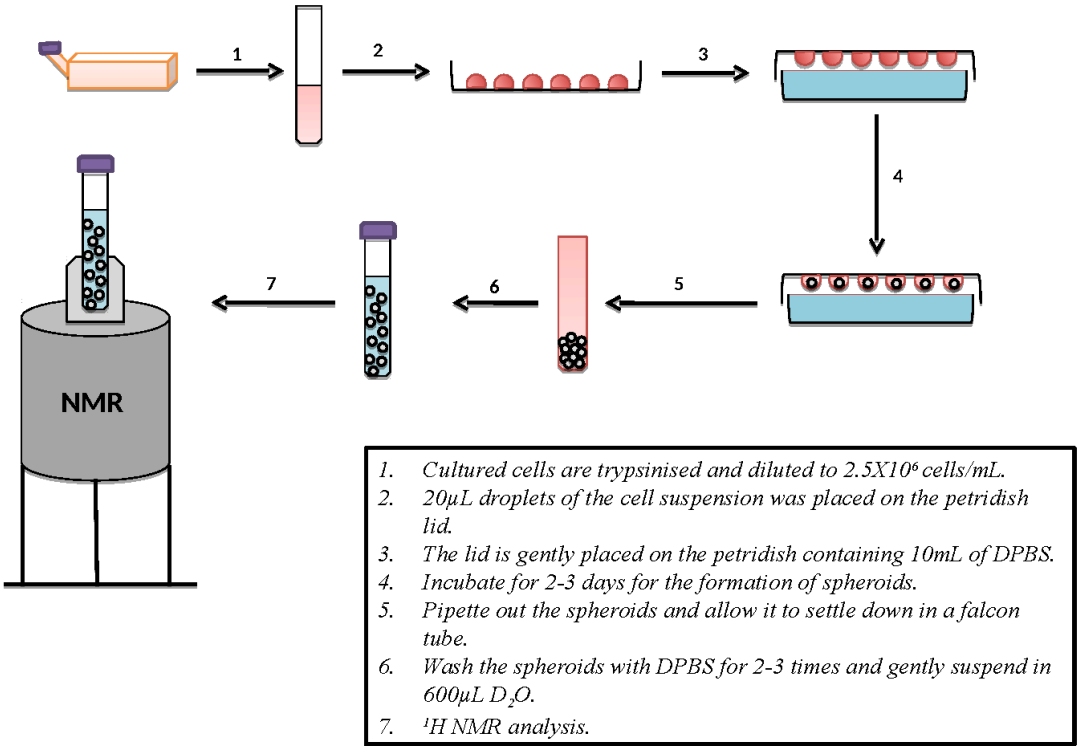

Figure 3.1: Methodology of sample preparation.

3.3. Results:

3.3.1. Spheroid formation:

Among the 12 gastric cancer cell lines, only 4 of them can form the spheroids using the hanging drop procedure mentioned above. The gastric cancer cell lines that can form spheroids were SNU484, NUGC 3, MKN28 and IST1. Among them, the spheroids formed by the SNU484 and MKN 28 were more compact compared to the spheroids formed by IST1 and NUGC 3 cell lines. It is already well documented that only a limited number of cell lines could form spontaneous spheroids whereas, many cell lines could form only the loose aggregates. In a previous study, it is reported that by the addition of reconstituted basement membrane (rBM, Matrigel™), these loose aggregates can be transformed into spheroids

[108]. Another study shows that egg white can be used as the substitute for the standard reconstituted basement membrane-like collagen and Matrigel™, whereby in this study they able to establish an angiogenesis assay using egg white whose characteristics were similar to the results obtained using collagen and Matrigel™ [109]. These studies motivated us to try forming the spheroids of YCC 11 cell lines, which could not undergo spontaneous spheroid formation using nutrient medium supplemented with different concentration of egg white (ranges from 2% to 50%). Unfortunately, we were unable to generate spheroid using egg white (Figure 3.2). In fact, the addition of egg white decreases the aggregation of the cells with the increase in the concentration of egg white.

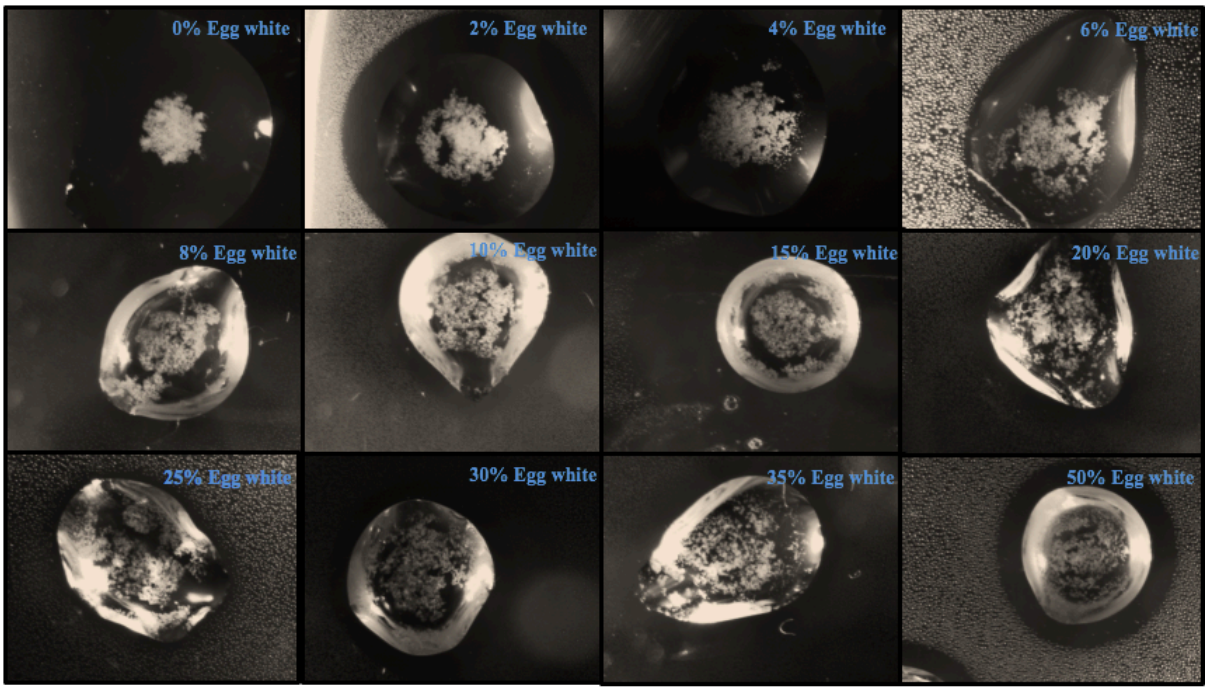

Figure 3.2. Stereo microscopic images of YCC 11 cell lines fed with RPMI + 10% FBS supplemented with various concentrations of egg white.

3.3.2. NMR spectrum of gastric cancer and normal gastric spheroids:

The peak lists of all NMR spectrums were obtained. The peaks were grouped together by the moving window of 0.03 ppm and a step of 0.015 ppm, which results in a group of 117 peaks. The pooled data was normalized using generalized log transformation and auto scaling.

3.3.3. Statistical analysis of the NMR spectrums of gastric cancer and normal gastric spheroids:

The statistical analysis the normalized peak lists shows 21 chemical shift peaks (Table 3.1) were significantly vary between the gastric cancer cell lines (SNU484, MKN28, IST1, and NUGC3) and normal gastric cell line (HS738). Among these 21 chemical shift peaks eight were present in higher intensity in the gastric cancer spheroids when compared to the normal gastric spheroids. These eight peaks could be the potential magnetic resonance based gastric cancer markers. The rest 13 were observed to be in higher intensity in the normal gastric spheroids compared to the gastric cancer spheroids. The NMR markers for the gastric cancer spheroids ranges from 1 ppm to 4 ppm (Figure 3.3) whereas, NMR markers for the normal gastric spheroids ranges from 3 ppm to 8 ppm (Figure 3.4).

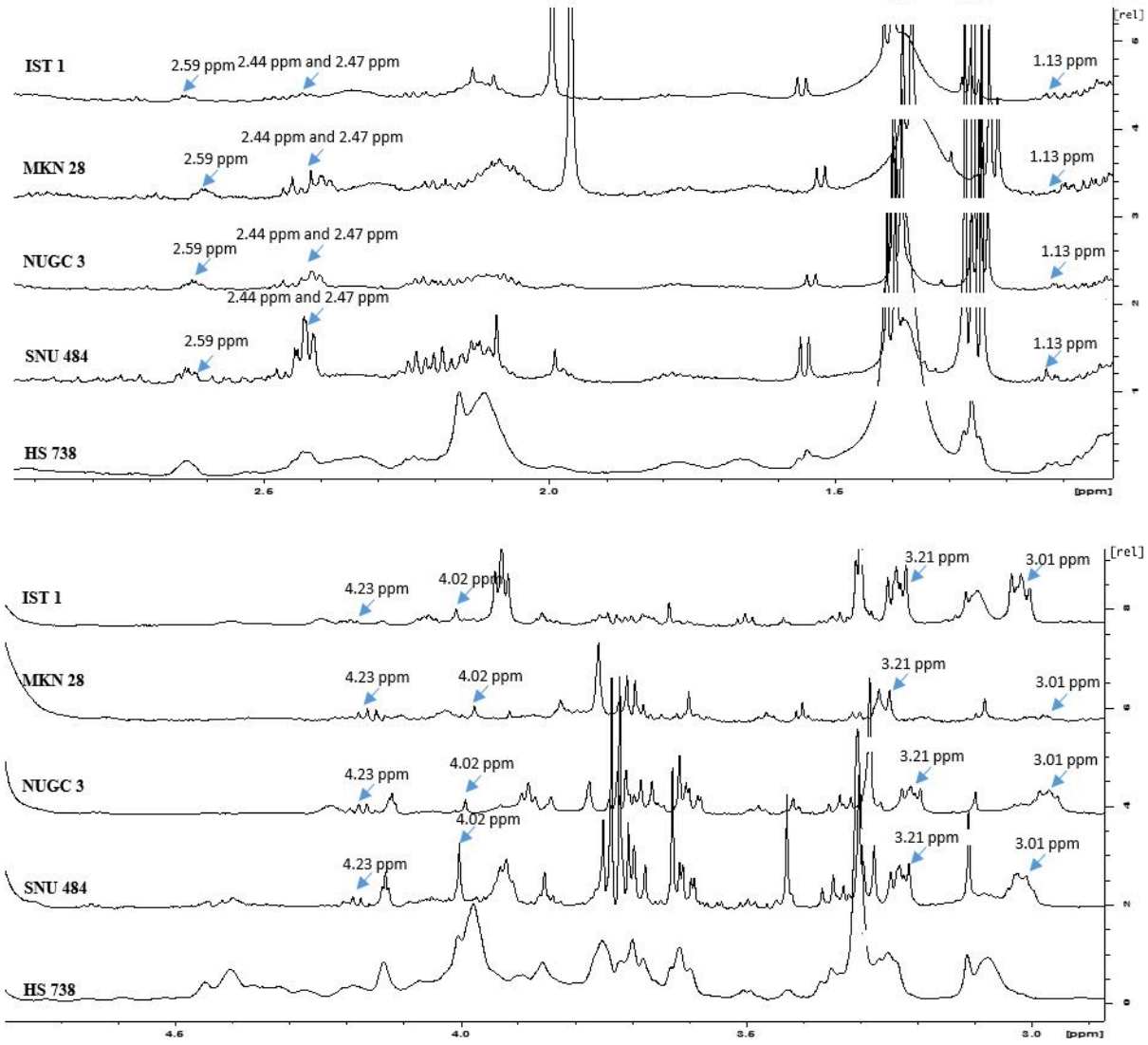

Figure 3.3: 1H NMR spectrum showing NMR markers of gastric cancer spheroids.

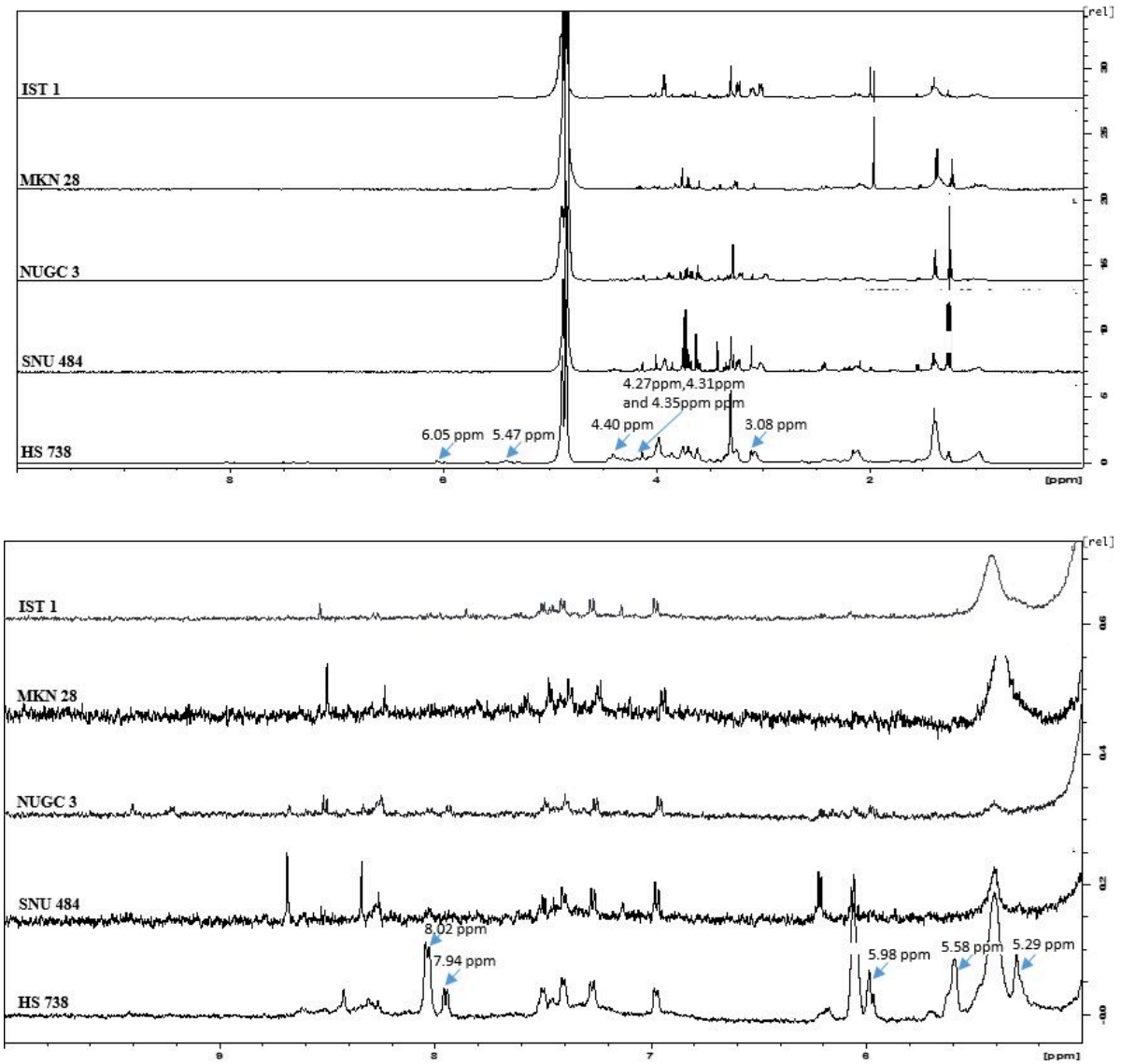

Figure 3.4: 1H NMR spectrum showing NMR markers of normal gastric spheroids.

S. No	Chemical shifts (ppm)	FC	log2(FC)*	p.value
1	3.21	332.77	8.3784	0.00021027
2	4.02	53.079	5.7301	0.00044346
3	4.23	44.809	5.4857	0.00096607
4	1.13	34.183	5.0952	0.00092528
5	2.59	16.297	4.0265	0.0067511
6	3.01	15.039	3.9107	0.0085235
7	2.44	7.5685	2.92	0.0012475
8	2.47	4.7224	2.2395	0.0011457
9	4.40	0.17478	-2.5164	0.0002721
10	7.94	0.12923	-2.952	0.00010053
11	3.08	0.12643	-2.9836	0.0088915
12	4.27	0.12609	-2.9874	0.0050839
13	5.29	0.11044	-3.1787	0.00038551
14	5.47	0.10526	-3.248	0.0046374
15	5.98	0.098221	-3.3478	5.67E-06
16	6.05	0.076551	-3.7074	0.00034459
17	4.35	0.05315	-4.2338	0.00074306
18	4.31	0.047047	-4.4098	0.00010888
19	5.58	0.045401	-4.4611	1.30E-11
20	4.72	0.042526	-4.5555	1.48E-16
21	8.02	0.02419	-5.3694	7.49E-12

Table 3.1: List of NMR chemical shift markers for the gastric cancer spheroids. *positive values represent the chemical shifts exhibit higher intensity in gastric cancer spheroids, and negative values represents the chemical shifts show high intensity in normal gastric spheroids.

Furthermore, principal component analysis (PCA) and clustering analysis performed between gastric cancer and normal gastric spheroids depict the gastric cancer spheroids and normal gastric spheroids into different groups, indicating the significant variance between these cell lines (Figure 3.5). Heat map analysis manifests the top 25 significant (p-value <0.05) chemical shift markers with its relative intensities (Figure 3.6).

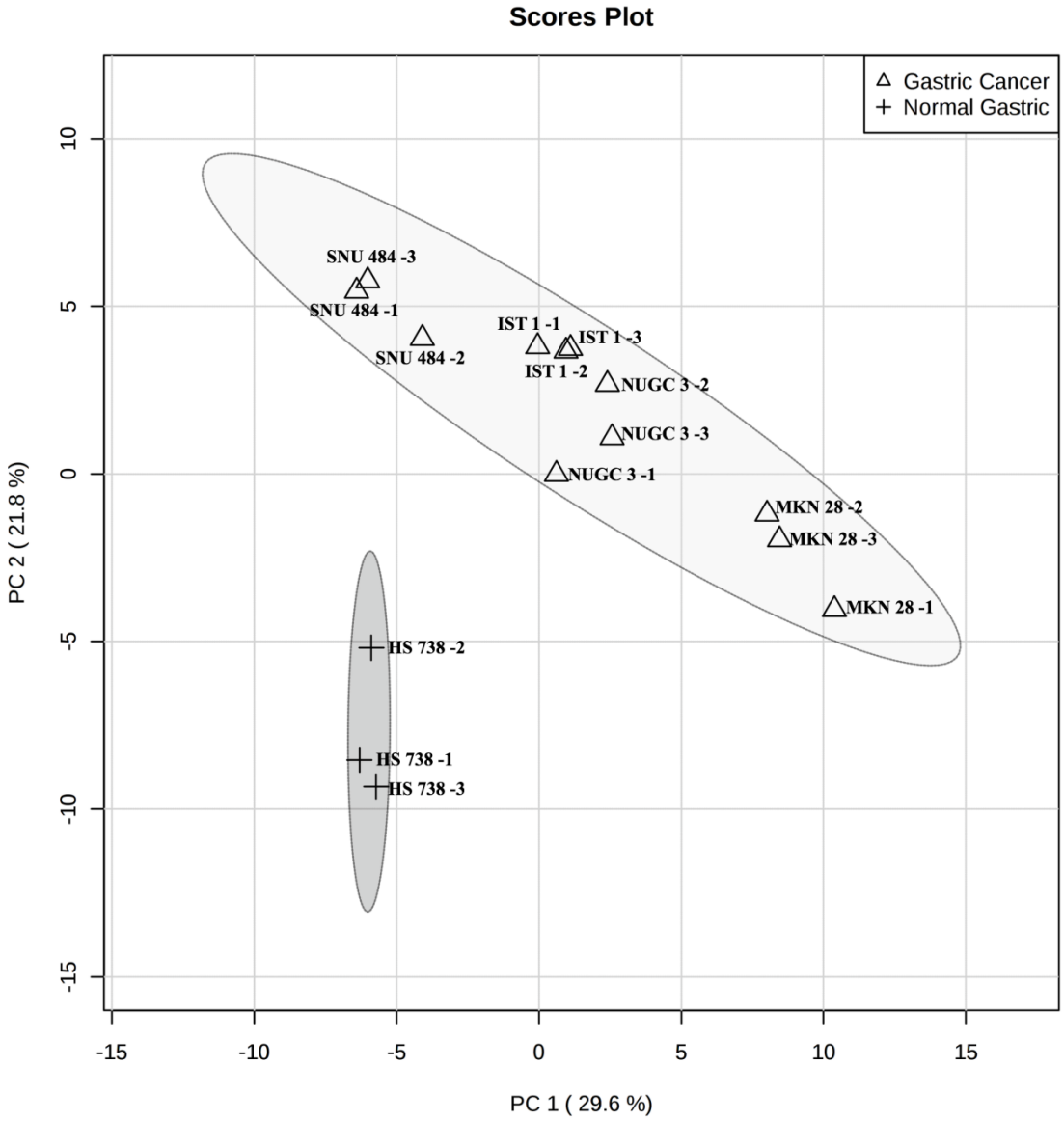

Figure 3.5: PCA plot depicting the variance between the gastric cancer spheroids and normal gastric spheroids.

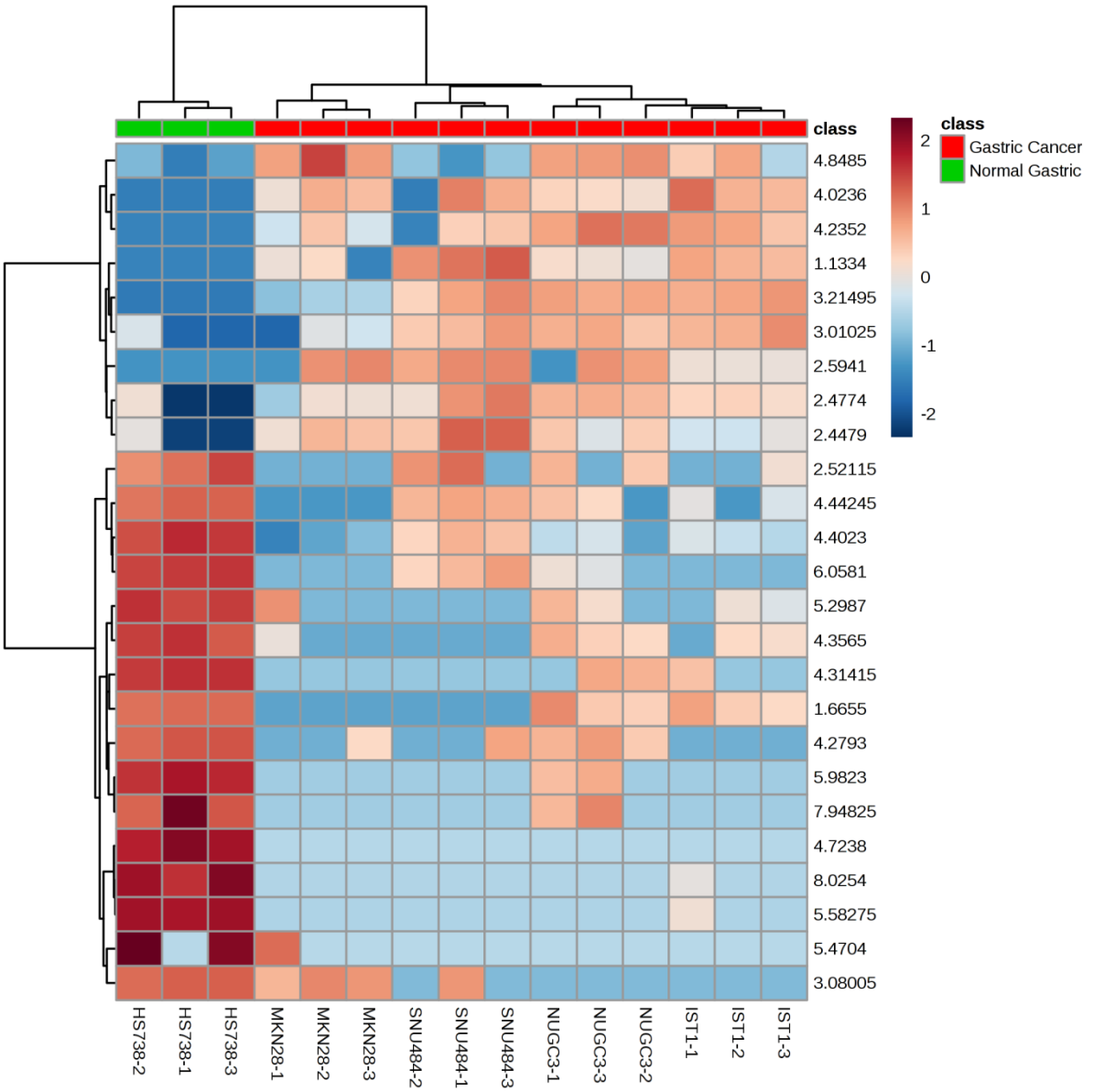

Figure 3.6: Heat map depicting the relative intensity of the top 25 significant chemical shifts (p-value <0.05).

3.4. Discussions:

3.4.1. Formation of gastric spheroids:

In this study, we have observed that spontaneous spheroid formation is not typical for all the cell lines only a few cell lines like IST 1, NUGC 3, MKN 28, SNU 484 and HS 738 can form spontaneous spheroids. This discrepancy is because cells interact with each other in a very complex and diverse manner which dictates the formation of the spontaneous spheroids *in-*

vitro. In a previous study which involves eight breast cancer cell lines show that the E-Cadherin plays a pivotal role in the formation of spontaneous spheroids in some cell lines whereas the interaction between the collagen I/integrin β1 drives the cells to form spontaneous spheroids. Interestingly some cell lines were able to form spheroids with the shared responsibility of both homophilic E-cadherin and integrin β1/collagen I [110].

3.4.2. Phospholipid metabolism is the major contributor of NMR markers for Gastric cancer:

We could observe a total of eight NMR markers that are overexpressed in gastric cancer spheroids than normal gastric spheroids. 3.2 ppm represents the choline and choline related compounds [111]. Choline has been identified as the tumor marker in breast cancer and lung cancer [101, 112]. Choline and its derivatives have been already reported as the markers of cell proliferation as they play a vital role in phospholipid metabolism that forms the cell membrane [69]. The chemical shift 1.13 ppm has been already identified as the marker for cervical cancer. The serum obtained from the cervical cancer patients shows 1.13 ppm shift as the marker for the diagnosis of cervical cancer [113].

Our study identifies chemical shift at 3.01 ppm as a marker for gastric cancer. This chemical shift represents creatine [114,115]. Creatine was reported to the biomarker for cervical cancer. Ex-vivo HR-MRS analysis of the cervical tumor tissue and healthy cervical tissue shows a significant ($p=0.004$) difference in creatine [116]. Creatine is named as a potential biomarker for lung cancer in a study which involves analyzing the methanol-chloroform - water extract of non-small cell lung cancer tissues from 21 lung cancer patients [112]. These studies support our data which shows creatine, represented by the chemical shift at 3.01 ppm as the marker for gastric cancer. Another important gastric cancer biomarker that we have discovered is the chemical shift at 4.02 ppm, which represents 2-hydroxyglutarate. World

Health Organization reported that two hydroxyglutarate is the key biomarker for the identification of IDH (Isocitrate dehydrogenase) mutated glioma as the mutation in these genes could result in the accumulation of the 2-hydroxyglutarate [117]. In our knowledge, we are the first to report 4.02 ppm as the biomarker for gastric cancer.

Another interesting chemical shift marker for gastric cancer is the chemical shift at 2.47 ppm. This marker indicates glutamine, a common amino acid. Previous studies have reported glutamine as the marker for the slightly malignant prostate cancer [118]. Our study depicts glutamine as the common NMR marker for gastric cancer as well as prostate cancer. The chemical shift marker 2.59 ppm is assigned to methylamine. Methylamine has been reported, as the key biomarker is cancers of the alimentary canal. Methylamine, as represented as the chemical shift 2.59 ppm, has been reported as the rectal cancer marker. Methylamine involves in the metabolism of another important cancer biomarker namely choline [69]. It is reported that methylamines can cause hepatocarcinogenesis in rats [119]. It is also reported that higher levels of methylamine could induce gastric cancer [120]. 2- oxoglutarate plays a pivotal role in the activity of the 2- oxoglutarate-dependent dioxygenases. Increase in the cellular level of 2- oxoglutarate elevates the activity of the 2- oxoglutarate-dependent dioxygenases, which will result in many crucial events like activation of hypoxia inducible factors (HIF 1), disturbances in the epigenetic regulation and reduction of the carnitine synthesis. These events eventually lead to tumor viability and metastasis [121]. Our study depicts the presence chemical shift marker for gastric cancer at 2.44 ppm which is assigned to 2 – oxoglutarate [122].

3.4.3. Glycosylated derivatives are the key NMR markers unique to the normal gastric spheroids:

We observed 13 NMR chemical shift markers that are unique to the normal gastric spheroid

that is not found or varies significantly ($p<0.05$) from the gastric cancer spheroids. The assignment of these markers and their role were as follows: The chemical shifts at 4.40 ppm and 4.27 ppm indicate the oligosaccharide alditols, these compounds consist of the Galβ1-3(GlcNAcβ1-6)- GalNAc-ol core. This core contains the O-glycosidic structures. These structures are represented by the chemical shifts of 4.40 ppm and 4.27 ppm [123,124].

Our data depicts the strong evidence for the presence of UDP-glucose. Chemical shift resonance at 8.02 ppm represents the proton in the NH group of the uracil ring [125,126], whereas the NMR resonances at 7.94 ppm and 5.98 ppm mark the presence of the protons linked to the C6 and C5 of the uracil ring [127]. The presence of the phosphate group is indicated by the chemical shift resonance at 4.35 ppm [128]. This evidence proves the existence of the uridine diphosphate in the normal gastric spheroids. There must be a glucose molecule which is hinted by the chemical shift resonance at 4.27 ppm, and that is linked with the UDP via anomeric carbon as we also observed a chemical shift resonance at 5.58 ppm which manifests the occupancy of the proton-linked with the anomeric carbon of glucose [129].

It is reported that increase in the synthesis of glycogen from glucose results in the decrease in the cellular concentration of the UDP-glucose [130]. On the other hand, the increased glycogen synthesis has been demonstrated in many types of cancer [131]. These studies support our data, which shows a significant increase in the UDP-glucose in the normal gastric spheroids compared to the gastric cancer spheroids. The chemical shift at 4.72 ppm and 4.31 ppm implies β (1-4) N-acetyl galactosamine, whereas the 4.72 ppm and 4.31 ppm denotes H-1β [132] and β(1-4) GalNAc respectively [133,134]. 4.31 ppm precisely indicates galactosamine as well as the acetylation of galactosamine in N-acetyl galactosamine [133,135]. Both 4.72 ppm, as well as the 4.31ppm, reveals the presence of β (1-4)

configuration [132,134].

Chemical shift at 5.47 points out the H linked to the C_1 of the N-acetyl galactosamine of UDP-GalNAc [136]. In another study, it also denotes the existence of a-D-GlcpNAc [137]. Another study describes this chemical shift for H-1 of α-Gal-1-P [138]. These observations strongly suggest the presence of UDP-GalNAc as we already have evidence for the presence of UDP. The chemical shift at 5.29 ppm manifests the proton from anomeric carbon [139] and specifically at β anomeric configuration [140]. Prior study has reported that this chemical shift indicates the galactopyranose residue at the reducing end of glycolipids [139]. Another report which characterizes the liver fats shows that 5.29 ppm belongs to the olefinic group in the triglycerides [141]. All this data suggests that the gastric cancer spheroids and normal gastric spheroids vary significantly in the composition of lipid and lipid derivatives. Another chemical shift marker which is considerably higher in normal gastric spheroids, 6.05 ppm is assigned to NH_2 group in a prior study [142,143]. Interestingly another report had assigned this chemical shift to the protons from the olefinic group [144,145].

Finally, the chemical shift at 3.08 is attributed to proton from the CH_2 group of the methyl lysine. 3.08 ppm was previously reported that this chemical shift manifests the presence of the SH_2 group in taurine [85]. Another study where proton nuclear magnetic resonance spectrometry is utilized for the identification of the neural cell types supports the assignment of 3.08 ppm to the SH_2 of taurine [86]. In these studies, the 3.08 ppm chemical shift has appeared as a triplet, but in our data, the 3.08 ppm shift appeared as a singlet. In a previous report, where the chromatin core particles were analyzed using proton nuclear magnetic resonance spectrometry encountered the 3.08 ppm chemical shift as a singlet, and it was assigned to the CH_2 group proton of the methyl lysine [75]. Methylated amino acids especially methyl-lysine and methylarginine in the chromatin plays a vital role in recruiting

proteins that induce structural changes in chromatin thus influencing gene expression and repression [87]. Our data suggests that the gastric cancer spheroids have significantly lesser methylated amino acids thus impairing its epigenetic control over gene expression.

3.4.4. Feasibility of clinical translation of this study:

In this study, we used the 3D spheroids, to minimize the limitations in its clinical translation. Flat monolayer cultures are the simple cancer models, where the cells adhere to the poly-D-Lysine treated plastic surfaces or glass surfaces. These cancer models have a physiologically stable environment and lack cell to cell attachment, which contradicts the actual tumor environment. In *in vivo* tumors, there exists cell to cell attachment, oxygen gradient, nutrition gradient and waste gradient. These features of *in vivo* tumor environment could be reproduced in the 3D spheroids with ease. Solid tumors proliferate in a differential manner whereas the proliferation is higher at the periphery than the core region which is attributed to the oxygen and nutrient gradient. This behavior could accurately be depicted by the 3D spheroids whereas, cells grown in 2D flat monolayer depicts uniform proliferation [88]. 2D flat monolayer cultured cells shows apical-basal polarity as only one side of the cell adheres to the surface, and that has a huge impact on the cellular function. As these 2D cultured cells always depict simple geometry, they do not show histological differentiation of the *in vivo* tumors, but by just growing cells as 3D spheroids one could obtain the histological morphology similar to that of the *in vivo* tumor type from which the cell lines were derived [89, 90]. The cells in a tumor exhibit phenotypic heterogeneity in the cell proliferation rate, gene expression and differentiation which leads to the heterogeneity in the function and morphology [91]. Tumor spheroids could capture this phenotypic heterogeneity as they have oxygen and nutrient gradients. Few cells exhibit the stem cell-like characteristics such as self-renewal and undifferentiated multipotent phenotype called cancer stem cells (CSCs)

[92]. These CSCs are observed in both *in vitro* 3D tumor spheroids and *in vivo* tumors [93] and these stemness-related genes are found to be upregulated in 3D spheroids compared to the 2D monolayers [94]. The gene expressions profiles including the expression of transcription factors of a cell line grown as 3D spheroids were divergent compared to the same cell line cultured 2D monolayers [90, 146, 147]. All the above studies show the cells grown as 3D spheroids resemble closely to the cells in the *in vivo* tumors. Thus, we expect there will not be any potential limitations in the clinical translation of the results of this study and of course an actual clinical translational research is necessary to corroborate this statement.

3.5. Conclusion:

In this study, we decipher the NMR markers for differentiating gastric cancer spheroids and normal gastric spheroids. We can identify eight markers that are unique to the gastric cancer spheroids that are analyzed in this study. We also demonstrated that 13 markers are significantly lesser in the gastric cancer spheroids compared to their normal counterpart. These markers indicate that the cancerous and non-cancerous spheroids differ majorly in the energy metabolism, composition of lipid and lipid derivatives. These results open up avenues for the researches focusing on identifying novel lipid targets in gastric cancer. This study also depicts that the formation of spontaneous spheroids is not a common trait for all the cell lines.

3.6. Summary:

Existing gastric cancer diagnosing methods were invasive; hence, a reliable non-invasive gastric cancer diagnosing method is needed. As a starting point, we used 1H NMR for identifying gastric cancer biomarkers using a panel of gastric cancer spheroids and normal gastric spheroids. We were able to determine eight chemical shift biomarkers for gastric

cancer spheroids. Our data suggests that the cancerous and non-cancerous spheroids significantly differ in the lipid composition and energy metabolism. These results encourage the translation of these biomarkers into in-vivo gastric cancer detection methodology using MRI-MS. Although proton NMR-based cancer detection is promising, the cost of MRI-MS and the need for the experienced operator suggest that this method is not suitable for developing and under developed nations. So, the decision to look for other alternative ways of cancer biomarker identification was taken and found prior studies where Volatile organic compounds (VOCs) were used as cancer biomarkers. But we discovered that all the existing literature on VOC based disease detection were based on the 2D monolayer cultures. Hence, the decision to develop and standardize a method for VOCs based characterization of *in vitro* cellular 3D models was taken.

Chapter 4

Comparison of the volatile organic compound signatures of primary melanoma cells (WM 115) in 2D cultures and 3D cultures.

4.1. Background:

The volatile organic compound (VOCs) signature of the cancer cells forms the basis of volatile-based cancer detection. There are several prior studies, demonstrating the unique VOC signatures of various cancer cells *in vitro*. Zimmerman et al. observed the qualitative differences in the VOC metabolites, methyl dodecane, undecan-2-ol, pentadecane-1-one, decane-1-ol, heptane-1-ol, and nonane-2-one. Between the colon cancer cell lines and the normal colon cell lines [148]. They concluded that the cancer cells and healthy cells differed mostly in the ketones and alcohols. Spring et al. observed the increased production of 2 ethyl-1-hexanol and 2-methyl pentane in the lung cancer cell lines when compared to the controls. They also validated that 2-methyl pentane was present in the breath of the lung cancer patients. They also observed the differential consumption of the headspace VOCs between the lung cancer cell lines and the controls [149]. Abaffy et al. found 3 VOCs that were differentially expressed in the melanoma cell lines and the normal skin cell lines. These VOCs were long chain alkanes, namely 4-methyl decane, dodecane and undecane [150]. Hanai et al. observed the differential expression of seven VOCs mostly ketones between the lung cancer cells and the healthy lung cells [151]. These seven compounds were dimethyl succinate, 2-pentanone, phenol,2-methyl pyrazine,2-hexanone, 2-butanone, and acetophenone. They validated the *in-vitro* experimental results with the *in-vivo* xenografted mice model. The VOCs observed in the xenografted mice urine, and the *in-vitro* cells were demonstrated to be statistically similar.

Troppmair et al. found that 2,3,3-trimethylpentane, 2,3,5-trimethylhexane, 2,4-

dimethylheptane, and 4-methyloctane were released by the lung cancer cell line CALU-1 and this cell line also consume acetaldehyde, 3-methylbutanal, butyl acetate, acetonitrile, acrolein, methacrolein, 2-methylpropanal, 2-butanone, 2-methoxy-2-methylpropane, 2-ethoxy-2- methylpropane, and hexanal. They also observed that there exists a difference in the consumption of the VOCs between different cell lines [149]. Pawel et al. found the hepatocellular carcinoma cells consumes nine and release twelve VOCs. The consumed VOCs include 2-methyl 2-propenal, 2-methyl propanal, 2-ethylacrolein, 3-methyl butanal, n-hexanal, benzaldehyde, n-propyl propionate, n-butyl acetate, and isoprene whereas the released VOCs were 2-pentanone, 3-heptanone, 2-heptanone, 3-octanone, 2-nonanone (dimethyl sulfide, ethyl methyl sulfide, 3-methyl thiophene, 2-methyl-1-(methylthio)-propane and 2-methyl-5-(methylthio) furan), n-propyl acetate, and 2-heptene [152].

Luca et al. found that the VOC signatures are capable of discriminating breast cancer cells for various characteristics, which include transformed condition, cell doubling time (CDT), Estrogen and Progesterone Receptors (ER, PgR) expression and HER2 overexpression [153]. Kristin et al. studied all the possible ways of VOC analysis such as in situ, gas subsampling and nutrient solution subsampling. They conclude that two-dimensional monolayer cell culture method which was currently employed is inappropriate for VOC analysis. Reena et al. studied the VOC signatures of the two lung cancer cell lines A549 and W138VA13. They observed decane and heneicosane in the A549 cell line and 1-heptanol and heptadecane in W138VA13 cell line [154].

All the prior studies in this research area were conducted using two-dimensional culture method, which is not directly representative of the *in vivo* condition. Thus, the results would not be comparable with the cells *in vivo*. Two-dimensional models have physiologically uniform cellular micro-environment and lack cell-to-cell attachment, but *in vivo*, there exists

cell to cell attachment, oxygen gradient, nutrition gradient and waste gradient. Solid tumors exhibit differential proliferation, i.e.; proliferation is higher at the periphery than the core region due to the gradients cells in 2D models depicts uniform proliferation [88]. Cells in two-dimensional models show apical-basal polarity due to their surface attachment, and that has a huge impact on the gene expression and cellular function. Further, these 2D cultured cells do not show histological differentiation of the *in vivo* tumor [89, 90]. The cells in a tumor exhibit phenotypic heterogeneity, which results in the heterogeneity in both function and morphology [91]. The gene expression profiles including the expression of transcription factors of a cell line grown in 3D are divergent compared to the same cell line cultured 2D [90, 146, 147]. It is possible to replicate all the features of the *in vivo* cellular microenvironment in three- dimensional models. All the above studies show the cells grown as 3D resemble closely to the cells in the *in vivo* tumors. Thus, we do not expect any potential limitations in the clinical translation of the results that are arrived using 3D models. The objective of this study is to develop a methodology for identifying VOCs signature of *in vitro* 3D models of cells lines. In this study, we analyzed and compared the volatile signatures of the primary melanoma cells (WM115) grown as conventional 2D models and 3D models.

4.2. Methods and materials:

4.2.1. Cell culture:

In this study, WM-115 (Human primary melanoma) cells were purchased from American Type Culture Collection (ATCC), USA. These cells were cultured in Eagle's modified essential medium (EMEM) with 10% fetal bovine serum (FBS) and 1% penicillin/streptomycin. All the experiments were carried out in triplicates along with control group that was devoid of cells.

4.2.2. Three-dimensional cancer model:

We developed 3D models of primary melanoma cells using hydrogel matrices. We used agarose as the hydrogel as it is non-cytotoxic and provides a mesh-like structure that simulates the extracellular matrix (ECM). We developed two types of 3D *in vitro* melanoma model: (1) Cells suspended in agarose matrix and (2) Spheroids suspended in the agarose matrix. As there are two different ways to generate *in vitro* 3D cancer models. We intend to analyze and compare the volatile signatures of these two types of 3D tumor models. The WM 115 cells were grown in the 2D until it reaches 95% confluence and harvested. The harvested cells were diluted to 1 x 10^7 cells/mL in various concentrations of agarose (0.5%, 1.0% and 2.0%). For each sample, 500µL of the aliquot is drawn and poured into the 3D printed mold for the agarose matrix formation. The mold has five wells with each well capable of holding 100µL (Figure 4.1). Once the agarose molds are gelled they are fed with the 50mL of fresh medium in the T75 flask and the caps and the vent were sealed using parafilm tape. The sealed flasks are incubated at 37°C and 5% of CO_2 for five days.

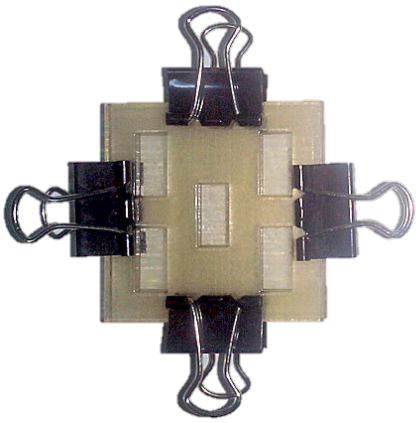

Figure 4.1: 3D printed mold to make agarose matrices for the 3D models.

For the spheroids based model, the harvested 2D cultured cells are diluted to 1 x 10^7 cells/mL. For each sample 500µL of the aliquot is drawn and further diluted to 2.5 x 10^6 cells/mL. This diluted cell suspension is placed on the lid of the Petri dish in droplets of 10µL each. 10mL of Dulbecco's phosphate buffered solution is poured into the Petri dish to make

the hydration chamber to prevent the dehydration of the droplets. The lid is gently flipped and placed over the Petri dish, which creates the hanging drops due to gravity [107]. The Petri dishes were incubated for three days, and the spheroids were harvested and suspended in various concentrations of agarose (0.5%, 1.0%, 1.5% and 2.0%) and poured in the 3D printed mold for curing and gelation (Figure 4.1). Once the agarose molds are gelled, they are fed with the 50mL of fresh medium in the T75 flask and the caps and sealed using parafilm tape. The sealed flasks are incubated at 37°C and 5% of CO_2 for five days which is followed by the VOC analysis. The incubated cells were histologically stained with modified Mason trichrome stain for nucleus and collagen then imaged in a light microscope (Figure 4.3).

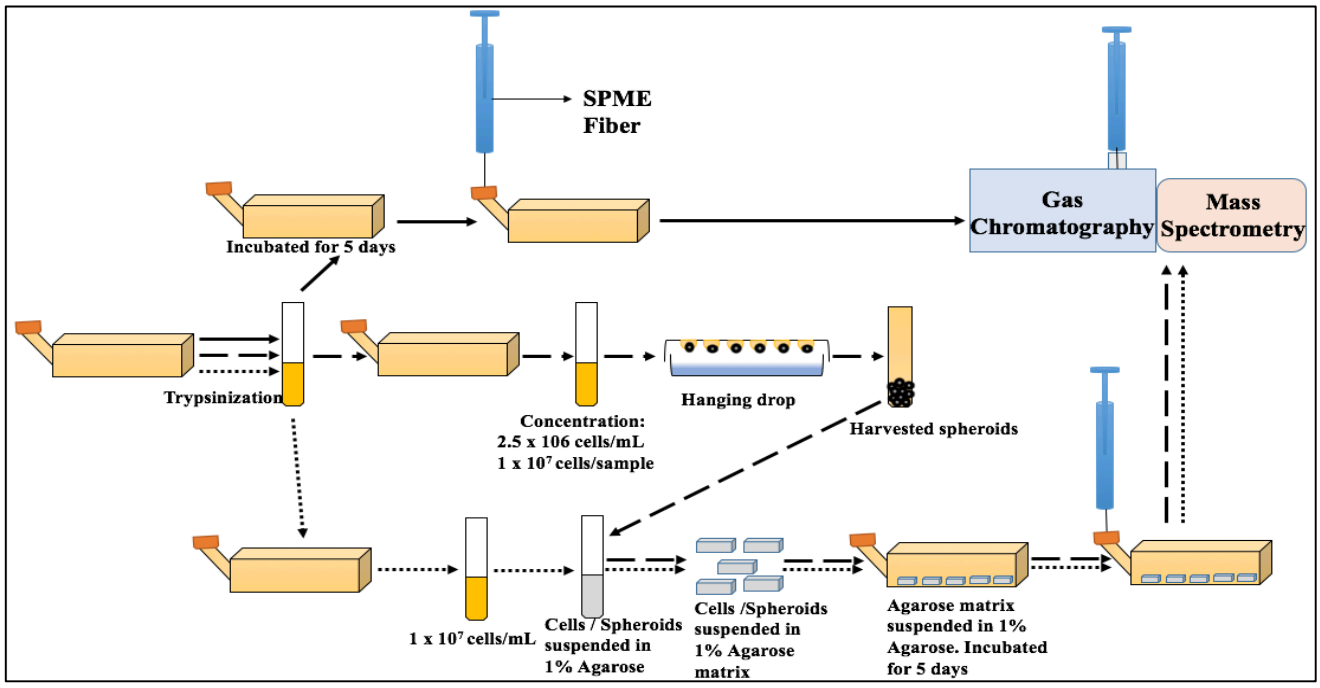

Figure 4.2: Experimental Methodology.

4.2.3. Solid Phase Micro-Extraction (SPME) sampling:

Solid-phase microextraction of the VOCs was performed using the CUSTODION® SPME Syringe, StableFlex needle, 23 GA with DVB/PDMS fiber (Torion Technologies Inc. USA). The DVB/PDMS fiber was carefully placed in the atmosphere of the culture vessel for 40 minutes 37°C and 5% of CO_2. After incubation, the fiber was carefully retracted into the syringe and taken out from the culture atmosphere. The VOC metabolites were then

identified using gas chromatography and mass spectrometry (GCMS) (Figure 4.2).

4.3.4. Gas chromatography and mass spectrometry (GCMS):

The VOC metabolites were identified using gas chromatography and mass spectrometry (Shimadzu GCMS-QP2010 Plus system, Japan, with a 0.25 mm x 30 m DB-5MS column that had a 0.25um phase film thickness). The SPME syringe needle was inserted into the GCMS injection port, in which the cotton wool is removed, and the fiber was extended for 10 minutes to allow for desorption of the VOC metabolites. Helium carrier gas was maintained at a flow rate of 1.0 mL/min. The initial GC oven temperature of 60°C was held for 2 minutes, followed by a temperature ramp of 8°C per minute up to 200°C followed by the second ramp of 5°C per minute up to 260°C then a final ramp of 10°C per minute up to 270°C which was held for 5 minutes. The mass spectrometer transfer line was maintained at 280°C, and the source temperature is 230°C. Mass spectra were repeatedly scanned from 20-700 m/z. The acquired mass spectrum was matched with the mass spectrums of the National Institute of Standards and Technology (NIST) MS spectral library and the mass spectrums NIST 08 mass spectral database, National Institute of Standards and Technology, Washington, DC, USA. The following quasi-linear equation for temperature-programmed retention indices was used to confirm the compound identification.

$$\mathbf{RI_X = [(t_X - t_n)/ (t_{n+1} - t_n)]100 + 100n}$$

where RI_X is the temperature-programmed retention index of interest and t_n, t_{n+1}, t_X the retention time in minutes of the two standard n-alkanes containing n and n + 1 carbons and index of interest, respectively [155].

4.3. Results:

4.3.1. 1% Agarose is the optimum matrix concentration for the development of 3D models of primary melanoma:

In 3D models of primary melanoma, cells and spheroids suspended in agarose were cultured for five days under standard conditions. After the incubation, the cells were fixed in 4.5% paraformaldehyde, and histology was performed using modified Mason trichrome stain. Our histological results clearly showed that in both 3D models, cell proliferation was much better in 1% agarose matrices compared to the 0.5% and 2% agarose matrices (Figure 4.3). These observations suggested that 1% agarose is the optimal concentration for the development of primary melanoma 3D models. In 0.5% agarose matrices, the cells might not get proper physical cues as the pore in the agarose matrices will be larger. On the other hand, in the 2% agarose matrix, the cells might have suffered from space constriction due to the small pore size, which may have restricted the cell proliferation. Hence, all the subsequent results have been obtained from the 3D models developed using 1% agarose.

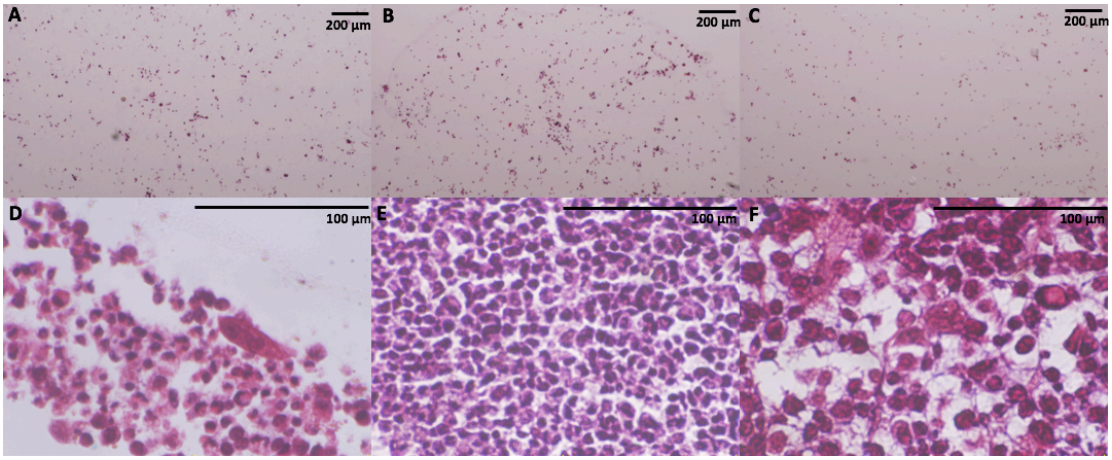

Figure 4.3: Modified mason trichrome staining of the 3D models- Cell suspended in agarose model: A- 0.5% agarose; B- 1% agarose; C- 2% agarose. Spheroids suspended in agarose model: D- 0.5% agarose; E- 1% agarose; F- 2% agarose.

4.3.2. VOCs signature for primary cells in 2D monolayer culture:

The GCMS chromatogram of the primary melanoma cells was compared with the negative control chromatogram to identify the VOCs produced by the primary melanoma cells. In

general, the chromatograms of both primary melanoma group and the medium control group looked very similar with high-intensity peaks, because the VOCs that are emitted by the cells were relatively lower in concentration than the background VOCs. We focused only on identifying the qualitative VOC biomarkers since qualitative biomarkers are preferred over the quantitative biomarkers in the clinical scenario. We were unable to observe any VOC biomarker released by the primary melanoma cells (WM115), but we found that these cells consume 1-tridecanol.

4.3.3. VOC signatures for primary melanoma 3D models:

From this study, we observed that the cells suspended in agarose and spheroids (micro tissue) suspended in agarose showed very similar VOC signatures. We noted that the two model showed differences in the consumption but not in VOC emission. We could also found that the concentration of the VOCs emitted by the cell suspended in agarose model is higher than the concentration of the VOCs emitted by the spheroids suspended in agarose model. This could be because of their difference in the proliferating cell number i.e., In the individual cells suspended in agarose model the individual cells are proliferating whereas in the spheroids suspended in agarose model the cells at the periphery are the proliferating cells whereas the cells at the core of the spheroids are not proliferating as a result of intra-spheroidal heterogeneity. The differences in the proliferating cell number may be the reason for the concentration drop in the VOCs of spheroids suspended in agarose model.

4.4. Discussion:

4.4.1. VOC profiles of the primary melanoma 2D models are different from 3D models:

As the number of cells in 2D culture and 3D culture were not the same, it does not make sense to compare them quantitatively. But, the qualitative comparison the VOC signatures of

the primary melanoma cells in 2D and 3D cultures makes sense. Hence, in this study, we focused on the qualitative differences in the VOC signatures. In the 2D models, the primary melanoma cells consume 1-tridecanol and do not release any VOCs, whereas the 3D models release 4-nonanol, 2-ethyl-1-dodecanol, and 3-tetradecanyl butyrate and consume cinnamic acid, 2,4-diaminotoluene, and 1-tetradecene. These results suggest that the VOC signatures of the cell lines would differ between 2D and 3D models, which supports our hypothesis. As 3D models are the closer replication of the *in vivo* cells than the 2D models, results observed in the 3D models would be relevant for the clinical translation of VOCs based biomarker studies [88-90, 146-147].

4.4.2. Both 3D models exhibit similar VOC signatures:

The VOCs released by both 3D primary melanoma models were very similar. We observed 13 peaks that differ qualitatively from the control chromatogram. Among these 13 peaks, three peaks were assigned to the compounds namely 4-nonanol, 2-Ethyl-1-dodecanol and 3-Tetradecanyl butyrate (Table 4.1).

	S. No	Compound Name	Retention time	Calculated Kovats Retention Index	Kovats Retention Index in library	NIST Similarity	CAS. No
Released by both 3D models	1.	4-Nonanol	14.393	1458.73	1467	83	5932-79-6
	2.	2-Ethyl-1-dodecanol	16.733	1612.76	1591 ± 41	82	19780-33-7
	3.	3-Tetradecanyl butyrate	21.092	1914.88	1914 ± 47	80	6221-98-3
Consumed by both 3D models	1.	Cinnamic acid	13.500	1402.64	1357 ± 51	78	621-82-9
Consumed by cells suspended in Agarose model	1.	2,4-Diaminotoluene	13.091	1378.31	1417 ± 83	84	95-80-7
	2.	1-Tetradecene	13.284	1389.72	1403 ± 39	90	1120-36-1

Table 4.1: Volatile signatures of the 3D models of primary melanoma cells (WM115).

Other ten peaks were not assigned as we cannot match similarity hits with the existing retention index databases (Table 4.2). These results suggest that the direct cell-cell contact does not play any role in the VOC signature of the primary melanoma cell line. However, the specific metabolic pathway and biological function of these VOC signatures of primary melanoma cells, 4-nonanol, 2-Ethyl-1-dodecanol and 3-Tetradecanyl butyrate are not yet known. But it is certain that the presence of these compounds is likely attributed to cellular metabolism. It is reported that nonanol exposure could promote cancer cell invasiveness and metastases by stimulating the olfactory receptors. Moreover, nonanol serves as an agonist for the olfactory receptor OR1G1 and increases the invasion index of the 3D cultured OR1G1 expressing BON cells (Embryonic carcinoma cell line) [156]. These prior studies suggested that primary melanoma cells in 3D models may release 4-nonanol as a signaling molecule to promote invasion. VOCs could act as chemical messengers that could alter the gene expression of the exposed cells. Prior studies show that the VOCs exposure affects the expression of GRP78, which could result in the accumulation of the misfolded and under-glycosylated proteins in the endoplasmic reticulum [157]. This further suggests that VOCs may act as chemical messengers.

S. No	Retention time	Calculated Kovat's Retention Index	Major M/Z
1	16.442	1592.80	27,41,45,55,56,67,71,85,87,97,98,105,111,119, 124,143.
2	16.875	1622.66	27,43,55,56,71,73,87,115,233.
3	16.975	1629.64	27,43,45,55,57,71,77,85,87,97,99,105,115,129.
4	17.908	1695.26	27,43,45,55,56,71,85,87,99.
5	18.617	1746.61	27,43,55,71,98.
6	18.867	1765.02	27,31,41,43,55,58,71.
7	19.492	1810.23	31,43,55,71,98,111,116,143.
8	20.292	1864.80	27,31,41,43,55,71,85,101.
9	20.425	1873.87	28,43,45,55,56,73,74,85,89,103,116,143
10	21.358	1928.81	31,43,45,66,56,71,85,89,101,117,143

Table 4.2: Unidentified Volatile signatures of primary melanoma cells (WM115) that are common for both 3D models.

4.4.3. Direct cell to cell contact does not play a role is VOCs release:

In the cells suspended in agarose model, all the single cells were grown in the 3D agarose mesh without direct cell-cell contact. The gradients of nutrition, CO_2, O_2, and wastes were maintained by the agarose matrix, i.e., the cells suspended in the periphery of the agarose matrix have higher accessibility to the resources than the cells in the core of the agarose matrix. In the spheroids suspended in agarose model, the cells were cultured in the three-dimensional agarose matrix with direct cell-cell contact. Similarly, the gradients were maintained within the spheroids, where the cells on the outer surface of the spheroids have higher accessibility to the resources than the cells in the core of the spheroids [88]. This study has demonstrated the process of obtaining VOC signatures of the 3D models of the primary melanoma cell line. We have deciphered the VOC signatures of the two possible hydrogel-based 3D models were similar to each other. This observation suggested that direct cell-to-cell contact does not play a role in VOCs release.

4.5. Conclusion:

In this study, we have demonstrated a novel method for the identification of the VOC signature of the cell lines using 3D models. We have shown that the VOC signatures of the 2D models were different from the 3D models. We have developed two types of 3D models and evaluated their VOC signatures. Moreover, we found that the VOC signatures of both the 3D models were very similar, which suggests that direct cell-cell contact does not play any role in the VOC signature, providing an insight that these released VOCs could function as intercellular signals. As 3D cell culture models are the closer replica of the *in vivo* cells than 2D models, the VOC signature results of the 3D cell culture models would be more relevant for the clinical translation of these studies.

4.6. Summary:

Identification of volatile signatures of cancer cells forms the basis for volatile-based cancer diagnosis and also for deciphering their unexplored volatile metabolism. All prior research in this area of volatile profiling is based on 2D-cultured cell lines, which drastically vary from the *in-vivo* cells, thus limiting the clinical translation of these studies. Previous studies indicated that culturing cells in 3D architecture mimic that of the *in-vivo* cells. In this study, we have developed 3D models of primary melanoma cells (WM115) and compared their volatile signatures with the volatile signatures of their corresponding 2D models. The two types of 3D models are 1) cells suspended in agarose matrix and 2) spheroids/micro-tissues suspended in the agarose matrix. We have found that the volatile signatures of the 2D and 3D cultured primary melanoma cells were completely different. Moreover, we have also observed that there were no differences in the volatile emission between the two types of 3D models as both 3D models released the same 13 compounds (3 identified and 10 unidentified). However, cells suspended in agarose model consumed 2 additional volatile organic compounds (VOCs) compared to the spheroids suspended in agarose model. Our results suggest that volatile signatures do not play a role in cell-cell contact, providing insight that they may act as signaling molecules. All the current literature addressing the VOC-based characterization of the cells shows the VOC biomarkers of a particular condition but does not link VOCs with a distinct phenotype. These results encouraged to study whether VOCs play a role in intercellular signaling in response to changes in the cellular microenvironment such as cell density.

Chapter 5

Cellular level quorum sensing is manifested by release of volatile organic compounds in human metastatic melanoma cells (WM266)

5.1. Background:

Quorum sensing (QS) is an interesting cell to cell communication phenomenon first observed in the marine bacterium *Vibrio fischeri,* where QS regulates bioluminescence [186]. Quorum sensing helps in the intraspecies or interspecies bacterial communication mediated by the chemical messengers known as autoinducers, secreted by the bacterial cells in a cell density-dependent manner. These secreted chemical messengers are related to cell density or as a metabolite indicating different growth stages of the bacteria [159,160]. Apart from bioluminescence, quorum sensing plays a pivotal role in sporulation (*Micrococcus gezantuse*) , Conjugation (*Enterococcus fecalis*), differentiated morphology (*Streptomyces Cuiceilar*), regulating gene expression in response to abiotic factors (*Vibrio cholera*), biofilm formation (*Pseudomonas aeruginosa* where QS controls over 600 genes), production of extracellular toxic proteins (*Enterococcus, Bacillus*, *Streptococcus, Streptomyces and Staphylococcus*), regulation of virulence factor synthesis (*Pseudomonas, Brucella, Erwinia, Ralstonia, Vibrio, Agrobacterium, Enterobacter, Serratia, Yersinia, Burkholderia and Vibrio*.), nitrogen fixation (*Rhizobium genus*) etc., [161,162].

It seems that QS is conserved across different domains of life as this phenomenon was recently observed in eukaryotic unicellular organism *Candida albicans,* where the quorum sensing molecule(QSM) is identified as farnesol [163]. Later, more molecules like aromatic alcohols, tyrosol, dodecanol, ɣ-butyrolactone, or ɣ-heptalactone have been reported as the QSM [164]. QS can be used as the mode of communication between different species and

even between different kingdoms of life. There are studies deciphering QS based communication between bacteria and fungi, fungi and plant hosts as well as mammalian hosts. In a very interesting study, it was shown that the *C. albicans* produced QSM that could attract leukocytes [165]. These studies hinted that even mammalian cells are compliant with the QS.

A recent study documented the role of organ level quorum sensing in the hair follicle regeneration in response to hair plucking mediated by chemokine (C-C motif) ligand 2 (CCL2). CCL2 promote hair follicle regeneration by attracting and recruiting TNF- α positive macrophages [166]. These studies motivated us to seek for the existence of quorum sensing in human cells. Due to the lack of readily observable phenotype like virulence, biofilm, bioluminescence, etc., in the human cells, makes the identification of cellular level quorum sensing very challenging. Fortunately, most of the human cells produce volatile organic compounds as indicators of their physiological and pathological status [148-154]. Another reason for selecting volatile organic compounds as our method of phenotyping is that VOCs production is conserved in all the domains of life ranging from bacteria to human cells [167 and references therein].

The objective of this study is to investigate the existence of quorum sensing in mammalian cells. We hypothesize that cell density based cell signaling, i.e., QS can be observed using the VOCs production of these cells. In this study, we used human metastatic melanoma cells (WM266) and cultured them in 3D architecture using hydrogel matrices at different cell densities. Even though the cell density is different, we maintained the total number of cells seeded, as constant across all the samples, to compare the results obtained from various cell density groups.

5.2. Methods and Materials:

5.2.1. Cell culture:

For this study, WM-266 (human metastatic melanoma) cells were purchased from American Type Culture Collection (ATCC), USA. These cells were cultured in Eagle's modified essential medium (EMEM) with 10% fetal bovine serum (FBS) and 1% penicillin/streptomycin. We used agarose as the hydrogel as it is non-cytotoxic and provides a mesh-like structure that simulates the extracellular matrix (ECM).

The WM 266 cells were grown in the 2D culture until it reaches 95% confluence and harvested by trypsinization. The harvested cells were diluted into 4 different concentrations such as 1 x 10^6 cells/mL, 2 x 10^6 cells/mL, 5 x 10^6 cells/mL and 10 x 10^6 cells/mL in 1.0% agarose. From each concentration 2 x 10^6 cells were drawn and poured in the 3D printed mold for curing and matrix bead formation (bead dimension: 10mmX5mmX2mm) i.e., 2mL from 1 x 10^6 cells/mL aliquot, 1mL from 2 x 10^6 cells/mL aliquot, 0.4 mL in 5 x 10^6 cells/mL aliquot and 0.2mL from 10 x 10^6 cells/mL aliquot. A single mold can form 5 agarose beads as they have 5 wells with each well capable of holding 100µL. Once the agarose molds were gelled, they were fed with the 35mL of fresh medium in the T75 flask. The sealed flasks were incubated at 37°C and 5% of CO_2 for 5 days.

Thus cell density in each agarose pellet will be different (1 x 10^5 cells/ agarose pellet, 2 x 10^5 cells/ agarose pellet, 5 x 10^5 cells / agarose pellet and 10 x 10^5 cells / agarose pellet in 1 x 10^6 cells/mL, 2 x 10^6 cells/mL, 5 x 10^6 cells/mL and 10 x 10^6 cells/mL samples respectively) but total number of cells seeded will remain constant across all the samples (Figure 5.1). All the experiments were carried out in triplicates along with control group, which was devoid of cells. After five days of incubation, the spent nutrient medium is collected and saved in the sterile 50 mL falcon tubes and preserved at -80^0 C until analysis.

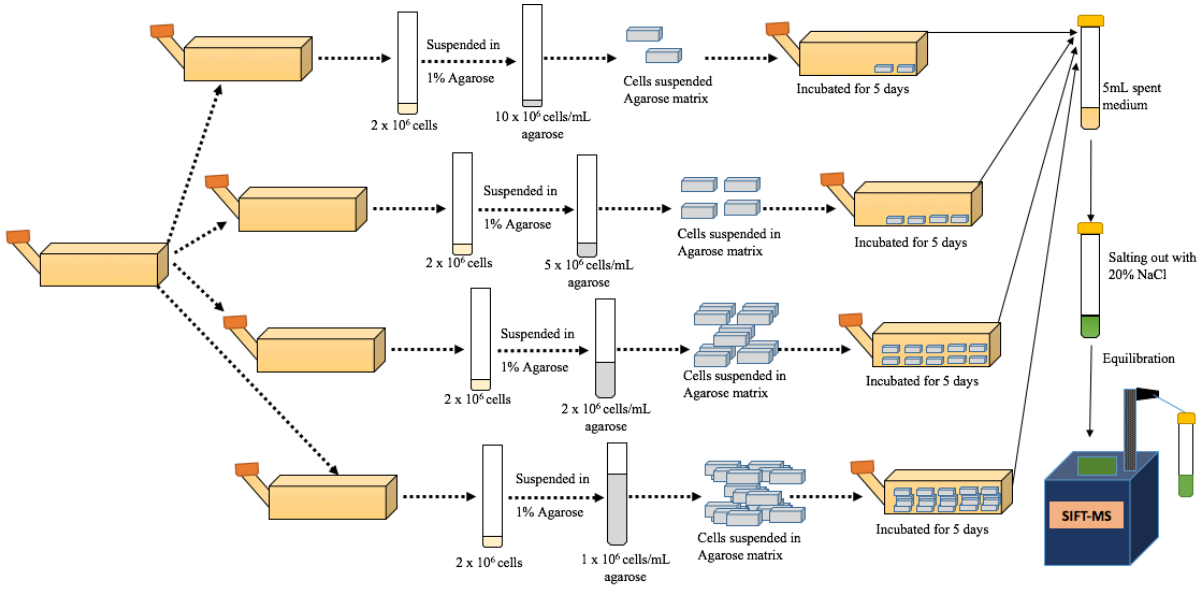

Figure 5.1: Research methodology followed in this study

5.2.2. Sample Preparation:

In *in vivo*, the volatiles produced by the cells tend to dissolve in blood and excreted during exhalation as a result of gaseous exchange in lungs. *In vitro*, the volatiles generated by the cells tend to dissolve in the nutrient medium. As gaseous exchange is not possible in *in vitro* condition, a reliable method of separating the volatiles dissolved in the spent nutrient medium is needed for the volatile analysis. We opted for salting out method using NaCl [167]. The preserved spent nutrient medium was thawed at room temperature. From the thawed spent nutrient medium 5 mL was drawn to the 60mL tube that contains 1 gram of NaCl (20%). The tube was then sealed with a stopper containing PFTE septa. The NaCl salt was dissolved in the medium by gentle agitation which results in the release of dissolved volatiles to the headspace of the 60 mL tube, as the solubility of NaCl is higher than the VOCs. The tubes were incubated for at least 2 hours in room temperature before volatile analysis for achieving equilibration.

5.2.3. Volatile Analysis Using SIFT-MS and Statistical Analysis:

The headspace volatiles of the equilibrated tubes was fed into the SIFT-MS (Voice 2000, New Zealand) at the rate of 25 standard cubic centimeters (sccm) using an 18-gauge needle.

A full mass scan (M/Z range: 18 – 200) was performed with three reaction ions namely H_3O^+, NO^+ and O_2^+. The M/Z ratios and their corresponding counts were collected. For the convenience of data comparison, all the samples were analyzed on the same day one after the other. All the statistical analysis was performed by the MetaboAnalyst 3.0, online statistical software (www.Metaboanalyst.ca/, Canada) [54]. The collected M/Z ratios with their counts were converted into single concatenated vector in order make it compatible for the MetaboAnalyst 3.0. The product ion count rate depends on the precursor ion count rate which varies from day to day; we conducted a normalization procedure in which product count rates of each sample were divided by corresponding H_3O^+, NO^+, and O_2^+ precursor count rates [168]. Statistical methods, such as heat map analysis of the significant product ion M/Z ratios, clustering analysis, t-test, etc., were performed using MetaboAnalyst 3.0 after logarithmic normalization and auto scaling. All the significant M/Z ratios mentioned in this article were having p-value lesser than 0.05. The ions comprise precursor, isotopologues and water clusters their isotopologues were removed as the precursors were carrier ions added to the sample, they need to be deleted from H_3O^+ product ion list. Hence, the M/Z of 19, 20, 21, 30, 32, 37, 38, 39, 55, 56, 57, 73, 74, 75, 91 in H_3O^+ were removed. Further M/Z in NO^+ product ions including 19, 30, 32, 37, 48, 50, 55, 57, 66, 73, 91, are removed and 19, 30, 32, 33, 34, 37, 50, 55, 56, 57, 73, from the O_2^+ product ion list [169]. However, the isotopologues that are highly significant (p-value <0.01) in t-test were retained. The compounds were predicted using the inbuilt database developed from various detailed selected ion flow tube (SIFT) studies of different classes of compounds (alcohols, aldehydes, ketones, hydrocarbons, etc.) with the three precursor ions mentioned above [170].

5.3. Results and discussion:

5.3.1. Statistical analysis of the SIFT-MS data:

Full mass scan SIFT–MS data obtained for the four cell density groups and statistically compared with the corresponding controls using Student T-test. The number of significant (p. value < 0.05) product ion M/Z ratios were found to be varying with the cell density (Table 5.1, Figure 5.2).

A

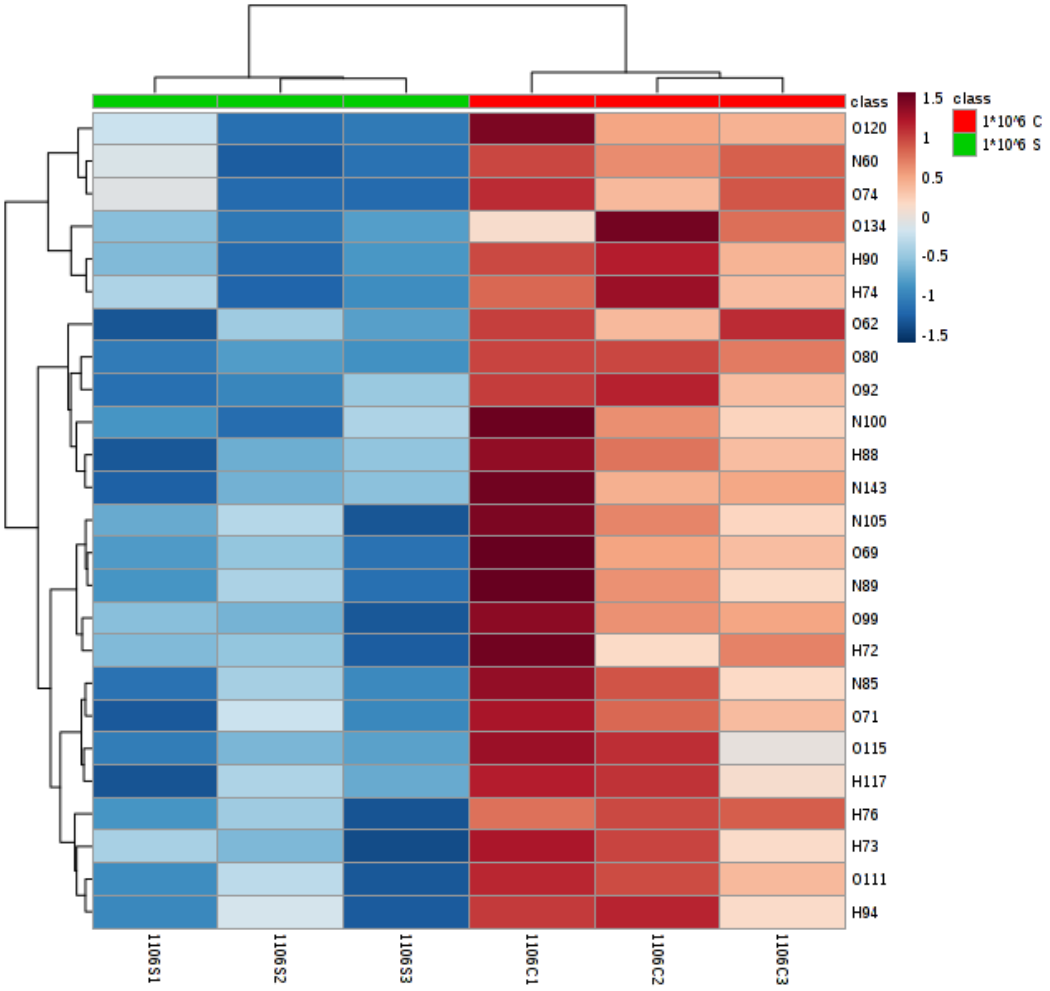

B

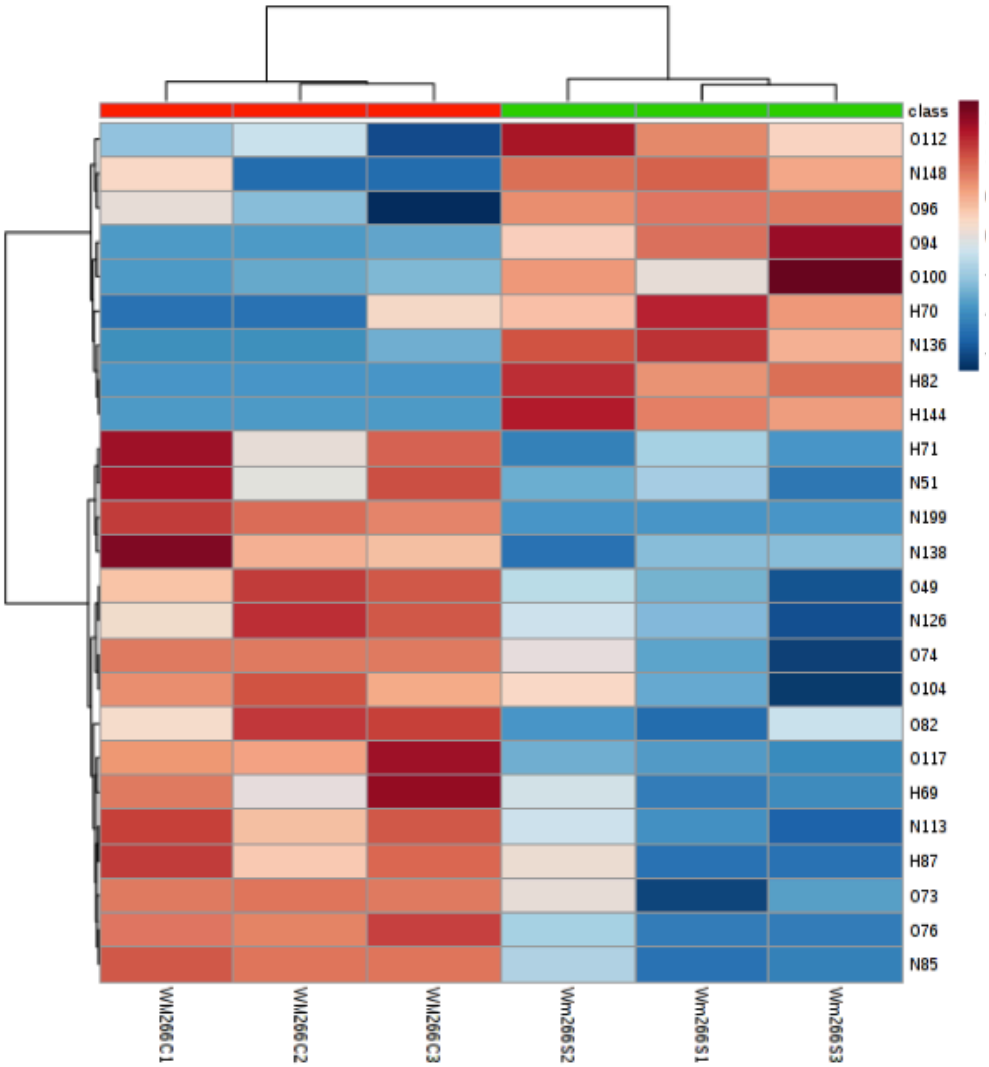
class
O112
N148
O96
O94
O100
H70
N136
H82
H144
H71
N51
N199
N138
O49
N126
O74
O104
O82
O117
H69
N113
H87
O73
O76
N85
WM266C1
WM266C2
WM266C3
Wm266S2
Wm266S1
Wm266S3

C

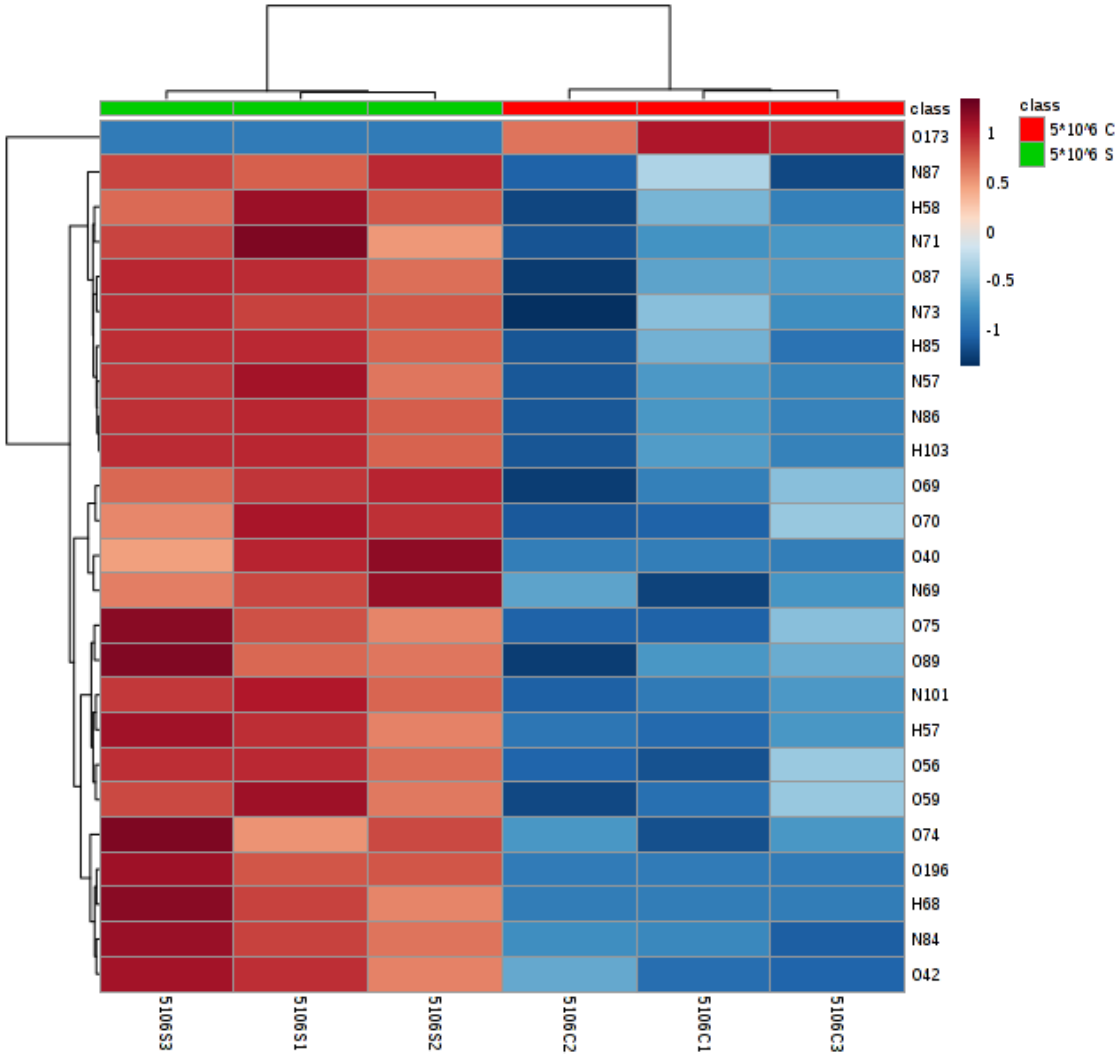
class
O173
N87
H58
N71
O87
N73
H85
N57
N86
H103
O69
O70
O40
N69
O75
O89
N101
H57
O56
O59
O74
O196
H68
N84
O42
510S3
510S1
510S2
510C2
510C1
510C3
class
5*10^6 C
5*10^6 S
1
0.5
0
-0.5
-1

D

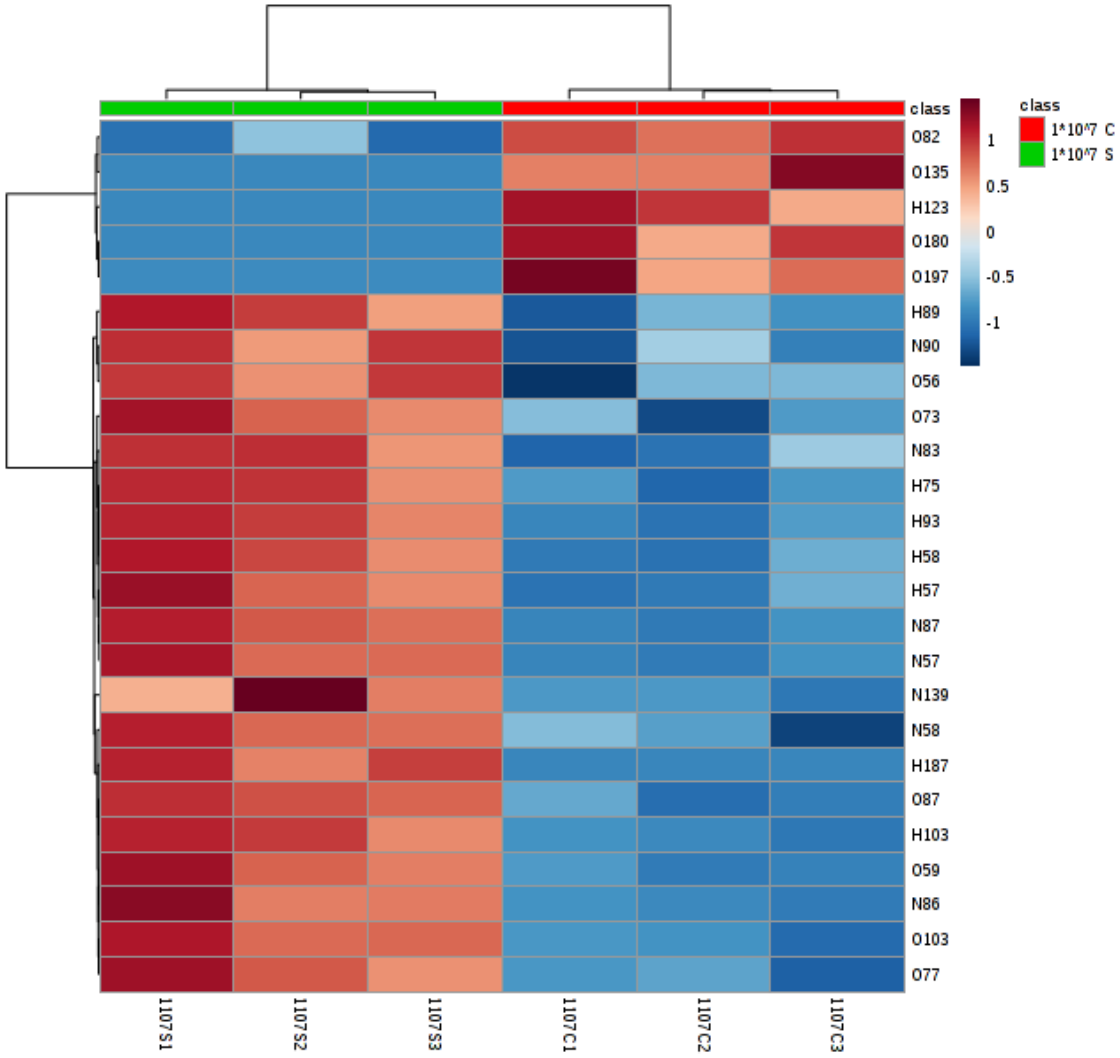

Figure 5.2: Heat Maps and clustering analysis of SIFT-MS product ion data of WM266 cells at various cell density. A- 1 x 10^6 cells/mL of 1% agarose; B- 2 x 10^6 cells/mL of 1% agarose; C- 5 x 10^6 cells/mL of 1% agarose; D- 10 x 10^6 cells/mL of 1% agarose.

Cell Density Cells/mL	SIFT-MS Reaction Ions	Statistically significant product ion M/Z (P-Value <0.05) Representing the VOCs released by the cells	Statistically significant product ion M/Z (P-Value <0.05) Representing the VOCs consumed by the cells
1 x 10^6	H_3O^+		33, 43, 45, 51, 71, 72, 76, 80, 86, 87, 88, 90, 94, 101, 108, 113, 117, 120, 129, 132, 139, 149, 159, 163, 167.
	NO^+		43, 60, 62, 71, 83, 85, 89, 99, 100, 104, 105, 118, 126, 143.
	O_2^+		18, 62, 69, 71, 74, 76, 80, 90, 92, 99, 100, 111, 115, 120, 134, 159.
2 x 10^6	H_3O^+	143, 144, 82	46, 72, 102, 107.
	NO^+	136, 148	
	O_2^+	94	43, 49, 74, 76, 82, 104, 106, 117.
5 x 10^6	H_3O^+	29, 35, 36, 58, 60, 61, 68, 71, 81, 85, 86, 89, 96, 103, 113, 115, 117, 121, 147.	
	NO^+	36, 56, 58, 69, 71, 83, 84, 86, 87, 101, 102, 104, 114, 115, 118, 126, 127, 129, 130, 144, 151.	51, 71, 85, 113, 126, 138, 199.
	O_2^+	17, 35, 41, 42, 43, 48, 59, 60, 69, 70, 71, 74, 75, 77, 80, 84, 85, 87, 88, 89, 92, 99, 103, 117, 191, 196.	54, 173.
10 x 10^6	H_3O^+	58, 60, 67, 69, 70, 76, 85, 89, 93, 103, 149, 187.	123, 145.
	NO^+	47, 56, 58, 63, 83, 84, 86, 87, 90, 101, 104, 108, 112, 114, 136, 139.	
	O_2^+	41, 42, 59, 74, 75, 77, 78, 87, 89, 103, 108.	82, 180

Table 5.1. List of all the significant (p-value <0.05) product ion M/Z ratios at different cell density representing the VOCs released and consumed by the WM266 (metastatic melanoma cells.

We observed that the number of significant M/Z ratios representing the VOCs released increases with the increase in cell density whereas the significant M/Z ratios representing the VOCs consumed tends to decreases with the increase in seeded cells density (Figure 5.3).

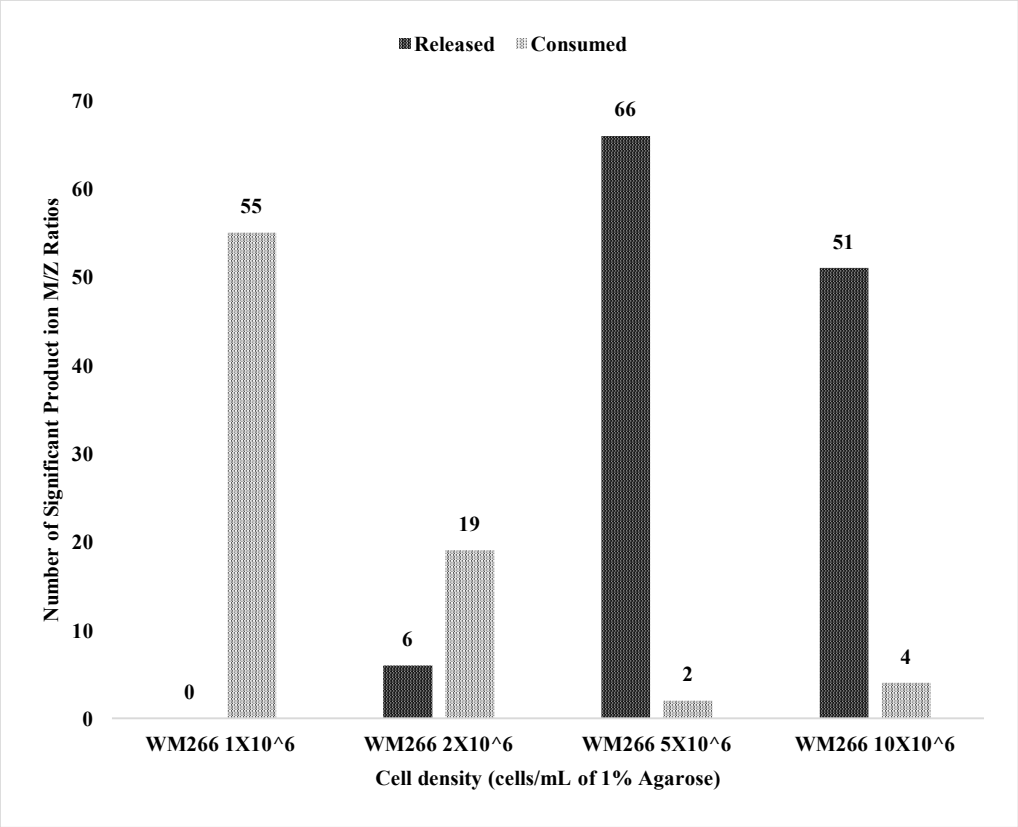

Figure 5.3. Number of Significant product ion M/Z representing the VOCs released and consumed by the cells at various cell densities

Likely that the WM266 cells consumed more VOCs at lower cell densities and when the cell density increases they releases more VOCs consuming fewer VOCs. Initially, this observation made us propose a hypothesis that the increase in cell density causes scarcity of the nutrients especially to the cells located at the core of the agarose matrix, causing the cell to undergo apoptosis and the VOCs we observed could be the indicator or the by-product of apoptosis. To validate this hypothesis, we performed histological analysis of the agarose matrices (that are previously fixed in 4.5% paraformaldehyde immediately after incubation) at three different depths namely at the outermost region, innermost region and in between outermost and innermost regions using H&E staining procedure. (Figure 5.4).

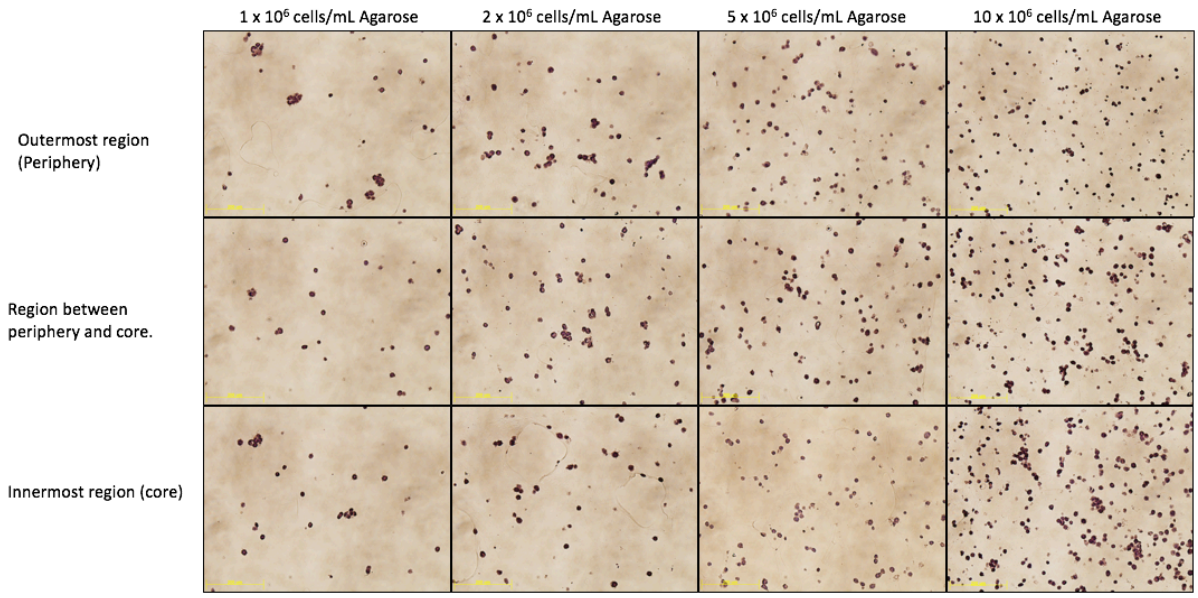

Figure 5.4: Histology of the agarose matrix containing WM266 cells at different cell densities on 5th of incubation, showing that the cell proliferation is not affected across the agarose matrix (Scale = 200µm).

The H&E staining of these slices clearly shows that cell proliferation is not constrained due to the increase in the cell density as we could observe active cell proliferation at all the three depths in all studied cell densities. Hence the significant product ion M/Z ratios we observed can be attributed solely to the increase in cell density rather than apoptosis or cell death. This observation is the clear indication that these cells alter their volatilome based on the cell density and provide insight about the existence of cellular level quorum sensing in these cells.

5.3.2. Volatiles could be the phenotypic manifestation of quorum sensing in metastatic melanoma cells:

Among the significant (p-value<0.05) product ion M/Z ratios, we could observe 29 M/Z ratios were present in both 5 x 10^6 cells/mL and 10 x 10^6 cells/mL groups and all these M/Z were highly significant (p-value<0.01) compared to their corresponding controls (Table 5.2).

Cell Density Cells/mL	SIFT-MS Reaction Ions	Statistically significant product ion M/Z (P-Value <0.05) Representing the VOCs released by the cells
5 x 10^6 and 10 x 10^6	**H_3O^+**	57, 58, 60, 75, 85, 89, 103.
	NO^+	56, 57, 58, 73, 83, 84, 86, 87, 101. 104, 114.
	O_2^+	41, 42, 56, 57, 59, 74, 75, 77, 87, 89, 101.

Table 5.2. List of the 29 highly significant (p-value < 0.01) product ion M/Z ratios, representing the VOCs released by the WM266 (metastatic melanoma cells that are observed in both at 5 x 10^6 and 10 x 10^6 cell densities.

Hence clearly these 29 M/Z ratios were the manifestation of the quorum sensing in WM 266 cells. We have identified 10 compounds using the inbuilt SIFT-MS library matches based on these 29 M/Z ratios (Table 5.3).

S. No	Volatile organic compound	Reagent ions	Reaction Rate (K)	Product ion M/Z	Product ions	Branching ratio
1	2-hexene	H_30^+	2.0E-9	85	C6H13+	1
		NO^+	1.9E-9	84	C6H12+	0.55
				83	C6H11+	0.45
2	Methyl tertiary butyl ether	H_30^+	3.0E-9	89	C5H12O.H+	0.4
				57	C4H9+	0.6
		NO^+	2.4E-9	86	C4H8.NO+	0.1
				57	C4H9+	0.9
		O_2^+	3.0E-9	89	C5H13O+	0.05
				73	C4H9O+	0.75
				57	C4H9+	0.2
3	Dipropenyl sulfide	NO^+	2.5E-9	114	(C3H5)2S+	1
4	Propanoic acid	H_30^+	2.7E-9	57	C2H5C0+	0.05
				75	C2H5COOH2+	0.95
		NO^+	1.5E-9	57	C2H5CO+	0.05
				104	NO+.C2H5COOH	0.95
		O_2^+	2.2E-9	74	C3H5COOH+	1
5	3,3-dimethyl-	H_30^+	3.0E-9	85	C6H12.H+	1

	2-butanol	NO^+	2.5E-9	101	C6H13O+	0.9
				85	C6H13+	0.1
		O_2^+	1.9E-9	87	C5H11O+	0.2
				57	C4H9+	0.35
				56	C4H8+	0.3
				45	C2H5O+	0.15
6	Isobutene	NO^+	1.5E-9	86	NO+.C4H8	0.15
				56	C4H8+	0.85
7	2-butene	H_30^+	1.6E-9	57	C4H9+	1
		NO^+	1.3E-9	56	C4H8+	1
		O_2^+	1.4E-9	41	C3H5+	0.5
				56	C4H8+	0.5
8	1-hexene	H_30^+	2.1E-9	85	C6H13+	1
		NO^+	1.8E-9	86	C4H8.NO+	0.35
				114	C6H12.NO+	0.25
				46	CH4.N0+	0.15
				72	NO+.C3H6	0.1
				69	C5H9+	0.1
				83	C6H11+	0.05
9	2-methyl-2-propanol	H_30^+	2.7E-9	57	C4H9+	1
		NO^+	2.0E-9	57	C4H9+	1
		O_2^+	2.1E-9	59	C3H7O+	1
10	Butyl hexanoate	H_30^+	3.0E-9	57	C4H9+	1
		NO^+	3.0E-9	73	C4H9O+	1
		O_2^+	2.0E-9	59	C3H7O+	0.4
				56	C4H8+	0.6

Table 5.3: List of identified VOCs released by WM266 (metastatic melanoma) cells at 5 x 10^6 and 10 x 10^6 cell densities.

Due to the lack of studies relating the volatile metabolites with the cellular physiology, it is very hard to understand the precise role of these VOCs in cellular biology. Among these predicted compounds methyl tertiary butyl ether and isobutene has been reported as volatile biomarkers for lung cancer cell line called A549 and interestingly isobutene is observed only in the higher A549 cell concentration as a qualitative biomarker. This study is noteworthy here because in that study higher cell concentration means higher cell density as the various cell concentrations were cultured in cell culture bottles of same dimensions, which supports the results of our study [171]. 2-butene has already reported as a VOC of normal human breath [172]. 1-hexene has been identified as the lung cancer-associated biomarker using discriminant analysis of the GC-MS data and using sensors made of carbon nanotube coated with non-polymeric organic materials [173,174]. 2-methyl-2-propanol has been observed to be released only by the normal lung cells and not by the transformed cells [208], but our results suggest that this might not be true with melanoma. It is also important to note that, all the existing cell line studies in the scientific literature were based on the 2D cultured cells. We adopted 3D culture as 3D cultured cells were very much similar to the *in vivo* cells as they showed all the characteristic features of *in vivo* cells [88-91, 146-147].

5.3.3. Quorum sensing model:

By these results, we propose the following quorum sensing model for the metastatic melanoma cells. Metastatic melanoma cells tend to secrete the quorum sensing molecule (QSM). When the QSM reaches a threshold limit, which is corresponding to the cell number, these cells release of specific VOCs that may act as cell signaling molecules (Figure 5.5). This hypothesis is possible as there are reports showing VOCs were capable of altering gene expression. In a recent study, VOCs exposure affects the expression of GRP78, which could result in the accumulation of the misfolded and under-glycosylated proteins in the

endoplasmic reticulum [157]. Previous studies on bacterial VOCs also claimed that volatile produced by bacteria helped in enhancing growth in many plants by modulating various genes [175-177]. The QSM might not be a VOC because we could not observe any consistent release of VOCs that are released by all the cell density groups. Thus clearly VOCs could not be a QSM at least for WM266 cells.

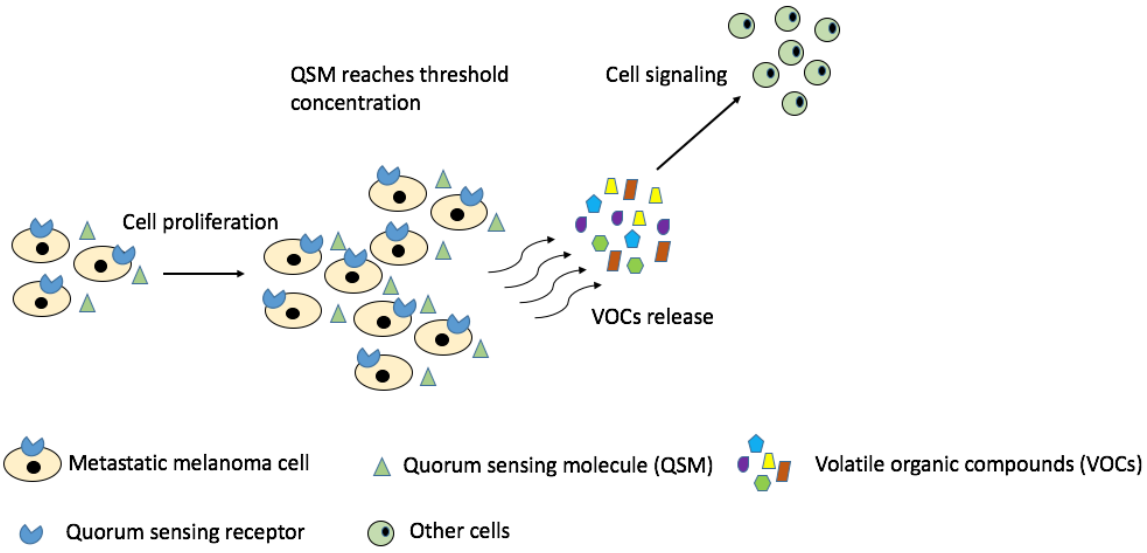

Figure 5.5: Proposed quorum sensing model

5.3.4. Clinical significance of cellular quorum sensing:

The clinical significance of cellular level quorum sensing is very high especially in the case of complex diseases like cancer. Once the quorum sensing molecule (QSM) of the cancer cells has been identified, we can target the QSM to neutralize it. So that, the progression of cancer cells could be restricted. This approach could open up novel treatment strategy in the century old fight of humanity against cancer.

5.4. Conclusion:

The significant product ion M/Z ratios obtained from the statistical analysis of the SIFT–MS data at higher cell density is highly significant and consistent. This study suggested the existence of the cellular level quorum sensing in the WM266 cells. According to the best of our knowledge, this is the first study to show the existence of cellular level quorum sensing in mammalian cells. We have also included the histological study to validate the existence of cellular level quorum sensing in WM266. We have also proposed a quorum sensing model and its probable role in VOCs based cell signaling.

5.5. Summary:

Quorum sensing is a cell to cell communication phenomenon, which was observed and extensively studied in various bacterial species. In the mammalian cells, it is very hard to observe quorum sensing as they lack in phenotypes, which can be observed without disturbing the cells. We have investigated the metastatic melanoma cells (WM266) for the existence of cellular level quorum sensing by observing the alteration in the cell's volatile organic compounds (VOCs) emission profiles. We had developed a series of 3D models with different cell densities while maintaining a constant number of cells. We extracted VOCs from the spent medium by salting out procedure. These extracted VOCs were analyzed using SIFT-MS full mass scan mode. Our study showed that, when the cell density was increased, the metastatic melanoma cells released characteristic VOCs. This finding proved that the metastatic melanoma cells could sense the cell density in their vicinity and respond to it by emitting certain VOCs, suggesting the existence of cellular level quorum sensing. Clinically, once the molecule responsible for the quorum sensing is identified, we can control cancer progression by neutralizing the quorum sensing molecule. The next step is to focus on gastric cancer and find out, is it possible to identify gastric cancer using their VOC signatures and

also to observe the dynamics of these VOC signatures in response to the anti-cancer compounds like curcumin.

Chapter 6

Volatile Biomarkers and Curcumin-Induced Volatile Signatures of Multicellular Gastric Cancer Tumor Spheroids.

6.1. Background:

Gastric cancer ranks as the third fatal cancer with 0.72 million deaths worldwide in 2012, and according to the World Health Organization, the highest incidence of gastric cancer is observed in the Asia-Pacific region, especially in Japan. Two important aspects of cancer research are diagnosing cancer and monitoring cancer treatment [1]. The gold standard for the diagnosis of gastric cancer is esophagogastroduodenoscopy (EGD) and biopsy. Although these invasive methods are widely accepted, they still create significant discomfort for the patients especially in children and elderly with potential complications such as perforation and aspiration if handled by poor operators. Furthermore, these are not cost-effective as screening tools. It is imperative to develop a non-invasive and cost effective gastric cancer diagnosing tool. Fortunately, most of the human cells produce volatile organic compounds as indicators of their physiological and pathological status [181, 88 - 91, 146-147]. This study aims to identify the volatile signatures of the gastric cancer cells, as our first to develop volatile based gastric cancer detection method. Cellular level volatile profiles might be useful to understand gastric cancer biology in the perspective of volatile metabolites.

Turmeric (*Curcuma longa*) is a spice containing the following ingredients; curcumin, dimethoxy curcumin, bisdemethoxycurcumin curcumin, and cyclo curcumin [178]. The antioxidant properties of these curcumins are attributed to the hydroxyl group whereas the anti-proliferative property is attributed to the methoxy groups [179]. Curcumin has been found to inhibit the signaling pathways of cancer cells, inhibit cell proliferation, invasion, angiogenesis, and metastasis. In the prospect as a chemo-protectant against cancer, Curcumin

is very promising as it can induce apoptosis by several molecular pathways. These pathways include and are not limited to activation of caspase, induction of death receptors, aggregation of Fas receptor, induction of p53/p21 pathway, release of apoptosis inducing factor, regulation of cell cycle, down-regulation of androgen receptors, activation of thioredoxin reductase, activation of c-Jun Kinase, induction of DNA fragmentation, depletion of intracellular Ca^{2+}, activation of mitochondrial activation, suppression of anti-apoptotic proteins, binding to microtubules, activation of proteasome, pro and antioxidant mechanisms, autophagy and inhibition of various cancer-related genes and gene products such as PI3K-AKT, mTOR, AMPK, COX2, 5 LOX, hTERT, STAT3, NF-κB, Wnt/beta-catenin signaling, growth factors and their receptors, ornithine decarboxylase, acidic sphingomyelinase, phospholipase D, glyoxalase etc. [180].

The objectives of this study are to identify the VOCs biomarker for gastric cancer spheroids and to investigate the alteration in the VOCs signature of gastric cancer spheroids in response to curcumin treatment. In this study, we hypothesize that gastric cancer cell lines have unique volatile signatures and these volatile signatures would change in response to the curcumin treatment. We examined four gastric cancer cells lines (SNU 484, IST 1, MKN 28, NUGC 3) and one normal gastric cell line (HS 738), for the identification of gastric cancer-specific volatile biomarkers. From these identified volatile compounds, biomarkers of the gastric cancer spheroids were deduced. We treated the above mentioned multicellular spheroids with curcumin and identified the volatile compounds produced by these spheroids in response to curcumin treatment. Our results suggest that the curcumin treatment triggers either the production of curcumin associated cell death related volatiles (as in SNU 484 and NUGC 3) or curcumin associated cell death evasion related volatiles (as in MKN 28, IST 1 and HS 738).

6.2. Methods and Materials:

6.2.1. Cell Culture:

Four gastric adenocarcinoma cell lines SNU484, MKN28, IST1, and NUGC3 and a normal cell line HS738 were used in this study. The gastric adenocarcinoma cells were cultured in Roswell Park Memorial Institute (RPMI) medium with 10% fetal bovine serum (FBS), and the normal gastric cell line was cultured in Dulbecco's modified essential medium (DMEM) with 10% FBS. All the experiments were carried out in triplicates along with the spent medium, which served as the background control.

S. No	Cell Line	Cancer/ Normal	Primary / Metastatic	Differentiation Status	Tissue	Morphology
1	SNU484	Adenocarcinoma	Primary	Poor	Stomach	Round oval
2	MKN 28	Tubular adenocarcinoma	Metastatic	Moderate	Lymph node	Polygonal
3	IST 1	Tubular adenocarcinoma	Metastatic	Moderate	Liver	Polygonal
4	NUGC 3	Adenocarcinoma	Metastatic	Poor	Brachial muscle	Polygonal
5	HS738	Normal	NIL	Good	Mixed, Stomach, Intestine	Fibroblast/ Spindle-like

Table 6.1: Characteristics of the gastric cell lines used in this study.

6.2.2. Formation of Cellular Spheroids:

For the spheroids formation, the cells were grown as a monolayer (2D culture) and harvested using trypsinization. The harvested cells were checked for their viability by dye exclusion method using bromophenol blue dye. The samples with required viability (95%) were diluted into $2.5x10^6$ cells/mL for spheroid formation. Each replicate contained 20 mL of the diluted cell suspension equivalent to $5X10^7$ cells. The diluted cell samples were drawn into drops of 10µL on the lid of the sterile petri dish. The petri dish was filled with 10mL of Dulbecco's Phosphate-Buffered Saline DPBS which will act as the hydration chamber. The petri dish lid was gently inverted and fixed over the petri dish and placed in the incubator for the spheroid formation [107]. After incubation for 3 days, the spheroids, observed by the naked eye as white spheres, were harvested and cultured in a custom made silanized glass culture flask.

The spheroids were further cultured for 6 days with 50mL of RPMI medium with 10% FBS with nutrient medium being replaced on every alternative day. On the sixth day, the spheroid culture was replaced with RPMI medium with 10% FBS supplemented with 75mg of 95% curcumin (100% pharmaceutical grade, Turmeric - Curcumin extract with 95% curcumin, 21st Century, Singapore). On the eighth day as well as on the tenth day, the spheroid culture was replaced with RPMI medium with 10% FBS supplemented with 150mg of 95% curcumin. The spheroids were observed under the light microscope on every alternative day just before replacing the nutrient medium.

6.2.3. Sample collection and time of sample collection:

The spent nutrient medium was the sample for this study. 50mL spent medium was collected on every alternative day before replacing the culture flask with fresh nutrient medium or curcumin supplemented nutrient medium. The collected spent nutrient medium was saved in the sterile 50 mL falcon tubes and preserved at -80^0 C until analysis.

6.2.4. Sample preparation:

In vivo, the volatiles produced by the cells tend to dissolve in blood and get excreted during exhalation as a result of gaseous exchange in lungs. In vitro, the volatiles generated by the cells tend to dissolve in the nutrient medium. As gaseous exchange was not possible in vitro, a reliable method of salting out method using sodium chloride (NaCl) was used to separate the volatiles dissolved in the spent nutrient medium needed for the volatile analysis. The preserved spent nutrient medium is thawed to room temperature. From the thawed spent nutrient medium, 5 mL was drawn to the 60mL tube that contains 1 gram of NaCl (20% W/V). The tube is then sealed with a stopper containing Polytetrafluoroethylene PFTE septa. The NaCl salt was dissolved in the medium by gentle agitation which results in the release of

dissolved volatile to the headspace as the solvation power of NaCl was higher than that of volatile organic compounds VOCs. The tubes were incubated for at least 2 hours before volatile analysis for achieving equilibration [154].

6.2.5. Volatile analysis using SIFT-MS and statistical analysis:

The headspace volatiles of the equilibrated tube were fed into the SIFT-MS at the rate of 25mL/min using 18-gauge needle. A full mass scan (M/Z range: 18 – 200) was performed with three reaction ions namely H_3O^+, NO^+ and O_2^+. The M/Z ratios and their corresponding counts were collected. For the convenience of data comparison, all the samples for a single cell line were analyzed on the same day one after the other. All the statistical analysis was performed by the MetaboAnalyst 3.0 online statistical software (www.Metaboanalyst.ca/, Canada) [54]. The collected M/Z ratios with their counts were formatted in order make it compatible for the MetaboAnalyst 3.0 before statistical analysis. We conducted a normalization procedure in which product count rates of each sample were divided by corresponding H_3O^+, NO^+, and O_2^+ precursor count rates [168]. Since the product ion count rate depended on the precursor ion count rate which varied from day to day, All the significant M/Z ratios mentioned in this article were having p-value lesser than 0.05 (Figure 6.1). The compounds were predicted using the inbuilt database developed from various detailed selected ion flow tube (SIFT) studies of different classes of compounds (alcohols, aldehydes, ketones, hydrocarbons, etc.) with the three precursor ions mentioned above [170]. However, we were not able to identify all the VOCs that are represented by the significant M/Z ratios mainly because of the limited number of compounds in the SIFT library, which is expected to increase in future.

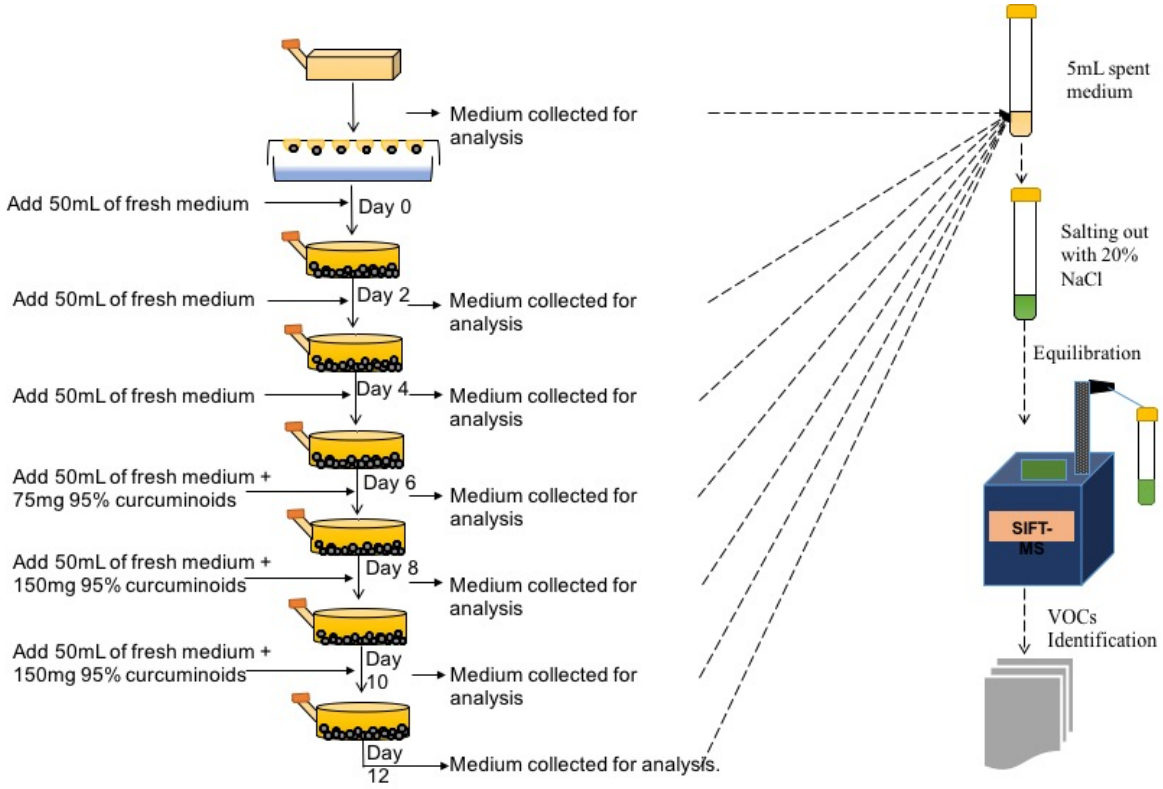

Figure 6.1. The experimental procedure of this study.

6.3. Results:

6.3.1. Volatile signatures of gastric cancer cells in monolayer (2D) culture:

In monolayer culture, we observed that the gastric cancer cells produce many VOCs, which was represented by the significant (p-value <0.05) M/Z ratios and the normal gastric cells (HS738) showed only 4 significant M/Z ratios (Table 6.2). Among those significant M/Z ratios of gastric cancer cells, 68 ratios were found to be observed in all the gastric cancer groups. It was also noted that 32 significant M/Z ratios were found to be present only in the metastatic gastric cancer groups. These results suggested that, under monolayer culture, VOC profiles were capable of classifying, normal gastric cells as well as primary and metastatic gastric cancer cells.

Cell line	Reaction Ion	Product ion M/Z ratios
HS738	H_3O^+	54,
	NO^+	118.
	O_2^+	31, 49.
MKN 28	H_3O^+	101, 105, 114, 117, 127, 133, 135, 137, 139, 140, 141, 147, 181, 189, 31, 33, 35, 36, 45, 46, 47, 48, 49, 51, 52, 53, 63, 64, 65, 66, 67, 69, 73, 74, 75, 82, 83, 84, 85, 89, 91, 92, 93, 94, 95.
	NO^+	102, 109, 110, 113, 116, 118, 121, 123, 128, 130, 132, 137, 139, 147, 158, 175, 31, 33, 36, 37, 39, 43, 45, 46, 47, 51, 55, 62, 63, 64, 65, 66, 67, 69, 73, 74, 75, 76, 81, 83, 84, 85, 89, 90, 91, 92, 93, 94.
	O_2^+	111, 112, 117, 119, 124, 127, 131, 133, 135, 137, 139, 140, 141, 143, 146, 147, 169, 175, 189, 191, 18, 19, 30, 31, 33, 36, 37, 39, 41, 43, 44, 45, 46, 47, 48, 49, 51, 52, 53, 54, 55, 57, 60, 63, 64, 65, 66, 67, 68, 69, 70, 71, 72, 73, 74, 75, 76, 77, 78, 81, 82, 83, 84, 85, 86, 88, 89, 90, 91, 92, 93, 94, 95.
IST 1	H_3O^+	101, 103, 104, 105, 113, 114, 117, 127, 128, 129, 135, 139, 143, 147, 149, 150, 153, 155, 163, 189, 31, 33, 36, 47, 48, 49, 51, 52, 53, 57, 58, 64, 65, 66, 67, 69, 70, 71, 72, 75, 83, 84, 85, 87, 89, 91, 92, 93, 94, 95.
	NO^+	100, 101, 102, 103, 105, 107, 112, 113, 114, 115, 116, 117, 118, 126, 130, 132, 133, 141, 142, 144, 147, 154, 156, 158, 36, 37, 43, 45, 46, 47, 51, 54, 55, 56, 57, 58, 62, 63, 64, 65, 66, 68, 69, 70, 71, 73, 76, 83, 84, 85, 86, 87, 88, 89, 91, 92, 93, 94, 96.
	O_2^+	101, 103, 105, 111, 113, 114, 115, 117, 118, 119, 122, 124, 126, 127, 129, 131, 135, 139, 141, 143, 145, 147, 173, 191, 18, 19, 30, 31, 33, 36, 41, 43, 45, 46, 47, 48, 49, 51, 52, 57, 58, 59, 60, 63, 64, 65, 66, 67, 68, 69, 70, 71, 72, 73, 75, 76, 77, 78, 83, 84, 85, 86, 87, 88, 89, 91, 92, 93, 94, 95.
SNU 484	H_3O^+	101, 102, 103, 104, 113, 117, 127, 128, 129, 135, 141, 150, 31, 33, 36, 47, 49, 51, 52, 53, 57, 58, 60, 69, 70, 71, 75, 83, 85, 87, 89, 93, 94, 99.
	NO^+	101, 102, 103, 112, 113, 114, 115, 116, 118, 123, 126, 128, 130, 132, 141, 142, 144, 146, 154, 156, 158, 36, 45, 46, 47, 51, 55, 56, 57, 58, 62, 63, 64, 65, 68, 69, 70, 71, 72, 73, 76, 83, 84, 86, 91, 93, 94.
	O_2^+	101, 103, 110, 111, 114, 117, 118, 127, 129, 135, 141, 142, 17, 18, 31, 33, 35, 36, 41, 47, 49, 51, 52, 57, 59, 60, 65, 66, 68, 69, 70, 71, 72, 75, 76, 77, 83, 85, 86, 87, 88, 91, 93, 94, 95.
NUGC 3	H_3O^+	101, 102, 105, 111, 113, 127, 133, 135, 137, 139, 147, 189, 31, 33, 36, 45, 46, 47, 48, 49, 51, 52, 53, 60, 63, 64, 65, 66, 67, 69, 75, 83, 84, 85, 91, 92, 93, 94, 95, 99.
	NO^+	102, 109, 113, 118, 123, 130, 133, 141, 156, 175, 31, 33, 36, 37, 43, 45, 46, 47, 51, 55, 62, 63, 64, 65, 66, 67, 69, 73, 74, 76, 81, 83, 84, 85, 88, 89, 91, 92, 93, 94.
	O_2^+	101, 103, 109, 111, 113, 117, 118, 122, 124, 135, 137, 139, 141, 142, 147, 153, 169, 185, 191, 18, 19, 28, 30, 31, 33, 36, 37, 41, 43, 45, 46, 47, 48, 49, 51, 52, 54, 55, 60, 63, 64, 65, 66, 67, 68, 69, 70, 73, 74, 75, 76, 77, 78, 83, 84, 85, 89, 91, 92, 93, 94, 95, 96.

Table 6.2: List of Significant M/Z ratios (P value <0.05) expressed by the Gastric cells cultured as monolayer.

6.3.2. Volatile signatures of gastric cancer cells in Spheroid (3D) culture:

Table 6.3 showed the list of significant M/Z ratios (p.value < 0.05) representing the VOCs released by the spheroids on alternate days till day 12. For HS 738 (normal gastric) spheroids produce 8, 5 and 4 significant M/Z ratios on day 2, 4, and 6 respectively. Nine significant M/Z ratios were observed after the treating with 75 mg curcumin on the day 8, whereas 19 and 36 significant M/Z ratios were found after treated with 150 mg curcumin on day 10 and day 12 day respectively. These results clearly showed that these spheroids produce volatiles in response to the curcumin treatment (Table 6.3). Among these M/Z ratios, 3 were consistent during the entire course of the curcumin treatment (H_3O^+ - 99; NO^+ - 98; O_2^+ - 98) and 11 M/Z ratios were consistently observed after 150mg curcumin treatment (H_3O^+ - 100, 129, 135, 137, 192; NO^+ -104, 128, 134, 136, 138, 154, 158; O^+ - 128). From figure 6.2, it was evident that the morphology of HS 738 spheroid was unaltered, which suggested that these volatiles were produced as a result of the cytoprotective mechanism against the curcumin or the byproducts of curcumin catabolism. These results showed that there was an interaction between HS738 spheroids and curcumin.

Name of the Spheroids	**SIFT-MS Reaction Ions**	**Age of the Spheroids**					
		2 Days	4 Days	6 Days	8 Days	10 Days	12 Days
		Curcumin concentration					
		NIL	NIL	NIL	75 mg	150 mg	150 mg
HS738	**H_3O^+**	59.	59.	198, 39, 59.	124, 139, 95, 99.	100, 129, 135, 137, 192, 99.	100, 129, 135, 136, 137, 139, 151, 153, 155, 178, 189, 192, 199, 30, 37, 38, 39, 55, 56, 57, 60, 81, 99.
	NO^+	117, 37, 88.	169, 88.		95, 98.	104, 128, 134, 136,	104, 128, 134, 136,

						137, 138, 144, 154, 158, 82, 98.	138, 143, 158, 98.
	O_2^+	102, 120, 175, 82.	121, 82.	160.	140, 98, 99.	128, 98.	144, 128, 155, 98, 99.
MKN 28	H_3O^+	154, 163, 178, 186, 198, 200, 21, 35, 42, 45, 46, 63, 64, 75, 92.	154, 178, 200, 21, 35, 45, 63.	35, 45, 63.	113, 45, 63,64,78, 81, 82, 89.	127, 135, 45, 63.	135, 137, 45, 46, 63, 64.
	NO^+	116, 141, 180, 43, 44, 74.	43, 74.	129, 43, 74.	128, 158, 43, 61, 62, 74, 98.	135, 43, 92, 98.	135, 43, 74, 79.
	O_2^+	154, 157, 180, 192, 193, 40, 43, 74.	164, 191, 193, 194, 40, 43, 74.	43, 74.	151, 43, 61, 98.	110, 81.	119, 136, 43, 81, 93.
IST 1	H_3O^+	101, 103, 104, 117, 121, 122, 125, 129, 137, 139, 141, 175, 191, 29, 43, 45, 46, 51, 52, 57, 58, 63, 64, 71, 75, 89, 90, 91, 92, 93.	122, 137, 141, 149, 150, 169, 181, 45, 54, 71, 72, 89, 90.	104, 169, 70, 71.	107, 110, 130, 29, 45, 78, 81.		141.
	NO^+	102, 103, 104, 127, 150, 156, 170, 43, 44, 57, 58, 61, 70, 73, 74, 79, 86, 87, 89, 91, 97.	101, 104, 130, 142, 43, 57, 58, 61, 73, 74, 86, 87, 97.	113, 130, 151, 167, 73, 74, 86, 90.	125, 147, 43, 57, 58, 59, 61, 74, 96,	136, 38.	134, 136, 139, 57, 84.
	O_2^+	103, 115, 121, 127, 133, 36, 43, 44, 45, 57, 59, 60, 61, 63, 64, 73, 75, 77, 79, 87, 89, 93.	140, 166, 36, 43, 73, 77, 79, 87, 89.	175, 36, 57, 59, 60, 70, 87, 89.	149, 43, 44, 58, 60, 61, 76, 81, 89.	154, 34, 70, 96.	108, 137, 139, 155, 59, 70, 78, 93.
SNU 484	H_3O^+		197.	162.	118, 137, 154, 99.	182.	43, 47, 61, 64, 79.
	NO^+	54.	129.	162.	101, 102, 104, 128,	108, 128, 136, 184,	136, 198, 45, 59,

					132, 158, 87, 98.	98.	60, 63, 65, 76, 77.
	O_2^+			113, 145, 83, 87, 88.	117, 125, 139, 155, 98.	101, 139, 36, 92.	177, 37, 45, 46, 47, 63, 65, 91.
NUGC 3	H_3O^+	103, 115, 149, 185, 45, 46, 57, 63, 64, 78, 89, 91, 95, 99.	161, 171, 45, 63.	109, 34, 42.	117, 165, 171, 30, 38, 45, 46, 5762, 63, 76, 89, 99.	105, 106, 107, 114, 124, 127, 134, 135, 173, 22, 62, 69, 71, 87.	104, 110, 123, 124, 127, 134, 135, 162, 166, 172, 173, 177, 180, 182, 183, 184, 186, 187, 200, 22, 27, 42, 49, 50, 68, 89, 90, 96.
	NO^+	158, 185, 43, 44, 56, 61, 74, 79, 90.	111, 143, 167, 197, 43, 44, 74.	169, 178, 74.	104, 124, 136, 138, 182, 43, 61, 74, 77, 79, 98.	103, 105, 116, 118, 135, 57, 85, 86, 87, 90, 92.	106, 107, 108, 118, 119, 134, 136, 143, 151, 152, 153, 160, 34, 82, 87.
	O_2^+	120, 41, 43, 59, 61, 70, 79.	120, 43.	171	111, 43.	105, 118, 135, 44, 62, 76, 87, 89.	109, 110, 118, 122, 128, 129, 135, 136, 146, 152, 153, 166, 191, 89, 93, 94, 95.

Table 6.3: List of Significant M/Z ratios (P value <0.05) expressed by the Gastric spheroids under the untreated condition and after subsequent treatment with curcumin.

MKN 28 spheroids produce 29, 16 and 8 significant M/Z ratios on day 2, 4, and 6 respectively. In response to the curcumin treatment, the number of significant M/Z ratios increased to 19 on day 8 (75 mg), 10 on day 10 and 15 on the day 12 (Table 6.2). Three significant M/Z ratios were produced during the entire curcumin treatment (H_3O^+ - 45, 63;

NO^+ - 43) and three M/Z ratios (H_3O^+ - 135; NO^+ - 135; O^+- 81) were observed specifically after 150mg curcumin treatment (day 10 and 12). IST 1 spheroids produce 73, 36 and 20 significant M/Z ratios on day 2, 4 and 6 respectively. After the 75 mg curcumin treatment, these spheroids release VOCs represented by 25 significant M/Z ratios, which reduced to 6 after 150mg curcumin treatment on day 10 and then increased to 14 on day 12 (Table 6.2). Seven significant M/Z ratios were produced consistently before curcumin treatment (H_3O^+ - 71; NO^+ - 73. 74, 86; O^+ - 36, 87, 89). The M/Z ratios NO^+ -136^+ and O_2^+- 70^+ were produced consistently during the 150mg curcumin treatment.

Figure 6.2 showed that the MKN 28 was completely unaffected and IST 1 spheroids were moderately affected due to the curcumin treatment, which suggested that both these cell lines survived by evading curcumin-induced cell death or apoptosis. Thus these significant M/Z ratios were representative of curcumin-induced cell death evasion. It was also important to note that both MKN 28 and IST 1 followed different mechanisms for evading curcumin-induced cell death, which is evident from the significant M/Z ratios. This differences might be due to the differences in the interaction of the curcumin with these spheroids, as the curcumin were capable of interfering vast array of metabolic pathways.

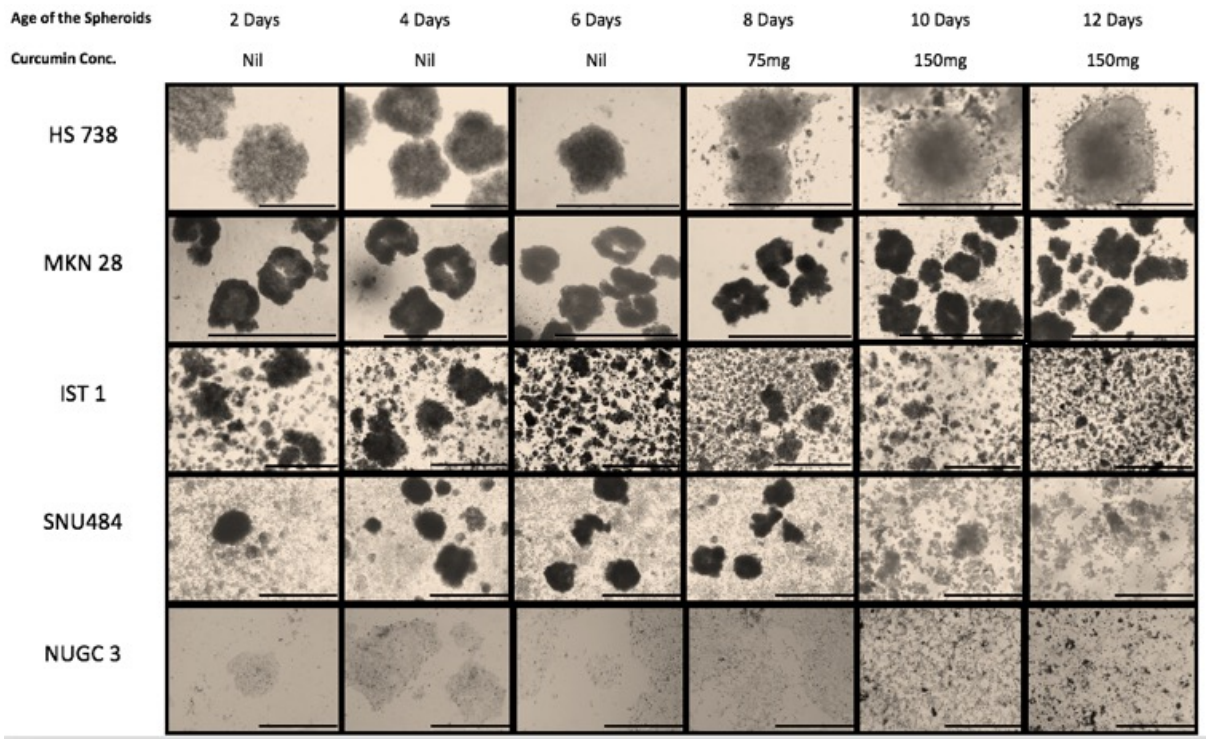

Figure 6.2: Micrographs Depicting the Effect of curcumin treatment on Normal Gastric spheroids and Gastric cancer spheroids (scale = 1 μm).

NUGC 3 spheroids produced 30, 13 and 7 significant M/Z ratios on day 2, 4 and 6 respectively. 26 M/Z ratios were observed after 75mg curcumin treatment, whereas 33 and 60 significant M/Z ratios were found after 150mg curcumin treatment on day 10 and day 12 respectively (Table 6.2). M/Z ratios H_3O^+ - 124, 127, 234, 135, 173, 22; NO^+ -118, 87; and O_2^+- 118, 135, 89 were produced consistently during the 150mg curcumin treatment. Three significant M/Z ratios were produced till day 8 i.e., till 75mg curcumin treatment (H_3O^+ - 45, 63; NO^+ - 74). This suggested that these spheroids had certain degree of resistance to 75mg curcumin treatment. SNU 484 spheroids produced 1, 2 and 9 significant M/Z ratios on day 2, 4 and 6 respectively. In response to the 75mg curcumin treatment, SNU 484 spheroids produced 17 significant M/Z ratios whereas, treating with 150 mg of curcumin resulted in the production of 10 and 29 significant M/Z ratios on day 10 and day 12 respectively (Table 6.2). From the microscopic observation, it was evident that the curcumin treatment on both NUGC 3 and SNU 484 spheroids resulted in the apoptosis. It was also clear that the in both

spheroids, the apoptosis was complete between day 10 and day 12. Hence the significant M/Z ratios produced on the day 12 represented the volatiles that were produced as a result of curcumin-induced cell death, and these M/Z ratios could be the potential biomarkers for curcumin-induced cell death/ apoptosis. On the other hand, the significant M/Z ratios observed on day 8 and 10 are the representation of these spheroids' initial response to 75mg and 150mg curcumin treatment respectively.

6.4. Discussion:

6.4.1. VOC signatures can classify normal gastric cells, primary gastric cancer cells and metastatic gastric cancer cells that are cultured as monolayer as well as spheroids:

In monolayer culture, the normal gastric cells (HS738) released methylamine (O_2^+ - 31), which was specific to the normal gastric cells among the cells studied here. As for gastric cancer cells, both the primary and metastatic gastric cancer cells released seven VOCs, which were not observed in normal gastric cells. Thus these seven VOCs could be considered as the biomarkers of gastric cancer. These seven VOCs were formaldehyde (H_3O^+ - 31; O_2^+ - 31, 60), methanol (H_3O^+ - 33, 51, 69; NO^+ - 62; O_2^+ - 31), cyanoacetylene (H_3O^+ - 52), cyclohexane (H_3O^+ - 83, 85), phenylamine (H_3O^+ - 94; NO^+ - 93; O_2^+ -93), 2-hexane (H_3O^+ - 85; NO^+ - 83, 84) and Methane (O_2^+ -47). Interestingly, the release of methylamine by the normal gastric cells and phenylamine by the gastric cancer cells suggested that there existed an alteration in the alkyl amine biosynthesis between the normal and cancerous gastric cells. Metastatic gastric cancer cells specifically released nitrous acid, nitric acid, and 2,3-butadiene. Thus these three VOCs could be considered as biomarkers of metastatic gastric cancer in monolayer culture (Table 6.4).

Identified Compounds		
Normal (HS-738)	**Gastric Cancer (MKN-28, IST-1, SNU-484 & NUGC-3)**	**Metastatic Gastric Cancer (MKN-28, IST-1 & NUGC-3)**
Methylamine	Formaldehyde Methanol Cyanoacetylene Cyclohexane Phenyl amine 2-hexane Methane	Nitrous acid Nitric acid 2,3-butadiene

Table 6.4: List of identified VOCs released by the Gastric cells cultured as monolayer.

On the other hand, in the spheroid culture, under the untreated condition, the normal gastric spheroids specifically released acetone (H_3O^+ - 59; NO^+ - 88), which was consistently released from day 2 to day 6. Hence, it was certain that acetone could be the biomarker for the normal gastric spheroids. It was previously reported that acetone was expressed by primary human bronchial epithelial cells [171]. We could not be able to identify common VOC biomarker for primary and metastatic gastric cancer spheroids as the primary gastric spheroids did not release any detectable VOCs. However, we identified acetaldehyde (H_3O^+ - 45; NO^+ - 43, 74; O_2^+ - 43) as the VOC biomarker for the metastatic gastric cancer spheroids. Acetaldehyde was observed consistently till day 6 (untreated condition) in all the metastatic spheroids (Table 6.5). Acetaldehyde has been already reported as a lung cancer biomarker in previous reports [181, 149].

Name of the Spheroids	Age of the Spheroids					
	2 Days	4 Days	6 Days	8 Days	10 Days	12 Days
	Curcumin concentration					
	NIL	NIL	NIL	75 mg	150 mg	150 mg
HS738	Acetone	Acetone	Acetone	Pentyl furan 3-methyl thiophene	Furaneol Pentyl furan 3-methyl thiophene	Furaneol Pentyl furan 3-methyl thiophene
MKN 28	Acetaldehyde Nitric acid Hydrogen sulfide	Acetaldehyde Hydrogen sulfide	Acetaldehyde Hydrogen sulfide	Acetaldehyde Furfuryl alcohol Furaneol	Acetaldehyde carveol	Acetaldehyde carveol
IST 1	Acetaldehyde Methyl tert butyl ether Nitric acid	Acetaldehyde Methyl tert butyl ether	Acetaldehyde	Acetaldehyde Carbonyl sulfide	4-Isopropyl toluene	4-Isopropyl toluene
SNU 484				3-Methyl thiophene Furaneol	3-Methyl thiophene Furaneol	2-propanol Formic acid/Nitrogen dioxide Nitric acid Methane Ethyl chloride
NUGC 3	Acetaldehyde	Acetaldehyde	Acetaldehyde	Acetaldehyde	Pentanal Benzaldehyde	Acetonitrile 1-nitropropane/ urethane Benzoic acid/ 2-Methyl-3-ethyl pyrazine

Table 6.5: List of identified VOCs released by the Gastric spheroids under the untreated condition and after subsequent treatment with curcumin.

6.4.2. VOCs signature of cells cultured as monolayer and as spheroids were dissimilar:

As the number of cells in the monolayer culture and spheroid culture were different, the volatile signatures obtained from monolayer culture and spheroid culture were not comparable in the quantitative aspect. However, comparing qualitatively, it was evident that the VOC signatures of all the studied gastric cells in monolayer culture were different from that of the same cells cultured as spheroids. Numerous previous studies showed the similarity of spheroid culture with the in vivo cells, as all the characteristics of the in vivo cells like

nutrient and waste gradients, cell proliferation gradients, heterogeneity, etc. were preserved in the cells cultured as spheroids [88-91, 146-147]. Thus the VOC biomarkers that were identified in the spheroids were suitable for the clinical translation and further basic biology investigation. These results were yet another proof of the differential behavior of cells in 2D culture and 3D cultures.

6.4.3. Effect of Curcumin Treatment on Normal Gastric Spheroids and Gastric Cancer Spheroids:

It is evident from the figure 6.2 that the HS738 and MKN 28 remain intact after the complete curcumin treatment whereas, curcumin treatment in IST 1 spheroids of results in the fragmentation of the tumor spheroids. On the other hand, in the case of SNU 484 and NUGC 3 spheroids curcumin treatment resulted in apoptosis. These results suggested that curcumin treatment was more effective for poorly differentiated gastric cancers than moderately differentiated gastric cancers and does not affect the normal gastric cells (Table 6.1).

6.4.4. Curcumin treatment alters the volatile signatures of the gastric spheroids:

The volatile signatures of all the gastric spheroids were modified by the curcumin treatment. Among the 5 gastric spheroids studied, two spheroids (HS 738 and MKN 28) evaded the cytotoxicity of the curcumin, whereas IST 1 was moderately affected resulting in the fragmentation of the spheroids but did not undergo cell death. However, the other two spheroids, namely SNU 484 and NUGC 3 have been affected by the curcumin treatment resulting in apoptosis of these spheroids. Hence, the VOCs observed in the HS 738, MKN 28 and IST 1 after curcumin treatment were the curcumin-induced cell death evasion associated volatiles whereas, the VOCs found in SNU 484 and NUGC 3 after the curcumin treatment were the curcumin-induced cell death associated volatiles.

Normal gastric spheroids (HS 738), did not release its signature volatile acetone after the curcumin treatment, instead released pentyl furan (H_3O^+ - 139; NO^+ - 138) and 3-methyl thiophene (H_3O^+ - 99; NO^+ - 98; O_2^+ -98) after treating with 75mg curcumin. With the 150mg curcumin treatment, they release additional volatiles one being furaneol. It is noteworthy that, curcumin treatment ceased the release of acetone and induced release of pentyl furan (H_3O^+ - 139; NO^+ - 138), 3-methyl thiophene (H_3O^+ - 99; NO^+ - 98; O_2^+ -98) and furaneol (H_3O^+ - 129; NO^+ - 128, 158; O_2^+ -128). This observation provided an insight that curcumin interacted with the metabolic pathway which synthesized acetone and it is evident that these three volatiles produced after curcumin treatment represents either by product of curcumin metabolism or volatiles associated with the cytoprotection mechanisms or both.

Interestingly, MKN 28 spheroids could retain its volatile signature namely acetaldehyde even after the complete curcumin treatment, but they released certain additional VOCs, in response to the curcumin treatment. The consistent acetaldehyde expression is coinciding with the unaltered morphology of the MKN 28 after the curcumin treatment suggesting that MKN 28 spheroids had a mechanism to prevent itself from curcumin treatment without compromising its normal metabolism. When treated with 75mg curcumin, MKN 28 spheroids responded with the production of furfuryl alcohol (H_3O^+ - 81; NO^+ - 98; O_2^+ -98). When the curcumin dosage was increased to 150mg, they released carveol (H_3O^+ - 135; NO^+ - 135). Carveol is a hydroxylated monoterpene, which was shown as a chemopreventive agent against mammary gland carcinogenesis [182]. IST 1 retains its acetaldehyde (H_3O^+ - 45; NO^+ - 43, 74; O_2^+ - 43) release even after treating with 75 mg curcumin but it ceased to release acetaldehyde after the 150mg curcumin treatment. However, after the 75mg treatment they released carbonyl sulfide (O_2^+ - 60) in addition of acetaldehyde but after the 150mg treatment they produce different volatiles like 4-isopropyl toluene (H_3O^+ - 135; NO^+ - 134; O_2^+ - 119). This finding suggested

that IST 1 spheroids were responding to curcumin treatment in a dose-dependent manner. Even though the curcumin treatment caused fragmentation of the IST 1 spheroids, the cells did not undergo apoptosis even after another dose to 150mg curcumin (data not shown). This observation revealed that volatiles like 4- isopropyl toluene could be the manifestation of cell death prevention mechanism but not the fragmentation of the spheroids.

SNU 484 spheroids were one of the two cell lines that underwent apoptosis. This primary gastric cancer spheroids, released 3- methyl thiophene (H_3O^+ - 99; NO^+ - 98; O_2^+ -98) and furaneol (NO^+ - 128, 158) when treated with 75mg of curcumin and 150mg of curcumin. From figure 6.2, it is evident that SNU 484 spheroids underwent apoptosis after the first dose of 150mg curcumin. Formic acid (H_3O^+ - 43, 61; NO^+ - 59; O_2^+ - 45)/ nitrogen dioxide (O_2^+ - 46), nitric acid (H_3O^+ - 64), methane (O_2^+ -47) and ethyl chloride (O_2^+ -63, 65) that were observed after the second dose could be the manifestation of apoptosis. Thus, these VOCs were the curcumin-induced cell death associated volatiles. Another cell line that underwent apoptosis in response to curcumin treatment was NUGC 3. These spheroids were resistant to the 75mg curcumin treatment, which was evident from the release of acetaldehyde even after 75mg of curcumin treatment. But once treated with the first dose of 150mg of curcumin, these spheroids ceased their acetaldehyde production and released other higher aldehydes, pentanal (H_3O^+ - 69, 87; NO^+ - 85; O_2^+ -44, 58) and benzaldehyde (H_3O^+ - 107; NO^+ - 105). On the second dose of 150mg curcumin the cells in the NUGC 3 spheroids underwent complete apoptosis and released acetonitrile (H_3O^+ - 42, 96), 1-nitropropane (H_3O^+ - 90; NO^+ - 119)/ urethane (H_3O^+ - 90; NO^+ - 119; O_2^+ -89), benzoic acid (H_3O^+ - 123; NO^+ - 152; O_2^+ - 122)/2-methyl-3-ethyl pyrazine (H_3O^+ - 123; NO^+ - 152; O_2^+ -122). These volatiles could also be regarded as the curcumin-induced cell death associated volatiles. It is noteworthy to mention that SNU 484 and NUGC 3 might have undergone apoptosis by following different

mechanisms, which was evident from their initial to response to curcumin treatment and also by the volatiles observed after complete apoptosis (Table 6.4).

6.4.5. Sensitivity to curcumin treatment varies between different gastric cells cultured as spheroids:

This study showed that the cell lines differ in their sensitivity to curcumin treatment. The gastric cancer spheroids of cell lines MKN 28 was completely immune to curcumin treatment whereas, IST 1 and NUGC 3 shows resistance to lower doses of curcumin, which was evident from the release of acetaldehyde. However, HS 738 and SNU 484 were highly sensitive to the curcumin even at the lower doses. It is imperative to note that, two out of five cell lines (HS 738 and SNU 484) studied, produces 3- methyl thiophene and furaneol as their response to curcumin treatment. Interestingly among these two cell lines SNU 484 underwent apoptosis whereas, HS 738 survived the curcumin treatment. This observation suggested that 3- methyl thiophene and furaneol did not play any role in either apoptosis or evasion of apoptosis. We could observe an additional VOC called pentyl furan released in HS 738 that is not released by SNU 484, which showed that pentyl furan could be released as a result of apoptosis evasion mechanism by HS 738.

Another interesting observation was these metastatic gastric cancer spheroids were able to retain the production of acetaldehyde even after 75mg curcumin treatment along with some new M/Z ratios and when treated with 150mg curcumin treatment they stop producing their volatile biomarker namely acetaldehyde (with the exception of MKN 28) and produced volatiles in response curcumin treatment. These significant M/Z ratios that were produced before and after 150mg curcumin treatment were completely different. This data suggested that the cytotoxicity of curcumin was dose dependent.

6.5. Conclusion:

This study used multicellular spheroids to reproduce the in vivo cellular microenvironment in vitro as close as possible. Acetaldehyde was found to be a potential volatile biomarker for diagnosing metastatic gastric cancer. All the normal gastric spheroids and gastric cancer spheroids studied produced specific volatiles in response to the curcumin treatment. Each and every cell line studied gave their unique response to the curcumin treatment by expressing unique volatile signatures. Observations on acetaldehyde expression by the metastatic gastric cancer spheroids after curcumin treatment suggest that these cells respond to curcumin in a dose-dependent manner. These volatile signatures would be useful in monitoring the progress of the curcumin treatment against cancer. This study was first of its kind, and still, there is a lot of research that needs to be done to relate the volatiles represented by the significant M/Z ratios with the established metabolic pathways, which would be indispensable in understanding the disease metabolism and developing better ways of diagnosis and treatment.

6.6. Summary:

Gastric cancer has the third highest mortality rate among all other cancers due to the lack of non-invasive and early detection methods. Various studies showed volatile signatures of the cancer cells could be used as biomarkers for cancer detection, where in the case of gastric cancer, curcumin was identified as a potential drug candidate for treatment. In this study, we investigated four gastric cancer cells lines (SNU 484, IST 1, MKN 28, NUGC 3) and one normal gastric cell line (HS 738), for the identification of gastric cancer-specific volatile biomarkers, where we intend to decipher the curcumin-induced volatile signatures of the gastric cancer spheroids. Among the five cell lines, three cell lines (MKN 28, IST 1 and HS 738) were wholly or partially resistant to curcumin treatment whereas the other two cell lines (SNU 484 and NUGC 3) were susceptible to the curcumin treatment which led to the cell

death. Our results suggests that the curcumin treatment triggers either the production of curcumin-induced cell death associated volatiles (as seen in SNU 484 and NUGC 3) or curcumin-induced cell death evasion associated volatiles (as seen in MKN 28, IST 1 and HS 738), which could be considered as potential biomarkers for accessing the outcome of curcumin treatment. This study opens up further research to decipher the role of these volatiles in curcumin associated cell death and curcumin associated cell death evasion. Any biomedical study is not considered complete without clinical translation of the experimental results. The aim of volatile signature identification experiments using 3D spheroid method is to prove the existence of gastric cancer associated volatile signatures. This *in vitro* confirmation is very important before pursuing a clinical study. Furthermore, a specialized breath collection instrument was developed to collect end-tidal breath from human subjects. Our next study is to collect and identify the VOCs in the exhaled breath samples of gastric cancer subjects and non-gastric cancer subjects. Our aim of this study is to compare the VOCs of gastric cancer cohort and non-gastric cancer cohort, to identify breath biomarkers of gastric cancer.

Chapter 7

Identification of Non-Invasive Breath Biomarkers for the Diagnosis of Gastric Cancer- A Clinical Study

7.1. Background:

According to World Health Organization, gastric cancer (0.72 million deaths) ranks third in cancer mortality worldwide in 2012, with the highest incidence in the Asia-Pacific region [1]. Given high global incidence rate, early diagnosis of gastric cancer appears to improve survival rates [183]. The gold standard for the diagnosis of gastric cancer is esophagogastroduodenoscopy (EGD) and biopsy. When a doctor identifies an abnormal tissue area through EGD, he/she will perform a biopsy of the suspected tissue followed by the microscopic examination. However, this is expensive and invasive; hence it is not a cost-effective screening tool for most countries.

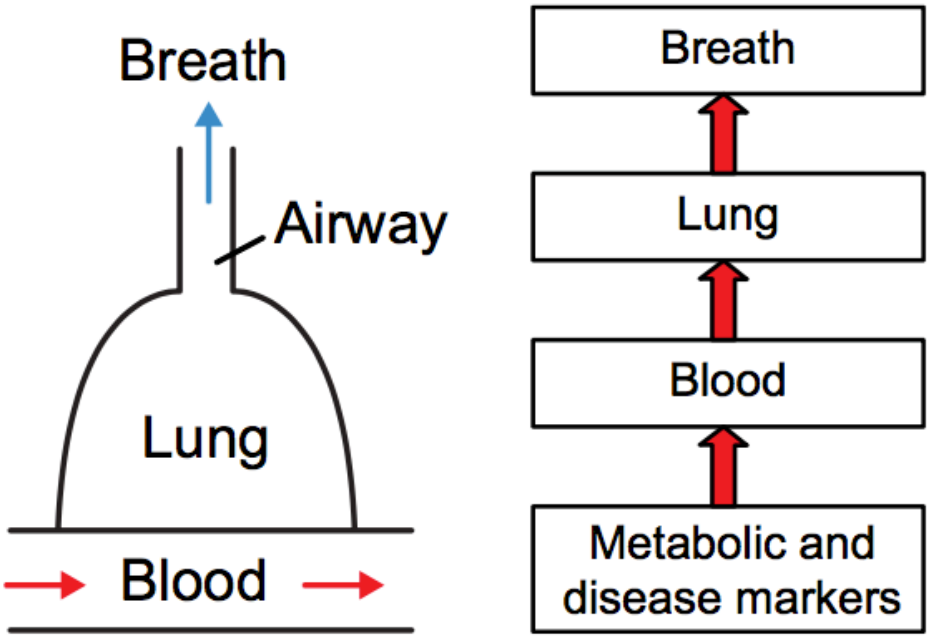

Figure 7.1: Schematic diagram showing the link between blood and exhaled breath [**Source:** 241].

Previous studies in this thesis have shown that cells release VOCs in response to its physiological and pathological conditions. The volatiles released by the cells are dissolved in the blood. These VOCs were carried to the alveoli via blood flow and excreted out during exhalation [184]. Many prior studies have identified several breath based biomarkers for various diseases including cancer. In breath research for cancer diagnosis, studies on lung cancer dominate due to lung's association in gaseous exchange and exhalation. Gordon et al. (1985) compared the breath VOCs of lung cancer subjects and healthy subjects and identified acetone, methyl ethyl ketone, and n-propanol as potential biomarkers of lung cancer [185]. Michael Phillips et al. (2003) developed a diagnostic, predictive model based on the VOCs identified in exhaled breath and identified primary lung cancer with a sensitivity of 89.6% and specificity of 82.9% Whereas, metastatic lung cancer was detected with a sensitivity of 66.7% [186].

In an another study Chen et al. reported styrene, decane, isoprene, benzene, undecane 1-hexene, hexanol, propyl benzene, 1,2,4-trimethyl benzene, heptanal, and methyl cyclopentane as breath markers of lung cancer [187]. Ligor et al. (2009) identified 8 VOCs 1-propanol, 2-butanone, 3-butyn-2-ol, benzaldehyde, 2-methyl-pentane, 3-methyl pentane, n-pentane and n-hexane as potential breath biomarkers of lung cancer [27]. Bajtarevic et al. (2009) identified a set of 21 VOCs as the breath markers of lung cancer [188]. Fuchs et al. (2010) identified pentanal, hexanal, octanal and nonanal as the breath biomarkers for lung cancer [181]. Wang et al. (2014) had identified caprolactam and propionic acid as the lung cancer biomarkers [189]. Filipiak et al. (2014) compared the VOCs released by the lung cancer transformed cell lines, lung cancer tumors and exhaled breath of lung cancer patients. They identified ethanol and octane as the lung cancer biomarkers as these two VOCs are observed in all the three types of lung cancer samples [190].

Few studies investigate the breath biomarkers of cancers in the alimentary canal. Kumar et al. (2013) discovered 4 VOCs hexanoic acid, phenol, methyl phenol and ethyl phenol as the breath markers for oesophagogastric cancer [191]. In the latest study by the same group, 12 breath VOCs pentanoic acid, hexanoic acid, phenol, methyl phenol, ethyl phenol, butanal, pentanal, hexanal, heptanal, octanal, nonanal, and decanal were identified as the potential biomarkers of esophageal and gastric adenocarcinoma [192].

It is evident from the studies focused on the identification of the breath based lung cancer biomarkers that those studies are incomparable mainly due to the complexity of the disease, sampling methodology, subject recruitment criteria and demographic differences [193]. This finding could be true for gastric cancer also. Thus identification of the breath biomarkers for gastric cancer in Singapore population becomes imperative. Breath biomarkers for gastric cancer in Singapore population can be identified by comparing the volatile organic compounds (VOCs) in the exhaled breath obtained from gastric cancer patients and non-gastric cancer subjects, using Gas chromatography and mass Spectrometry (GC-MS). Given that the 13C urea breath test has become a popular non-invasive rapid diagnostic procedure for detecting H. pylori infection in the human stomach in the clinic [194]. Our objective is to develop a non-invasive method for gastric cancer detection through the volatile organic compounds (VOCs) biomarkers in the exhaled breath.

7.2. Methods and Materials:

7.2.1. DSRB approval and Subject recruitment:

This clinical study has been approved by the Domain specific review board (DSRB) Singapore. The DSRB approval letter has been included as appendix 3. A total of 22 exhaled breath samples (gastric cancer = 11 and Non-gastric cancer = 11) were collected and analyzed in this study. All the subjects were recruited after screened by the current gold standard diagnostic procedure namely esophagogastroduodenoscopy (EGD) (Table 7.1).

Subject Parameter	Gastric cancer Cohort	Non-gastric cancer cohort
Mean age (S.D) in years	62.2 (15.2)	62.3 (9.9)
Median age in years	67	64
Male	9	8
Female	2	3
Race: Chinese	9	10
Race: Others	2	1
Total number of subjects	11	11

Table 7.1: Details of the subjects participated in the study.

7.2.2. A sampling of exhaled breath:

The main criteria for the selection of gastric cancer and non-gastric cancer subjects were the presence and absence of gastric cancer tumor respectively, confirmed by the gold standard diagnostic method. All the other intragroup variations were allowed. These intra-group variations were intentionally allowed after considering the real clinical scenario. The main aim of this study is to differentiate between the gastric cancer subjects from non-gastric cancer subjects irrespective of the stage of gastric cancer. The two groups were age and gender matched. The subjects were in fasting and restricted from diet, smoking and alcohol consumption for 8 hours before esophagogastroduodenoscopy in order to minimize the background noises. The non-gastric cancer subjects were the people underwent the esophagogastroduodenoscopy because of their gastro intestinal problems other than cancer, which was also done intentionally in due consideration of the real clinical scenario where who come for the gastric cancer diagnosis will have either have gastric cancer of some other gastro intestinal problem. The breath samples were collected by trained paramedics. A demo video detailing the breath collection procedure is shown to the subjects before breath collection. For the breath sampling, the subjects need to undergo a simple procedure, which involves 3 minutes of lung flushing and followed by breath sampling. The lung flushing involves the deep inhalation (where the depth of inhalation is depends on the comfortability of the subjects) followed by exhalation for 3 minutes. The three minutes breathing was

performed to increase the volumetric lung capacity to maximize the gaseous exchange. Breath sampling involves the collection of end tidal breath in the custom-made glass end tidal breath collection device. The glass end tidal breath collection device was designed for capturing the last 55-60mL of the exhaled breath. Another glass collection device was used to trap the ambient air, which will act as the environmental control. An average human exhales approximately 500mL of air during each exhalation. In that 500mL only the last 350mL air is the result of gaseous exchange in lungs, which contains the crucial chemical information for the disease diagnosis [195]. The cancer patients will be either weak or aged so that they exhale a lesser volume of air when compared to the healthy volunteers. We took this into consideration and made the sampling volume to 55-60mL.

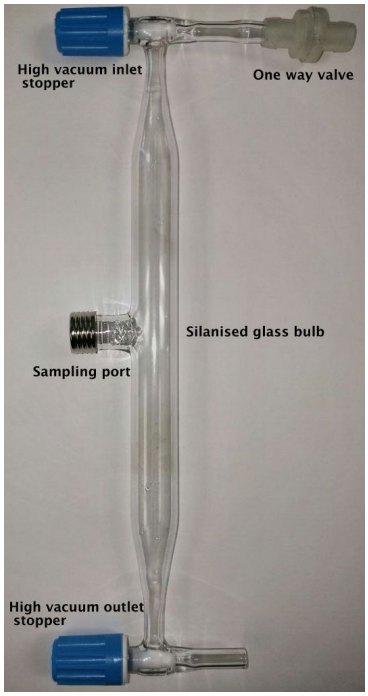

Figure 7.2 Custom-made silanized end-tidal breath collection tube.

The prime motivation for designing the custom-made silanized end-tidal breath collection tube was that the commercially available breath bags were found to be not suitable for our

study. These breath bags collect the entire breath which leads to the dilution of the end-tidal gas and increases background noise. In our previous study where we used the breath bags for breath, the collection gives only the background noise. So we designed our end tidal breath collection device (figure 7.2). Our device has 5 components namely one-way valve, high vacuum inlet stopper, glass bulb, sampling port and high vacuum outlet stopper. The design of the glass bulb is crucial. The slope between the inlet tube and the glass bulb should be minimum to reduce the air recirculation phenomenon. Another important factor is the silanization of the glass bulb. Silanisation will deactivate the highly reactive silanol groups on the glass surface. If silanization is not performed, these silanol groups will react with the polar gas compounds thus affecting the outcome of the experiment. When the subject blow air through the one-way valve the air travels through the glass bulb and exit through the outlet stopper. The subject is instructed to close the outlet stopper first when they are about to complete their exhalation, followed by the closure of the inlet stopper, thus trapping the last 55-60 mL of the end tidal breath. The trapped breath can be sampled from the sampling port, which is lined with gas tight replaceable Teflon septa.

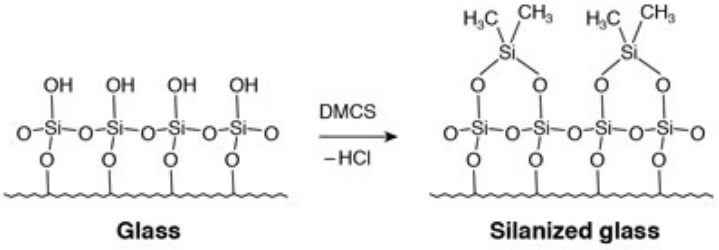

7.2.3. Solid Phase Micro-Extraction (SPME) sampling:

Solid-phase microextraction of the VOCs was performed using the CUSTODION® SPME Syringe, StableFlex needle, 23 GA with DVB/PDMS fiber (Torion Technologies Inc. USA). The DVB/PDMS fiber was carefully placed in the atmosphere of the end-tidal breath collection flask through the sampling port for 45 minutes at room temperature. After incubation, the fiber was carefully retracted into the syringe and taken out from the culture

atmosphere. The VOC metabolites were then identified using gas chromatography and mass spectrometry (GCMS) (Figure 7.3).

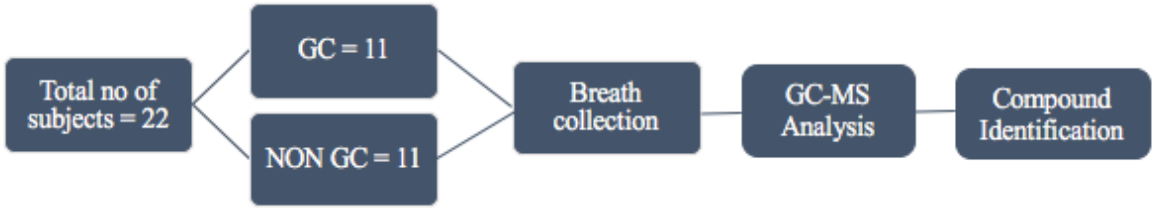

Figure 7.3: Experimental procedure of the clinical study.

7.2.4. Gas chromatography and mass spectrometry (GCMS):

The VOC metabolites were identified using gas chromatography and mass spectrometry (Shimadzu GCMS-QP2010 Plus system, Japan, with a 0.25 mm x 30 m DB-5MS column that had a 0.25um phase film thickness). The SPME syringe needle was inserted into the GCMS injection port and the fiber was extended for 10 minutes to allow for desorption of the VOC metabolites. Helium carrier gas was maintained at a flow rate of 1.0 mL/min. The initial GC oven temperature of 40°C was held for 5 minutes, followed by a temperature ramp of 5°C per minute up to 200°C followed by the second ramp of 10°C per minute up to 270°C. The mass spectrometer transfer line was maintained at 280°C, and the source temperature is 230°C. Mass spectra were repeatedly scanned from 20-700 m/z. The acquired mass spectrum was matched with the mass spectrums of the National Institute of Standards and Technology (NIST) MS spectral library and the mass spectrums NIST 08 mass spectral database, National Institute of Standards and Technology, Washington, DC, USA. The following quasi-linear equation for temperature-programmed retention indices was used to confirm the compound identification.

$$\mathbf{RI_X = [(t_X - t_n)/(t_{n+1} - t_n)]100 + 100n}$$

where RI_X is the temperature-programmed retention index of interest and t_n, t_{n+1}, t_X the retention time in minutes of the 2 standard n-alkanes containing n and n + 1 carbons and

index of interest, respectively [155].

7.2.5. SIFT-MS analysis for accessing the working of end-tidal breath collection tubes:

To access the suitability of the custom made end-tidal breath collection device, the collected breath samples were fed into the SIFT-MS (Voice 2000, New Zealand) at the rate of 25 standard cubic centimeters (sccm) using an 18-gauge needle. A full mass scan (M/Z range: 18 – 200) was performed with three reaction ions namely H_3O^+, NO^+ and O_2^+. The M/Z ratios and their corresponding counts were collected. For the convenience of data comparison, all the samples were analyzed on the same day one after the other. All the statistical analysis was performed by the MetaboAnalyst 3.0, online statistical software (www.Metaboanalyst.ca/, Canada) [54]. The collected M/Z ratios with their counts were converted into single concatenated vector in order make it compatible for the MetaboAnalyst 3.0. The product ion count rate depends on the precursor ion count rate which varies from day to day; we conducted a normalization procedure in which product count rates of each sample were divided by corresponding H_3O^+, NO^+, and O_2^+ precursor count rates [168]. Statistical methods, such as heat map analysis of the significant product ion M/Z ratios, clustering analysis, t-test, etc., were performed using MetaboAnalyst 3.0 after logarithmic normalization and auto scaling.

7.3. Results and Discussions:

7.3.1. The efficiency of breath collection tube:

The assessment of the effectiveness of breath collection tube in separating the end tidal breath from the total tidal volume is critical. To study this, we have compared the SIFT-MS breath profiles of the ambient air and the breath collected at the same place. The breath tubes are apt for the breath studies, if and only the difference between these samples mentioned above were strikingly different. Figure 7.4 shows eight heat map depicting the significant variation in the volatile profiles between eight breath samples (VB series) and their

corresponding ambient samples (Control). From the heat maps, it is clear that the variation of the breath profiles is radically different from its ambient samples. Thus, we conclude that these breath collection tubes were suitable for the end tidal breath collection.

7.3.2. Breath biomarkers of gastric cancer:

GC-MS analysis of the breath samples results in the identification of 69 VOCs. Among the 69 VOCs, 19 were observed only in the gastric cancer cohort and 35 VOCs were found exclusively in the non-cancer group. However, 15 VOCs were noted in both cancer and non-cancer group (Figure 7.5). Among these 19 breath markers associated with the gastric cancer group only 9 markers were identified by retention index identity. In a complex disease like cancer, where each and every tumor is unique, it is highly impossible to determine a single or few compounds that could identify all the gastric tumors. Hence, the aim of this study is to define a panel of VOCs that are observed only in the gastric cancer cohort. In this perspective, the 19 VOCs (Table 7.4) found in gastric cancer were considered as gastric cancer specific breath biomarkers.

7.3.3. Lipid peroxidation is the major origin for the gastric cancer breath markers:

Silva et al. (2011) identified cymene as a volatile urinary biomarker for various cancers including colorectal cancer, leukemia, and lymphoma. Bajtarevic et al. (2009) and Mochalski et al. (2014) described that cymene could be of exogenous origin and excluded this compound from their biomarker list [188, 196, 197]. Hence considering cymene as VOC biomarker of gastric cancer remains inconclusive. Sethi et al. (2013) observed tetradecanoic acid as one of the seven breath biomarkers for tuberculosis [167]. Perhaps, tetradecanoic acid and hexadecanoic acid or palmitic acid could be the product of lipid peroxidation induced by reactive oxygen species (ROS) [198]. Further, hexadecanoic acid was already reported as the biomarker for *in-vitro* cultured melanoma cells [199]. Alkanes and methylated alkanes were well known as the standard breath markers of lipid peroxidation in cancer cells [20, 21, 186

and 195]. Hence, compounds like isohexadecane, 2,6,10,15, tetramethyl heptadecane also could be the result of lipid peroxidation in gastric cancer cells which is a common event in cancer cells.

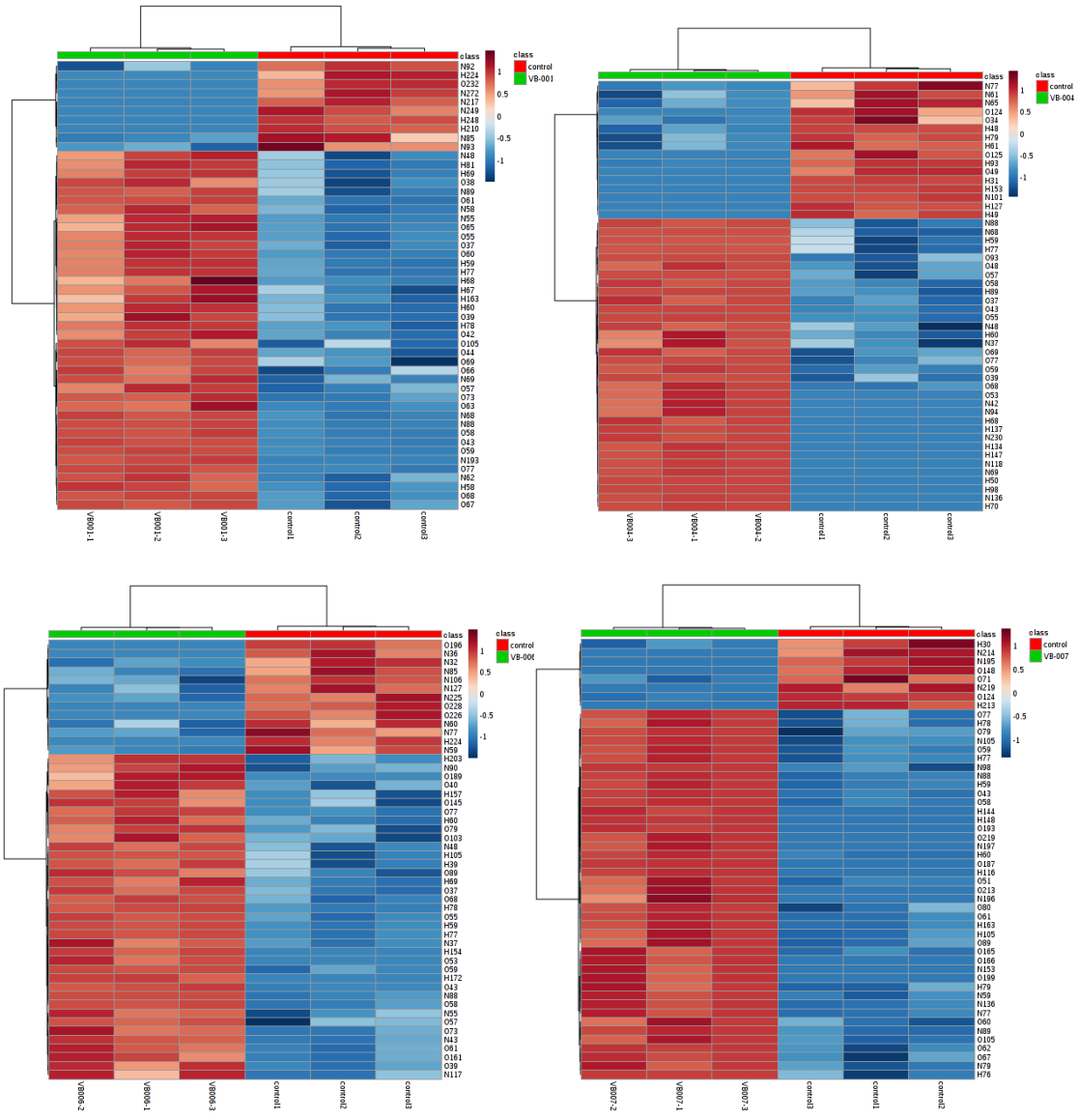

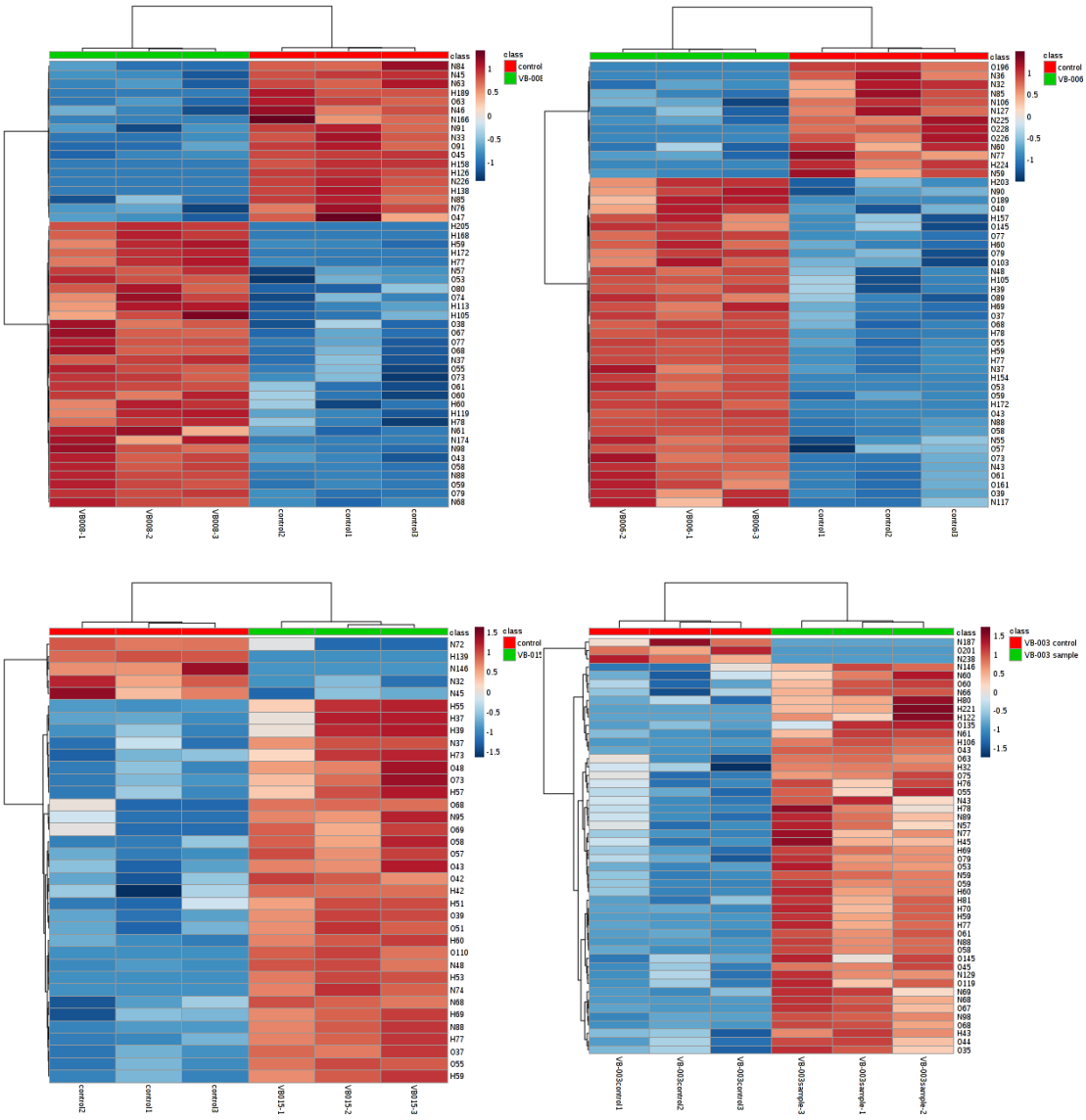

Figure 7.4: Heat maps showing eight heat map depicting the significant variation in the volatile profiles between eight breath samples (VB series) and their corresponding ambient samples (Control).

Figure 7.5: Venn diagram showing the number of breath biomarkers.

S. No	Breath markers		
	Gastric Cancer cohort	Non-Gastric cancer cohort	Observed in both cohorts
1	2,6,10-trimethyl dodecane	1-iododecane	Phenol
2	1-iodoheptane	1-iodo nonane	Indole
3	2-heptyl thiophene	Diisobutyl phthalate	Menthol
4	Tetradecanoic acid	2,3 pentanedione	Anethol
5	Palmitic acid	4-dodecanol	Carvone
6	Isohexadecane	Menthone	Limonene
7	2,6,10,15, tetramethyl heptadecane	Isomenthol	1,3-Dichlorobenzene
8	Cymene	Isopropyl phenol	1-Hydroxy-2,4,4-trimethyl-3-pentanyl 2-methylpropanoate
9	1-Iodododecane	Bornyl acetate	Eucalyptol
10	RT = 19.125	2,4-dimethylbenzaldehyde	Anisole
11	RT = 22.483	2-heptyl-1,3-dioxolane	Farnesene
12	RT = 22.967	7-Methoxy-3,7-dimethyloctanal	RT = 17.85
13	RT = 23.183	1-iodononane	RT = 23.358
14	RT= 23.267	3,5-Di-tert-butylphenol	RT = 28.625
15	RT = 26.442	1-iodoundecane	RT = 32.117
16	RT = 27.608	Menthofuran	
17	RT = 28.150	Neoisomenthol	
18	RT = 28.2	Caryophyllene	
19	RT = 28.675	Camphor	
21		6-Ethyl-2-methyldecane	
22		1,1'-[1,2-Propanediylbis(oxy)]di(2-propanol)	
23		4,5-Diethyl-3,6-dimethyl-3,5-octadiene	
24		Undecane, 2-methyl-2-phenyl-	
25		11-heptadecenal	
26		1-Iodoheptane	
27		3-Methyltridecane	
28		2-Ethyl-3-hydroxyhexyl 2-methylpropanoate	
29		RT = 13.508	
30		RT = 17.475	
31		RT = 17.983	
32		RT = 21.633	
33		RT = 21.908	
34		RT = 21.992	
35		RT = 26.692	

Table 7.2: List of identified breath biomarkers (RT- Retention time).

7.3.4. Probable origins of the breath VOCs observed in both cohorts:

Phenol, Anethol, and menthol were two common ingredients of commercial mouthwashes [200, 201]. Thus, these two compounds were exogenic, arise from the mouthwashes used by the subjects. Carvone belongs to the terpenoid family of compounds usually, present in the caraway seeds and spearmint. Caraway oil (60% carvone) and spearmint oil (80% carvone) is a common ingredient in any commercial toothpastes and mouthwashes [202, 203].

Indole was observed as a result of oral malodor as this compound is closely associated with oral halitosis [204]. Limonene is commonly used in foodstuff and cleaning agents and halogenated compound like 1,3-dichlorobenzene should also potentially from exogenous origin [188]. 1,3-dichlorobenze had been identified in the breath of lung cancer patients, but it is not considered as a biomarker as the standard deviation is not within the acceptable range [205]. Eucalyptol (1,8-cineol) was observed potentially due to the administration of certain common medications as it is an active agent in the common non-prescription drugs used to remove airway blockages [206]. Anisole was also from exogenous sources, which traces its origin from medications or perfumes as anisole is a common precursor for pharmaceuticals and perfumes [207]. It is noteworthy that anisole is also claimed as urinary VOC biomarker for colon cancer [196]. Sophia et al. identified farnesene as one of the three breath biomarkers for invasive aspergillosis [208] but we consider farnesene could be exogenous from unidentified sources. The other unidentified compounds might also trace their origin either in the halitosis or from the products used for oral hygiene, diet and medications but yet to be confirmed.

7.3.5. Critics of the prior studies focused on identifying breath biomarkers for gastric cancer:

In the previous studies by Kumar et al. Phenol has been reported as gastric cancer breath marker, which contradicts our results. In the prior studies mentioned above, the authors suggested that the phenol was observed as a consequence of the increase in tyrosine breakdown by citing the studies of Deng et al. (2012) [191, 192]. Deng et al. showed that the elevated levels of aromatic amino acids like tyrosine and phenylalanine were associated with gastric cancer [209]. Unfortunately, there are no prior studies to show high levels of tyrosine breakdown in gastric cancer. Thus making the Kumar et al.'s proposal on explaining the phenol in breath invalid. In an another study, Amal et al. (2015) accessed the validity 8 VOCs as gastric cancer breath markers [210]. The authors concluded that 7 of these 8 VOCs were capable of detecting gastric cancer, but their data suggests that the standard deviation (SD) of the cancer cohort is too high and not acceptable if SD was taken into account. This discrepancy is attributed to the complexity of the disease making it tough identify VOCs that are unique to all the cases of gastric cancer. Thus, the better approach for detecting gastric cancer from exhaled breath is to define a panel of Breath markers that are only observed in the gastric cancer cohort. Gastric cancer could be diagnosed by looking at any one or more identified panel of breath markers in the subject's exhaled end-tidal breath.

7.3.6. Differences in the volatile biomarkers of gastric cancer *in vitro* and *in vivo*:

It is evident from the chapter 6 and chapter 7 that there is no correlation between the volatile biomarkers identified from the *in vitro* models and *in viv*o studies. This is expected because in the *in vitro* condition the volatile signatures of the specific cancer tumor model could be identified, whereas in the *in vivo* condition the volatile signatures we identify would be the collection of the volatiles released by the all the cells in the body due to their physiological and pathological status and the reaction products of these released volatiles. The idea behind

identifying cancer specific volatile biomarker *in vivo* is that cancer cells would produce unique volatile organic compounds (VOCs) as by product of cancer specific metabolism and get dissolved in the blood. These VOCs could react with the other VOCs that are produced by other cells and results in the reaction products that could be observed only in the presence cancer. These unique cancer-related VOCs can be observed in the exhaled breath as a result of alveolar gaseous exchange.

7.4. Conclusion:

This study showed the successful employment of the custom made end-tidal breath collection tubes in the gastric cancer biomarker identification from exhaled breath. A panel of 17 compounds associated with gastric cancer was identified, and their possible origin was discussed. Previous studies and their conflicts with the current study were addressed and explained. The effect of oral hygiene product usage was reflected in this study, which suggests that it is better to avoid the oral care products before breath collection.

7.5. Summary:

This study portrays the discovery phase of the clinical study for the identification of gastric cancer biomarkers in exhaled breath. The custom made reusable end-tidal breath collection tube was successfully used in this gastric cancer biomarker identification studies. 17 VOCs that are associated with gastric cancer were identified, and among these 17 only 8 compounds names were identified. The majority of the identified compounds were associated with the lipid peroxidation of the cell membranes. 8 VOCs were observed in both gastric cancer and non-gastric cancer cohorts. All these 8 compounds trace their origin in either oral halitosis or oral care products. Hence, it is better to avoid the use of oral care products before breath collection to increase the signal to noise ratio. Though breath based non-invasive biomarkers for gastric cancer is identified, a low-cost, reliable, easy to operate, reusable and a compact

diagnostic tool is essential for mass screening procedures. Hence, the next step is to develop a novel chemiresistive sensing tool that satisfies all the requirements mentioned above.

Chapter 8

Florisensors: A novel flower-based chemiresistive volatile sensors

8.1. Background:

Olfaction in animals depended on their nose. Nose is a very delicate chemical sensor that can detect and discriminate between various gases [211]. Nose is an array of sensors with less specificity. Hence one sensing molecule can respond to many gases, and one gas can stimulate many sensing molecules present in the nose. These stimulations of the sensing molecules are interpreted by the olfactory cortex in the brain resulting in the odor detection [212-214]. There many continuous effects to replicate this olfaction using chemical sensors. Chemical sensor arrays were developed leading to the electronic nose that can simulate olfactory system of animals. In the electronic noses, the odors were detected from the pattern obtained from the responses of all the individual chemical sensors in the electronic nose [215]. The commonly used chemical sensors in e-nose were known as chemiresistors. The chemiresistive sensors change its resistances in response to their chemical environment. Chemiresistive sensors consist of a sensing material coated across the metal electrodes. When chemical vapors were exposed to these sensors, the vapors tend to percolate into the sensing materials and results in the swelling of the sensing material. This swelling alters the resistivity of the sensing material, thus increasing the resistance. The extent of percolation is depended on the partition coefficient of the gaseous vapor to the corresponding sensing material. This percolation phenomenon is reversible, thus making these sensors reusable [216].

Conducting polymer composites, intrinsically conducting polymers and metal oxides are the commonly used sensing materials in the chemiresistive sensors. In the case of metal oxide

sensors, in particular, a heater is used as the high temperature is the prerequisite for the proper functioning of these sensors, thus making these sensors less energy efficient [217, 218]. Conducting polymer composite based sensors are another class of chemiresistive sensors that uses conducting particles interspersed in insulating polymer matrices [219]. Most of the constituents of the conducting polymer composite based sensors were either expensive or hazardous. For instance, the most common conducting particle used is polypyrrole, which is prepared by the polymerization of pyrrole using phosphomolybdic acid in a solution of insulating polymer [220]. The resistance changes of polypyrrole sensors in response to the odor molecules were tough to predict as the chemical interaction of the odor molecules with the conducting polymer can also change in the intrinsic conductivity of the polypyrrole molecules. Another common type is the carbon black based composite sensor, which is hazardous as carbon black is a well-known carcinogen.

Further nanomaterials such as functionalized gold nanoparticles, graphene and carbon nanotubes (CNTs) were also used as chemiresistors [221-226]. DNA functionalized graphene and nanomaterials were shown to exhibit chemiresistive properties in a sequence-dependent manner [226]. The drawbacks of these materials are that they are very expensive and requires hazardous chemicals and conditions for their preparation. Moreover, pristine graphene and CNTs were not sensitive enough for the chemiresistive applications. Hence additional step of creating defects in graphene and CNTs were required to enhance sensitivity [225].

Hence, a new sensing material, that is low-cost, easy to prepare and environmental friendly is highly needed. In this study, the possibility of using plant based extracts as the sensing material for developing chemiresistors was investigated. Reports from early 1980's showed that herbivore-induced volatiles released by the damaged leaves act as volatile cues for the undamaged leaves for enhancing their defenses against herbivore damage [227-229]. Plants,

when exposed to a green leaf volatile such as cis-3-hexenyl acetate and others results in the priming of the defense genes that mediate oxylipin signaling and direct defenses and defense metabolites like jasmonic acid and linolenic acid [230, 231]. *Cuscuta pentagona,* parasitic plant of *Lycopersicon esculentum* (Tomato) used the volatile cues for identifying the location of the host [232]. It is also demonstrated that the tobacco plant suffered lesser herbivore attack when grown near the clipped sagebrush than the tobacco plants grown near unclipped sagebrush [233 - 235]. An interesting study shows that lima beans produced more extrafloral nectar for attracting predators in response to the herbivore attack [236]. These studies clearly suggested that plants can perform olfaction, which means plants can detect and discriminate volatile compounds and respond to these volatile cues. Hence, we hypothesize that plant extracts can be utilized as chemiresistive sensing material in the volatile sensors. The objective of this study is to investigate the feasibility of using plant extracts as the volatile sensing material in the chemiresistive sensors. In this study, we show the capability of the plant extracts to function and sensing material in the chemiresistive sensors. As plant extracts are low-cost, non-hazardous, environmentally friendly and renewable, plant extracts have high potential in substituting energy inefficient, expensive and hazardous chemiresistive sensing materials.

8.2. Methods and materials:

8.2.1. Extraction of sensing material:

Two plant species were selected for the fabrication of the florisensors namely *Caesalpinia pulcherrima* (*C.pulcherrima*) and *Ixora coccinea (I.coccinea)*. Sepals and petals from the Caesalpinia pulcherrima were separated and used to make two florisensors one with sepals and other with petals. Whereas, in Ixora coccinea, only the petals were used to make florisensors. Thus, in this study, we are investigating three florisensors. The flower materials

of these two plants were freshly collected and ground with a pestle as soon as possible. Ethanol was added as the extraction solvent in the concentration of 1μL/5mg of the grounded flower material, followed by further grinding of the flower material with ethanol. The extract was separated from the plant debris by ultracentrifugation at 10,000 rpm for 15 mins. The supernatants were saved forming the sensing material of the florisensors.

8.2.2. Fabrication of the sensor:

Commercially available wire glue is used as the base conductive layer. PET sheets are cut into required dimensions and terminals were created using copper strips and connecting pins. The flower based sensing material is embedded on the base conductive layer by drop casting method. In total 250 μL of the sensing, material was drop cast of the base layer. For the control sensor, 250μL of ethanol (extraction solvent) alone was drop cast on the base layer. Four sensors were mounted on the plastic lid a sensor array. The estimated cost of fabrication of the florisensor version described in the thesis would be 0.15-0.20 SGD per florisensor excluding work force cost. The cost of the florisensor array would depend on the number of florisensors used in the array(n). Hence, the total cost of florisensor array excluding workforce cost would be equal to n x (0.15) SGD to n x (0.20) SGD.

8.2.3. Sensing milk to yogurt conversion:

To test the chemiresistive functionality of the florisensors, we set up an experiment to check whether these sensors could detect the milk spoilage. 5 mL of cow's milk is taken from the 1L milk pack bought from the local supermarket. A 100 μL of yogurt is added to the 10mL milk followed by closing it with a lid on which the sensor array was mounted. The resistance of the sensors at time zero was deduced and noted. Resistance readings were recorded for every 1 minute till the total duration of 12 hours using the voltage divider circuit connected to

the micro controller (Arduino Mega 2650). This entire experiment is repeated thrice, and the change in resistance is calculated from the obtained resistance readings (Eq. 1).

$$\Delta R = R_t - R_0 \qquad \text{Eq.1}$$

8.2.4. Chemiresistive sensing of different flavors of smoothies:

We set up another experiment, wherein the ability of the florisensor array to sense different flavors of smoothies were accessed. 5 mL of smoothie is taken in a glass beaker, and the beaker is closed with the lid on which the florisensor array is mounted. The resistance readings of the sensor array were recorded every 1 minute using the voltage divider circuit connected to the micro controller (Figure 8.1). This entire experiment was repeated thrice for each smoothie flavor, and the change in resistance is calculated from the obtained resistance readings (Eq. 1)

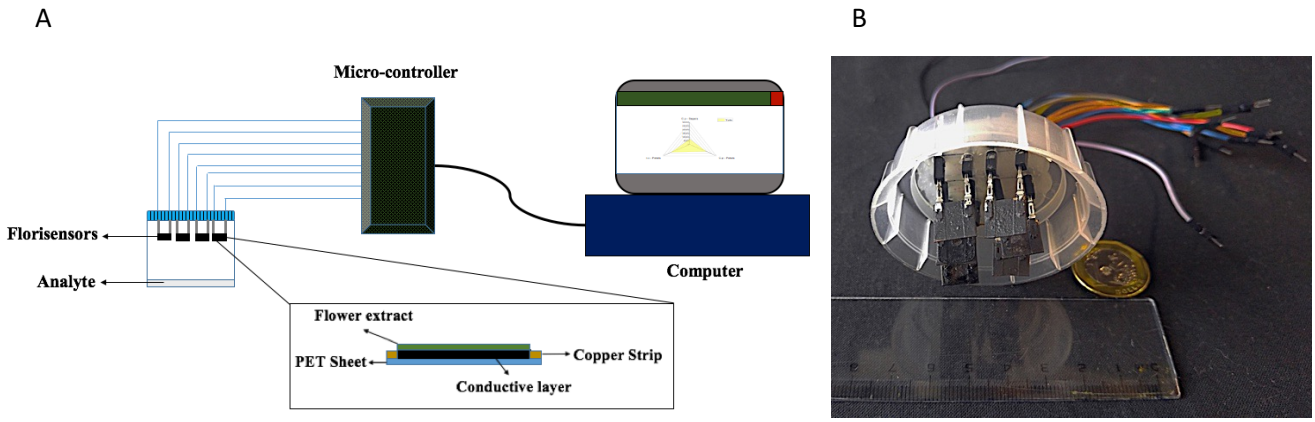

Figure 8.1: A: Experimental setup and schematic representation of the florisensor. B: Florisensor array.

8.3. Results and discussion:

8.3.1. Discriminating different flavors of smoothies:

The differential resistance (ΔR) values from the recorded resistance values were calculated followed by deducing the mean differential resistance and standard deviation. Figure 8.2

shows the ΔR responses of all the four sensors to the headspace volatiles of different flavors of smoothies. It is evident that the responses of the florisensors vary with the various flavors of smoothies and the control sensors did not show any significant variation, thus proving the chemiresistive properties of these florisensors. It is also observed that each flavor provoked distinct response pattern in the florisensor array, which suggests that, it is possible to discriminate different flavors of the smoothie based on the response pattern of the florisensors array. Radar chart was plotted using the ΔR values at which the sensor responses get saturated to visualize these distinct patterns, (Figure 8.3). It becomes evident that each and every flavor of the smoothie shows a distinct pattern in the radar chart. Thus the responses from these three florisensors were sufficient to discriminate all the 6 flavors of the smoothie tested. It is interesting to note that the strawberry flavor and mixed berry flavor shows very slight differences, which might be because of the phylogenetic closeness of berries.

The variation in the resistances when exposed to the smoothies was attributed to the percolation of the volatiles into the sensing layer causing swelling and resulting in the resistance change. The specificity of these sensors was attributed to the partition coefficient of the volatiles in the sensing layer. If the exposed volatiles have high partition coefficient to the sensing layer, more volatiles percolate into the sensing layer causing more swelling resulting more change in resistance. Whereas, if the partition coefficient is low to the sensing layer, only few volatiles percolate causing less swelling leading to the minor change the resistance. Here, the partition coefficient depends on the plant extract which is used as the sensing layer. Hence, different plant extract responds differently to different volatiles thus creating distinct response patterns. The control sensor does not respond to the volatiles. Hence the partition coefficient of these volatiles in this sensor should be near zero.

Interestingly the sensor, in which *C.pulcherrima* sepal extract is used as the sensing layer does not vary drastically between different smoothies. This observation might be because partition coefficients of these volatiles were not radically different in this sensor, unlike the other two sensors. Hence, petal extract base florisensors were more informative than sepal extract based florisensors.

Time taken by these sensor arrays to produce a stable saturated reading when exposed to an analyte is the limitation which was around 120 minutes. This limitation can be solved if we consider the rate of change in resistance as output instead of the saturated change in resistance reading.

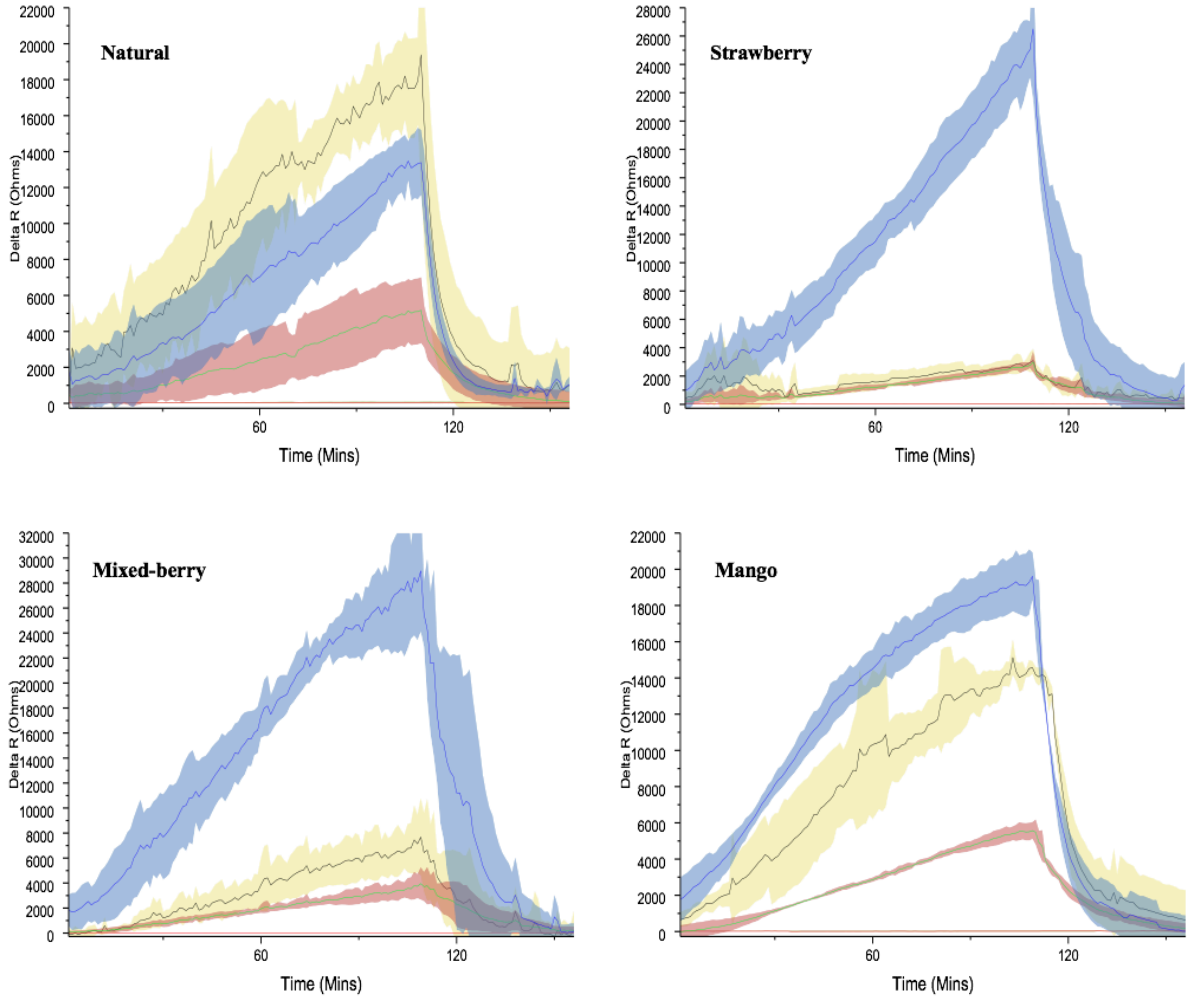

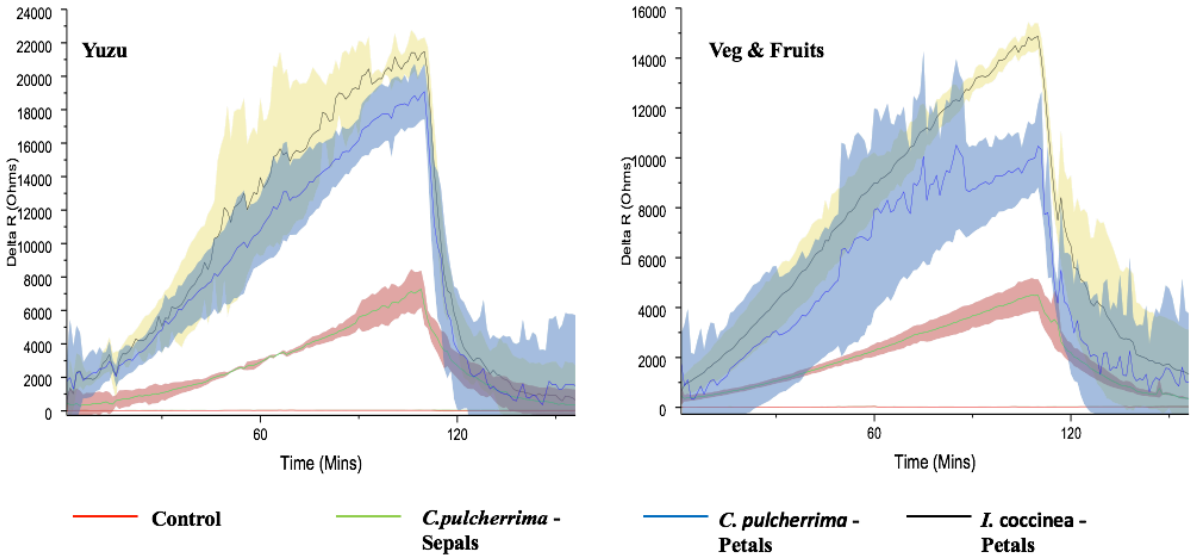

Figure 8.2: Chemiresistive responses of the florisensors and control when exposed to different flavors of smoothies.

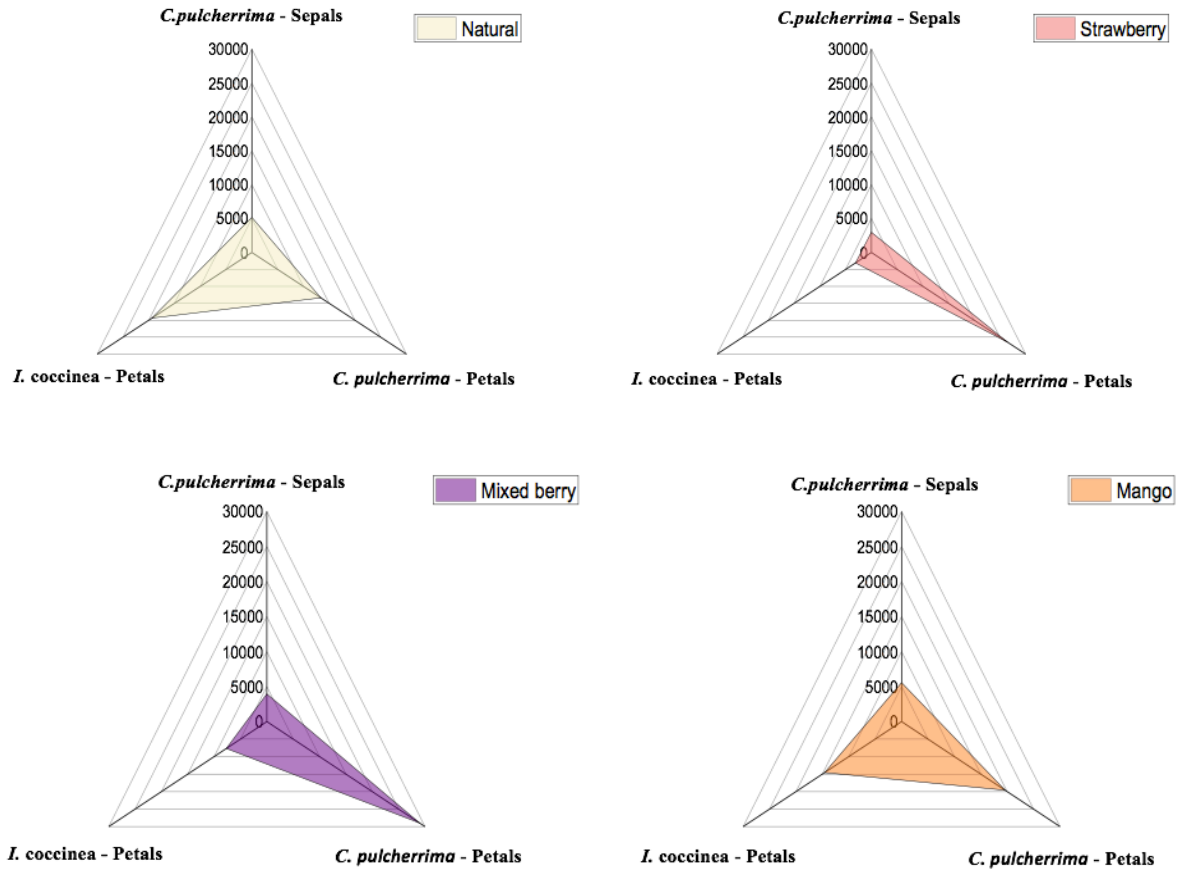

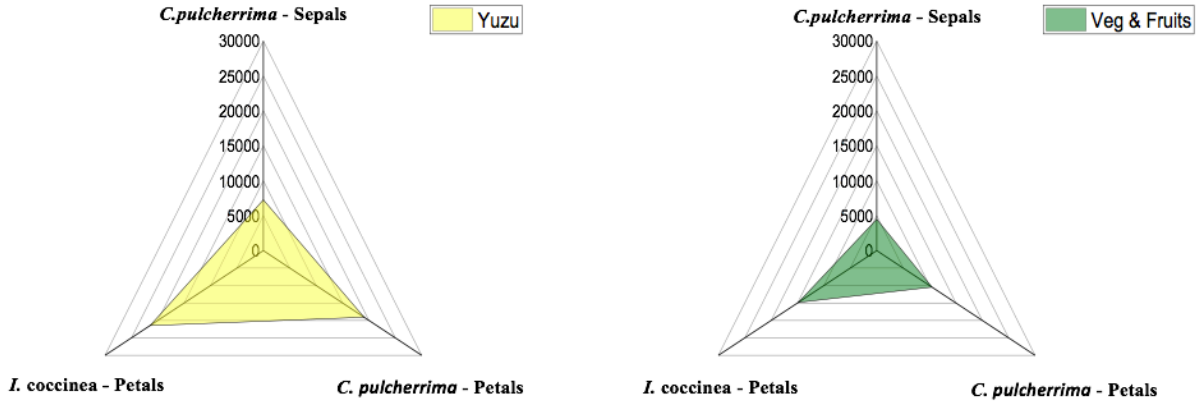

Figure 8.3: Radar plot showing the distinct pattern of the florisensor responses when exposed to different flavors of smoothies.

8.3.2. Milk to yogurt conversion:

Figure 8.4 shows the responses of the florisensor array in response to the conversion of milk to yogurt. From this plot, it was evident from the sensors drop-casted with *C.pulcherrima* petals and *I.coccinea* petals that milk to yogurt conversion completes in about 4 hours. The *C.pulcherrima* sepals based florisensor does not saturate and tend to have a linear curve. This data shows that this sensor does not have specificity towards the volatiles produced due to yogurt formation. Thus, this sensor allows percolation of all the volatiles in the headspace resulting in the linear curve as the concentration of the headspace volatiles would increase with the yogurt formation. However, this sensor indicates the continuous changes undergone by the analyte (Milk) due to the yogurt inoculation. It is important to note that these sensors tend to recover spontaneously when the volatiles were removed. There were nanoparticle based sensors which need other external stimuli like UV exposure, thermal energy for the sensor recovery [237, 238]. This feature makes these sensors more energy efficient over those expensive and energy inefficient chemiresistive sensors.

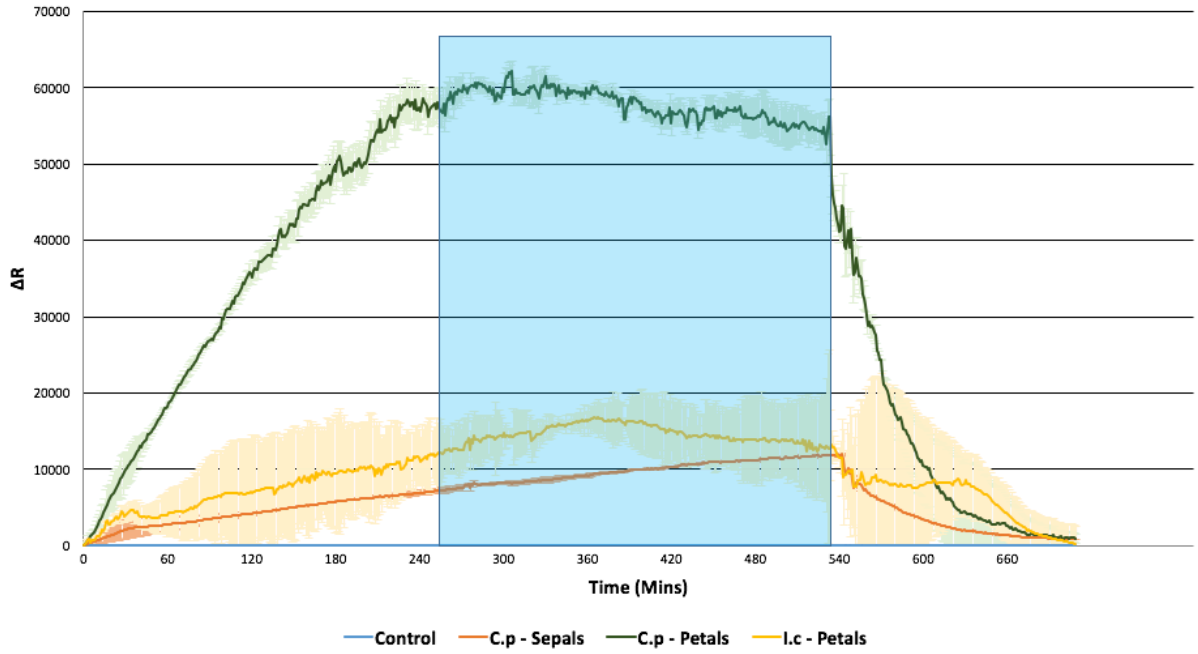

Figure 8.4: Chemiresistive responses of the florisensors and control to the conversion of milk to yogurt.

8.3.3. Specificity and sensitivity:

The specificity of the florisensors in identifying different analyte has been demonstrated. As florisensor array can able to detect and distinguish between different flavors of yogurt smoothies with the florisensor finger prints. The specificity of this florisensor array could be further improved by adding more florisensors in the array, thus increasing the dimensionality of the florisensor fingerprints. The reproducibility of the florisensor array (n=3) along with standard deviation values at each data point has shown in figure 8.2 and figure 8.4. This is a proof of concept demonstrating a novel way of volatile sensing by using the flower extracts. The future direction is to characterize these sensors, compare them with the existing volatile sensing platform regarding sensitivity and other sensor parameters and finally use this florisensor array to identify breath biomarkers.

8.4. Conclusion:

This study shows the capability of the flower extracts to act as the chemiresistive gas sensors. These were the first chemiresistive sensors that are made from renewable source. We also demonstrated that these sensor responses were reproducible as the standard deviation values were less enough to discriminate between different samples. The sensor fabrication is straightforward, easy, does not use hazardous or environment detrimental chemicals and low cost. This study shows that these florisensors were reusable and applicable to various real-time situations where gas sensing is indispensable. This study is a proof of concept demonstrating a novel way of volatile sensing by using the flower extracts. The future direction is to characterize these sensors, compare them with the existing volatile sensing platform regarding sensitivity and other sensor parameters. We also aim to investigate the feasibility of using these florisensor arrays in volatile based disease diagnosis such as cancer, tuberculosis, etc.

8.5. Summary:

Chemiresistors are the class of sensors widely used in volatile sensing. All the existing chemiresistors were expensive or use hazardous chemicals and physical conditions or energy inefficient. This study shows the development of a novel class of chemiresistors made from flower extracts, thus making these sensors renewable, low-cost and environmentally friendly. The chemiresistive abilities of these sensors were demonstrated by discriminating different flavors of smoothies and tracing the conversion of milk to yogurt. The spontaneous recovery of this sensor without any external stimulus is shown, thus making the sensor reusable. The future direction of this study is to increase the number of florisensors by incorporating various other flower extracts to increase the dimensionality, thus increasing the resolution of these florisensor arrays. The ultimate aim to develop a low-cost, reusable and reliable florisensor-array-based disease diagnostic device for the diagnosis of gastric cancer.

Chapter 9

Conclusion and Future Directions

This thesis is a series of comprehensive studies conducted to decipher the non-invasive ways of diagnosing cancer. On the course of pursuing these studies, novel methodologies and hypothesis were explored such as revealing the volatile signatures of *in vitro* 3D cancer models, cellular level quorum sensing, effect of curcumin treatment on the volatile signature of the cancer and non-cancer cells and florisensors – a novel low cost, renewable, reusable and eco-friendly chemiresistors for volatile sensing.

This thesis showed that two closely associated cell lines, which were obtained from the same donor and differed only in the stages of melanoma could be identified as different cell lines by employing 1D 1H NMR spectrometry, which proves the specificity of cell surface signatures in characterizing cancer cell lines. This study suggested that the glucose accumulation and phospholipid composition vary significantly between the primary and metastatic cells lines that were obtained from a single donor and also with the cell culturing methods. These results encourage further researches on understanding the effects of phospholipid and glucose accumulation in cancer development, progression, and invasion. This study also showed that the method of cell culture would drastically affect the phospholipid composition of the cells.

Proton NMR markers for differentiating gastric cancer spheroids and normal gastric spheroids were deciphered. Eight chemical shift markers that are unique to the gastric cancer spheroids were identified. We also demonstrated that 13 markers are significantly lesser in the gastric cancer spheroids compared to their normal counterpart. These markers indicate

that the cancerous and non-cancerous spheroids differ majorly in the energy metabolism, composition of lipid and lipid derivatives. This study opens up avenues for the researches focusing on identifying novel lipid targets in gastric cancer. This study also depicts that the formation of spontaneous spheroids is not a common trait for all the cell lines.

The *in vitro* results suggested the possibility of developing a non-invasive cancer diagnostic procedure based on the cancer specific cell-surface signatures using the MRI coupled with MRS. As this mode of diagnostic procedure requires a sophisticated and expensive facility, this method would not be a right choice to be employed in the developing and under developed regions of the world, which suffers high cancer-related mortality. Hence we did not proceed with the clinical study and found volatile biomarkers could be the potential alternative for developing non-invasive cancer diagnostic procedure.

Thus, the research focus changed towards identifying VOCs based cancer biomarkers. A novel method for the identification of the VOC signature of the cell lines using 3D models was shown. The VOC signatures of the 2D models were different from the 3D models. Two types of 3D models were developed, and their VOC signatures were evaluated. VOC signatures of both the 3D models were very similar, which suggests that direct cell-cell contact does not play any role in the VOC signature, providing an insight that these released VOCs could function as intercellular signals. As 3D cell culture models are the closest replica of the *in vivo* cells than 2D models, the VOC signature results of the 3D cell culture models would be more relevant for the clinical translation of these studies.

The cellular level quorum sensing in a human cell line was explored using the SIFT-MS. The significant product ion M/Z ratios obtained from the statistical analysis of the SIFT–MS data at higher cell density is highly significant and consistent. This study suggested the existence of the cellular level quorum sensing in the WM266 cells. According to the best of our

knowledge, this is the first study to show the existence of cellular level quorum sensing in mammalian cells. Histological study to validate the existence of cellular level quorum sensing in WM266 is also conducted. A cellular level quorum sensing model and its likely role in VOCs based cell signaling were proposed.

VOCs biomarkers for gastric cancer and effect of the anti-cancer drug curcumin were studied. This study used multicellular spheroids to reproduce the in vivo cellular microenvironment *in vitro* as close as possible. Acetaldehyde was found to be a potential volatile biomarker for diagnosing metastatic gastric cancer. These results were promising, hence translating this study into exhaled breath based gastric cancer detection is possible. All the normal gastric spheroids and gastric cancer spheroids studied produced specific volatiles in response to the curcumin treatment. Each and every cell line studied gave their unique response to the curcumin treatment by expressing unique volatile signatures. Observations on acetaldehyde expression by the metastatic gastric cancer spheroids after curcumin treatment suggest that these cells respond to curcumin in a dose-dependent manner. These volatile signatures would be useful in monitoring the progress of the curcumin treatment against cancer. This study was first of its kind, and still, there is a lot of research is yet to be done for relating the volatiles represented by the significant M/Z ratios with the established metabolic pathways, which would be indispensable in understanding the disease metabolism for the better ways of diagnosis and treatment.

A clinical study where the successful employment of the custom made end-tidal breath collection tubes in the gastric cancer biomarker identification from exhaled breath was demonstrated. A panel of 19 compounds associated with gastric cancer was discovered, and their possible origin was discussed. Previous studies and their conflicts with the current study were addressed and explained. The effect of oral hygiene product usage is reflected in this study, which suggests that it is better to avoid the oral care products before breath collection.

In future, more subjects will be recruited and more gastric cancer associated breath markers will be discovered. The future direction of this study will be the validation phase, where the results obtained in the discovery phase will be validated. The validation phase will be performed by selectively investigating the presence of this identified panel of VOC biomarkers in fresh breath samples. This validation study will provide us the specificity and sensitivity of the identified panel of VOC biomarkers.

A novel low-cost, reusable and reliable chemiresistive sensors were required to develop a VOCs based cancer diagnosis platform. A study was conducted showing the capability of the flower extracts to act as the chemiresistive gas sensors. These were the first chemiresistive sensors that are made from renewable source. We also demonstrated that these sensor responses were reproducible as the standard deviation values were less enough to discriminate between different samples. The sensor fabrication is straightforward, easy, does not use hazardous or environment detrimental chemicals and low cost. This study shows that these florisensors were reusable and applicable to various real-time situations where gas sensing is indispensable. The future direction is to increase the number of florisensors by incorporating various other flower extracts to increase the dimensionality, thus increasing the resolution of these florisensor arrays. These florisensor arrays may also hold great potential in volatile-based disease diagnosis such as cancer, tuberculosis, etc.

References

1. Globocan 2012, IARC.
2. http://www.cancer.org/acs/groups/cid/documents/webcontent/002048-pdf.pdf.
3. Gallucci BB. Selected concepts of cancer as a disease: From the Greeks to 1900. Oncol Nurs Forum. 1985; 12:67-71.
4. American Society of Clinical Oncology. Progress & Timeline. Accessed at www.cancerprogress.net/timeline/major-milestones-against-cancer.
5. Diamandopoulus GT. Cancer: An historical perspective. Anticancer Res. 1996;16:1595-1602.
6. Devita VT Jr, Rosenberg SA. Two Hundred Years of Cancer Research. N Engl J Med. 2012;366(23):2207-2214.
7. Frush DP, Donnelly LF, Rosen NS. Computed tomography and radiation risks: what pediatric health care providers should know. Pediatrics 2003; 112(4):951–957.
8. Pearce MS, Salotti JA, Little MP, et al. Radiation exposure from CT scans in childhood and subsequent risk of leukemia and brain tumors: a retrospective cohort study. Lancet 2012; 380(9840):499–505.
9. https://www.cancer.gov/publications/patient-education/skin.pdf.
10. http://www.cancer.org/acs/groups/cid/documents/webcontent/003141-pdf.pdf.
11. American Cancer Society. Cancer Facts & Figures 2016. Atlanta, Ga: American Cancer Society; 2016.
12. American Joint Committee on Cancer. Stomach Cancer. In: AJCC Cancer Staging Manual. 7th ed. New York, NY: Springer; 2010: 117–121.
13. Chen, J. et al Metabolomics of gastric cancer metastasis detected by gas chromatography and mass spectrometry. World Journal of Gastroenterology 2010; 16, 5874.
14. Wu, H. et al. Metabolomic investigation of gastric cancer tissue using gas chromatography/mass spectrometry. Analytical and bioanalytical chemistry 2010; 396, 1385–95.
15. Hu, J.-D., Tang, H.-Q., Zhang, Q., Fan, J., Hong, J., Gu, J.-Z., & Chen, J.-L. Prediction of gastric cancer metastasis through urinary metabolomic investigation using GC/MS. World Journal of Gastroenterology 2011; WJG, 17(6), 727–34. http://doi.org/10.3748/wjg.v17.i6.727.
16. Buszewski B, Kesy M, Ligor T, et al. Human exhaled air analytics: biomarkers of diseases. Biomed Chromatogr 2007;21:553-66.
17. Donovan A, Antoine Lavoisier: Science, Administration, and Revolution. Cambridge science biographies series. 1996, Cambridge; New York: Cambridge University Press.
18. Mueller J. Über die Ausscheidungsstätten des Acetons und die Bestimmung desselben in der Athemluft und den Hautausdünstungen des Menschen. Arch Exp Pathol Pharmacol 1898; 40: 315 - 362.
19. Pauling, L., Robinson, a B., Teranishi, R. & Cary, P. Quantitative analysis of urine vapor and breath by gas-liquid partition chromatography. Proc. Natl. Acad. Sci. U. S. A. 1971; 68, 2374–6.
20. Phillips, M. et al. Volatile markers of breast cancer in the breath. Breast J. 2003; 9, 184–91.

21. Phillips, M. et al. Breath biomarkers of active pulmonary tuberculosis. Tuberculosis (Edinb) 2010; 90, 145–51.
22. Boots, A. W. et al. The versatile use of exhaled volatile organic compounds in human health and disease. J. Breath Res. 2012; 6, 027108.
23. Amann, A. et al. The human volatilome: volatile organic compounds (VOCs) in exhaled breath, skin emanations, urine, feces and saliva. J. Breath Res. 2014; 8, 034001.
24. Calenic, B., Filipiak, W., Greabu, M. & Amann, A. Volatile Organic Compounds Expression in Different Cell Types: An *In vitro* Approach. 43–51 (2013).
25. Understanding NMR Spectroscopy, James Keeler, John Wiley & Sons. ISBN-13 978-0-470-01786-9.
26. K.D. Bartle, P. Myers, History of gas chromatography, TrAC Trends in Analytical Chemistry 2002; 21: 547-557.
27. M. Ligor, T. Ligor, A. Bajtarevic, C. Ager, M. Pienz, M. Klieber, H. Denz, M. Fiegl, W. Hilbe, W. Weiss, P. Lukas, H. Jamnig, M. Hackl, B. Buszewski, W. Miekisch, J. Schubert, A. Amann, Determination of volatile organic compounds in exhaled breath of patients with lung cancer using solid phase microextraction and gas chromatography mass spectrometry, Clinical Chemistry and Laboratory Medicine 2009; 47: 550-560.
28. Vas.G., Ve´ key .K. Solid-phase microextraction: a powerful sample preparation tool prior to mass spectrometric analysis. J. Mass Spectrom. 2004; 39: 233–254.
29. N. Adams, D. Smith, The selected ion flow tube (SIFT); a technique for studying ion-neutral reactions, Int. J. Mass Spectrom. Ion Phys.1976; 21: 349-359.
30. D. Smith, P. Španel l, Application of ion chemistry and the SIFT technique to the quantitative analysis of trace gases in air and on breath, International Reviews in Physical Chemistry 1996; 15: 231-271.
31. P. Španel, D. Smith, A selected ion flow tube study of the reactions of NO+ and O2+ ions with some organic molecules: The potential for trace gas analysis, J. Chem. Phys. 1996; 104: 7.
32. D. Smith, P. Spanel, Ions in the terrestrial atmosphere and in interstellar clouds, Mass Spectrom. Rev., 1995; 14: 255-278.
33. P. Španel, D. Smith, Progress in SIFT-MS: Breath analysis and other applications, Mass Spectrometry Reviews, 2011; 30: 236-267.
34. P. Španel, K. Dryahina, D. Smith, Microwave plasma ion sources for selected ion flow tube mass spectrometry: Optimizing their performance and detection limits for trace gas analysis, International Journal of Mass Spectrometry, 267 (2007) 117-124.
35. P. Španel, D. Smith, Advances in on-line absolute trace gas analysis by SIFT-MS, Current Analytical Chemistry, 2013; 9: 525-539.
36. Negendank, W. Studies of Human Tumors by MRS: a Review. NMR in Biomedicine 1992; 5: 303-324.
37. Ruiz-cabellot, J., & Cohen, J. S. Phospholipid Metabolites as Indicators of Cancer Cell Function, NMR in Biomedicine 1992; 5: 226-233.
38. Bolan, P. J., Meisamy, S., Baker, E. H., Lin, J., Emory, T., Nelson, M., Everson, L. I., Yee, D., Garwood, M. In Vivo Quantification of Choline Compounds in the Breast with ^{1}H MR Spectroscopy. Magnetic Resonance in Medicine 2003; 50: 1–10.

39. Bolan, P. J., Nelson, M. T., Yee, D., & Garwood, M. Imaging in breast cancer: Magnetic resonance spectroscopy. Breast Cancer Research 2005; 7: 149-152.
40. Jacobs, M. A., Barker, P. B., Bottomley, P. A., Bhujwalla, Z., & Bluemke, D. A. (2004). Proton Magnetic Resonance Spectroscopic Imaging of Human Breast Cancer: A Preliminary Study. Journal of Magnetic Resonance Imaging. 2004; 19: 68-75.
41. Gillies, R. J., & Morse, D. L. In vivo magnetic resonance spectroscopy in cancer. Annu. Rev. Biomed. Eng. 2005; 7: 287–326.
42. Koh, S. S., Wei, J.-P. J., Li, X., Huang, R. R., Doan, N. B., Scolyer, R. Binder, S. W. et al. Differential gene expression profiling of primary cutaneous melanoma and sentinel lymph node metastases. Modern Pathology 2012; 25(6): 828–837.
43. Riker, A. I., Enkemann, S. a, Fodstad, O., Liu, S., Ren, S., Morris, C., Matta, J. et al. The gene expression profiles of primary and metastatic melanoma yields a transition point of tumor progression and metastasis. BMC Medical Genomics 2008; 1: 13.
44. Le, T. T., Huff, T. B., & Cheng, J.-X. Coherent anti-Stokes Raman scattering imaging of lipids in cancer metastasis. BMC Cancer 2009; 9: 42.
45. Sounni, N. E., Cimino, J., Blacher, S., Primac, I., Truong, A., Mazzucchelli, G., Noel, A. et,al., Blocking lipid synthesis overcomes tumor regrowth and metastasis after antiangiogenic therapy withdrawal. Cell Metabolism 2014; 20(2): 280–294.
46. Sparling, M. L. Analysis of mixed lipid extracts using 1H NMR spectra. Computer Applications in the Biosciences: CABIOS 1990; 6(1): 29–42.
47. Podo, F. Tumor phospholipid metabolism, NMR in Biomedicine 1999; 12: 413–439.
48. Bolan, P. J., Baker, E. H., Bliss, R. L., Gulbahce, E., Everson, L. I., Nelson, M. T., Emory, T. H., Tuttle, T. M., Yee, D., Garwood, M. Neoadjuvant Chemotherapy of Locally Advanced Breast Cancer : Predicting Response with in Vivo 1 H MR Spectroscopy — A Pilot Study at 4 T^1. Radiology 2004; 233: 424-431.
49. Stretch, J. R., Somorjai, R., Bourne, R., Hsiao, E., Scolyer, R. a, Dolenko, B., … Lean, C. L. Melanoma metastases in regional lymph nodes are accurately detected by proton magnetic resonance spectroscopy of fine-needle aspirate biopsy samples. Annals of Surgical Oncology 2005; 12(11), 943–9.
50. Guitera, P., Bourgeat, P., Stretch, J. R., Scolyer, R. A., Ourselin, S., Lean, C., … Bourne, R. Diagnostic value of 8.5 T magnetic resonance spectroscopy of benign and malignant skin lesion biopsies. Melanoma Res 2010; 20(4), 311–317.
51. Bourne, R. M., Stanwell, P., Stretch, J. R., Scolyer, R. A., Thompson, J. F., Mountford, C. E., & Lean, C. L. In vivo and ex vivo proton MR spectroscopy of primary and secondary melanoma. European Journal of Radiology 2005; 53(3 SPEC. ISS.), 506–513.
52. Pohost GH, Elgavish GA, Evanochko WT. Nuclear magnetic resonance: with or without nuclear? J Amer Coll Cardiol. 1986; 7:709-710.
53. Manganas, L. N., Zhang, X., Li, Y., Hazel, R. D., Smith, S. D., Wagshul, M. E., Henn, F., Benveniste, F., Djuric, P. M., Enikolopov, G., Maletic-Savatic, M. Magnetic resonance spectroscopy identifies neural progenitor cells in the live human brain. Science 2007; 318: 980–985
54. Xia, J. & Wishart, D. S. Web-based inference of biological patterns, functions and pathways from metabolomic data using MetaboAnalyst. Nature protocols 2011; 6:743–60.

55. Guleria, A., Kumar Bajpai, N., Rawat, A., Khetrapal, C. L., Prasad, N., & Kumar, D. Metabolite Characterization in Peritoneal Dialysis Effluent Using High-resolution 1 H and 1 H-13 C NMR. Spectroscopy Magnetic Resonance in Chemistry 2014; 52(9): 475-479.
56. Allen, J. R., Prost, R. W., Griffith, O. W., Erickson, S. J., & Erickson, B. In vivo proton (H1) magnetic resonance spectroscopy for cervical carcinoma. American Journal of Clinical Oncology 2001; 24(5), 522–9.
57. Lean, C., Doran, S., Somorjai, R. L., Malycha, P., Clarke, D., Himmelreich, U., … Mountford, C. Determination of grade and receptor status from the primary breast lesion by magnetic resonance spectroscopy. Technol Cancer Res Treat 2004; 3(6), 551–556.
58. Behar, K. L., & Ogino, T. Assignment of resonance in the 1H spectrum of rat brain by two-dimensional shift correlated and J-resolved NMR spectroscopy. Magnetic Resonance in Medicine 1991; 17(2), 285–303.
59. Cheng, L. L., Lean, C. L., Bogdanova, A., Wright, S. C., Ackerman, J. L., Brady, T. J., & Garrido, L. (1996). Enhanced resolution of proton NMR spectra of malignant lymph nodes using magic-angle spinning. Magnetic Resonance in Medicine 1996; 36(5), 653–658.
60. Martínez-Granados, B., Monleón, D., Martínez-Bisbal, M. C., Rodrigo, J. M., del Olmo, J., Lluch, P., … Celda, B. Metabolite identification in human liver needle biopsies by high-resolution magic angle spinning 1H NMR spectroscopy. NMR in Biomedicine2006; 19(1), 90–100.
61. Mutsaers, J. H., van Halbeek, H., Vliegenthart, J. F., Wu, a M., & Kabat, E. Typing of core and backbone domains of mucin-type oligosaccharides from human ovarian-cyst glycoproteins by 500-MHz 1H-NMR spectroscopy. European Journal of Biochemistry / FEBS 1986; 157(1), 139–46.
62. Feng, J., Isern, N., Burton, S., & Hu, J. Studies of Secondary Melanoma on C57BL/6J Mouse Liver Using 1H NMR Metabolomics. Metabolites 2013; 3(4), 1011–1035.
63. Soliman, F. M. A., Dawoud, N. T. A., & Hamza, R. M. Synthesis, Biological and Anti-Tumor Evaluation of Some New Nucleosides Incorporating Heterocyclic Moieties. American Journal of Organic Chemistry 2015; 5(5), 137–148.
64. Abramov, Y., Carmi, S., Anteby, S. O., & Ringel, I. Ex vivo 1H and 31P magnetic resonance spectroscopy as a means for tumor characterization in ovarian cancer patients. Oncology Reports 2013; 29(1), 321–328.
65. Gottschalk, M., Ivanova, G., Collins, D. M., Eustace, A., O'connor, R., & Brougham. D.F. Metabolomic studies of human lung carcinoma cell lines using *in vitro* 1H NMR of whole cells and cellular extracts. NMR in Biomedicine 2008; 21: 448–467.
66. Asiago, V. M., Nagana Gowda, G. A., Zhang, S., Shanaiah, N., Clark, J., & Raftery, D. Use of EDTA to minimize ionic strength dependent frequency shifts in the 1H NMR spectra of urine. Metabolomics 2008; 4(4), 328–336.
67. Cox, I. J., Aliev, A. E., Crossey, M. M. E., Dawood, M., Al-Mahtab, M., Akbar, S. M., … Taylor-Robinson, S. D Urinary nuclear magnetic resonance spectroscopy of a Bangladeshi cohort with hepatitis-B hepatocellular carcinoma: A biomarker corroboration study. World Journal of Gastroenterology 2016; 22(16), 4191–4200.
68. Swanson, M. G., Zektzer, A. S., Tabatabai, Z. L., Simko, J., Jarso, S., Keshari, K. R., … Kurhanewicz, J. Quantitative analysis of prostate metabolites using 1H HR-MAS spectroscopy. Magnetic Resonance in Medicine 2006; 55(6), 1257–1264.

69. Wang, H., Wang, L., Zhang, H., Deng, P., Chen, J., Zhou, B., … Zhao, Y.-L. ^{1}H NMR-based metabolic profiling of human rectal cancer tissue. Molecular Cancer 2013; 12(1), 121.
70. Bell, J. D., Sadler, P. J., Macleod, A. F., Turner, P. R., & La Ville, A. 1H NMR studies of human blood plasma. Assignment of resonances for lipoproteins. FEBS Letters 1987; 219(1), 239–43.
71. 71. Eisner, R., Stretch, C., Eastman, T., Xia, J., Hau, D., Damaraju, S., … Baracos, V. E. Learning to predict cancer-associated skeletal muscle wasting from 1H-NMR profiles of urinary metabolites. Metabolomics 2011; 7(1), 25–34.
72. Swanson, M. G., Keshari, K. R., Tabatabai, Z. L., Simko, J. P., Shinohara, K., Carroll, P. R., … Kurhanewicz, J. Quantification of choline- and ethanolamine-containing metabolites in human prostate tissues using 1H HR-MAS total correlation spectroscopy. Magnetic Resonance in Medicine 2008; 60(1), 33–40.
73. Andronesi, O. C., Rapalino, O., Gerstner, E., Chi, A., Batchelor, T. T., Cahill, D. P., … Rosen, B. R. Review series Detection of oncogenic IDH1 mutations using magnetic resonance spectroscopy of 2-hydroxyglutarate. Journal of Clinical Investigation 2013; 123(9) 2013; 3659–3663.
74. Ramachandran, G. K., Yong, W. P., & Yeow, C. H. Identification of Gastric Cancer Biomarkers Using 1H Nuclear Magnetic Resonance Spectrometry. Plos One 2016; 11(9), e0162222.
75. Cary, P. D., Moss, T., & Bradbury, E. M. High-resolution proton-magnetic-resonance studies of chromatin core particles. European Journal of Biochemistry / FEBS 1978; 89(2), 475–82.
76. Tate, a R., Foxall, P. J., Holmes, E., Moka, D., Spraul, M., Nicholson, J. K., & Lindon, J. C. Distinction between normal and renal cell carcinoma kidney cortical biopsy samples using pattern recognition of 1H magic angle spinning (MAS) NMR spectra. NMR in Biomedicine 2000; 13(2), 64–71.
77. Schenetti, L., Mucci, A., Parenti, F., Cagnoli, R., Righi, V., Tosi, M. R., & Tugnoli, V. HR-MAS NMR spectrometry in the characterization of human tissues: Application to healthy gastric mucosa. Concepts in Magnetic Resonance Part A 2006; Vol. 28A (6) 430–443.
78. Guo, Q.-X., Li, Z., Ren, T. A. N., Zhu, X., & Liu, Y. (1994). Inclusion Complexation of Sodium Alkyl Sulfates with ☙-Cyclodextrin. A 1H NMR Study, Journal of lnclusion Phenomena and Molecular Recognition in Chemistry 1994; 17: 149-156.
79. Kriat, M., Vion-Dury, J., Confort-Gouny, S., Favre, R., Viout, P., Sciaky, M., … Cozzone, P. J. Analysis of plasma lipids by NMR spectroscopy: application to modifications induced by malignant tumors. Journal of Lipid Research 1993; 34: 1009–1019.
80. Hay, N. Reprogramming glucose metabolism in cancer: can it be exploited for cancer therapy? Nature Reviews Cancer 2016; 16(10), 635–649.
81. Kurosaka, A., Nakajima, H., Funakoshi, I., Matsuyama, M., Nagayo, T., & Yamashina, I. Structures of the major oligosaccharides from a human rectal adenocarcinoma glycoprotein. Journal of Biological Chemistry 1983; 258(19), 11594–11598.

82. Tsikas, D., Thum, T., Becker, T., Pham, V. V., Chobanyan, K., Mitschke, A., … Stichtenoth, D. O. Accurate quantification of dimethylamine (DMA) in human urine by gas chromatography-mass spectrometry as pentafluorobenzamide derivative: Evaluation of the relationship between DMA and its precursor asymmetric dimethylarginine (ADMA) in health and disease. Journal of Chromatography B: Analytical Technologies in the Biomedical and Life Sciences 2007; 851(1–2), 229–239.
83. Chowdhury, R., Yeoh, K. K., Tian, Y., Hillringhaus, L., Bagg, E. A., Rose, N. R., … Kawamura, A. The oncometabolite 2-hydroxyglutarate inhibits histone lysine demethylases. EMBO Reports 2011; 12(5), 463–9.
84. Dang, L., White, D. W., Gross, S., Bennett, B. D., Bittinger, M. A., Driggers, E. M., … Su, S. M. Cancer-associated IDH1 mutations produce 2-hydroxyglutarate. Nature 2009; 462(7274), 739–44.
85. Florian, C. L., Preece, N. E., Bhakoo, K. K., Williams, S. R., & Noble, M. D. Cell Type-specific Fingerprinting of Meningioma and Meningeal Cells by Proton Nuclear Magnetic Resonance Spectroscopy Cell Type-specific Fingerprinting of Meningioma and Meningeal Cells by Proton Nuclear Magnetic Resonance Spectroscopy. Cancer Research 1995; 55: 420–427.
86. Urenjak, J., Williams, S. R., Gadian, D. G., & Noble, M. Proton nuclear magnetic resonance spectroscopy unambiguously identifies different neural cell types. The Journal of Neuroscience: The Official Journal of the Society for Neuroscience 1993; 13(3), 981–989.
87. Arrowsmith, C. H., Bountra, C., Fish, P. V, Lee, K., & Schapira, M. Epigenetic protein families: a new frontier for drug discovery. Nature Reviews. Drug Discovery 2012; 11(5), 384–400.
88. Lin, R. Z. and Chang, H. Y. Recent advances in three-dimensional multicellular spheroid culture for biomedical research. Biotechnology journal 2008; 3(9-10): 139-151.
89. Baker, B. M. and Chen, C. S. Deconstructing the third dimension: how 3D culture microenvironments alter cues. Journal of cell science 2012; 125(Pt 13): 3015-3024.
90. Myungjin Lee, J., Mhawwech-Fauceglia, P., Lee, N., Parsanian, L. G., Lin, Y. G., Gayther, S. A. and Lawrenson, K. A three-dimensional microenvironment alters protein expression and chemosensitivity of epithelial ovarian cancer cells *in vitro*. Laboratory investigation; a journal of technical methods and pathology 2013; 93(5): 528-542.
91. Marjanovic, N. D., Weinberg, R. A. and Chaffer, C. L. Cell plasticity and heterogeneity in cancer. Clinical chemistry 2013; 59(1): 168-179.
92. Schiavoni, G., Gabriele, L. and Mattei, F. The tumor microenvironment: A pitch for multiple layers. Frontiers in oncology 2013; 3: 90.
93. Chitcholtan K., Sykes, P. H. and Evans, J. J. The resistance of intracellular mediators to doxorubicin and cisplatin are distinct in 3D and 2D endometrial cancer. Journal of translational medicine 2012; 10:38.
94. Busse, A., Letsch, A., Fusi, A., Nonnenmacher, A., Stather, D., Ochsenreither, S., Regenbrecht, C. R. and Keilholz, U. Characterization of small spheres derived from various solid tumor cell lines: are they suitable targets for T cells? Clinical and experimental metastasis 2013; 30(6): 781-791.
95. Rugge, M., Fassan, M., and Graham, D. Y. Epidemiology of gastric cancer. World Journal of Gastroenterology 2006; 12(3): 23–34.

96. Pourhoseingholi MA, Vahedi M, Baghestani AR. Burden of gastrointestinal cancer in Asia; an overview. Gastroenterol Hepatol Bed Bench 2015; 8(1): 19-27.
97. Kanavos, P. The rising burden of cancer in the developing world. Annals of Oncology 2006; 17: 15–23.
98. Martin U., Lucas M. B., Ulrike H., Thomas M. K., Tullio S., Dominik W., et al. Combined Magnetic Resonance Imaging and Magnetic Resonance Spectroscopy Imaging in the Diagnosis of Prostate Cancer: A Systematic Review and Meta-analysis. Eur Urol. 2009; 55(3): 575–590.
99. Jayalakshmi, K., Sonkar, K., Behari, A., and Kapoor, V. K. Lipid profiling of cancerous and benign gallbladder tissues by 1 H NMR spectroscopy. NMR in Biomedicine 2011; 24: 335–342.
100. Zietkowski, D., M, N., Davidson, R. L., and Payne, G. S. Characterisation of mobile lipid resonances in tissue biopsies from patients with cervical cancer and correlation with cytoplasmic lipid droplets. NMR in Biomedicine 2013; 26: 1096–1102.
101. Saito, K., Kaminaga, T., Muto, S., Ide, H., Nishio, K., Kamiyama, Y., et al. Clinical Efficacy of Proton Magnetic Resonance Spectroscopy (^{1}H-MRS) in the Diagnosis of Localized Prostate Cancer. Anticancer Research 2008; 28: 1899–1904.
102. Tozaki, M., Fukuma, E., Characterizing Breast Lesions. AJR 2009; 193: 840–849.
103. Heerschap, A., Jager, G. J., Van Der Graaf, M., Barentsz, J. O., De La Rosette, J. J. M. C. H., Oosterhof, G. O. N., et al. In vivo proton MR spectroscopy reveals altered metabolite content in malignant prostate tissue. Anticancer Research 1997; 17: 1455–1460.
104. Podo, F. Tumour phospholipid metabolism, NMR in Biomedicine 1999; 12: 413–439.
105. Jorgensen P. and Tyers M. How Cells Coordinate Growth and Division. Current Biology 2004; 23: 1014–1027
106. Bryant DM. and Mostov KE. From cells to organs: building polarized tissue. Nat Rev Mol Cell Biol. 2008; 9(11):887-901.
107. Foty, R. A simple hanging drop cell culture protocol for generation of 3D spheroids. Journal of Visualized Experiments: JoVE 2011; 51: 4–7.
108. Ivascu A and Kubbies M. Rapid generation of single-tumor spheroids for high-throughput cell function and toxicity analysis. J Biomol Screen 2006; 11: 922-932.
109. Mousseau, Y., Mollard, S., Qiu, H., Richard, L., Cazal, R., Nizou, A.,Sturtz, F. G. et al. *In vitro* 3D angiogenesis assay in egg white matrix: comparison to Matrigel, compatibility to various species, and suitability for drug testing. Laboratory Investigation; a Journal of Technical Methods and Pathology 2014, 94(3), 340–9.
110. Ivascu, A., and Kubbies, M. Diversity of cell-mediated adhesions in breast cancer spheroids. International Journal of Oncology 2007; 31(6): 1403–1413.
111. Huang, Y., Zhang, Z., Chen, H., Feng, J., Cai, S., and Chen, Z. A high-resolution 2D J-resolved NMR detection technique for metabolite analyses of biological samples. Scientific Reports 2015; 5: 8390.
112. Yokota, H., Guo, J., Matoba, M., Higashi, K., Tonami, H., and Nagao, Y. Lactate, choline, and creatine levels measured by vitro 1H-MRS as prognostic parameters in patients with non-small-cell lung cancer. Journal of Magnetic Resonance Imaging 2007; 25(5): 992–999.
113. Yong J. K. The Possibility of Cancer Diagnosis by Human serum NMR Measurement. Journal of KOSOMBE 1989; 10(3): 285-288.

114. Jordan, B. F., Black, K., Robey, I. F., Runquist, M., Powis, G., and Gillies, R. J. Metabolite changes in HT-29 xenograft tumors following HIF-1 ✔ inhibition with PX-478 as studied by MR spectroscopy in vivo and ex vivo. NMR in Biomedicine 2005; 18(7): 430–439.
115. Radermacher, K., Magat, J., Bouzin, C., Laurent, S., Dresselaers, T., Himmelreich, U., et al. Multimodal assessment of early tumor response to chemotherapy: Comparison between diffusion-weighted MRI, 1H-MR spectroscopy of choline and USPIO particles targeted at cell death. NMR in Biomedicine 2012; 25(4): 514–522.
116. Mahon, M. M., Williams, A. D., Soutter, W. P., Cox, I. J., McIndoe, G. A., Coutts, G., et al. 1H magnetic resonance spectroscopy of invasive cervical cancer: An in vivo study with ex vivo corroboration. NMR in Biomedicine 2004; 17: 1–9.
117. Choi, C., Ganji, S. K., DeBerardinis, R. J., Hatanpaa, K. J., Rakheja, D., Kovacs, Z., et al. 2-hydroxyglutarate detection by magnetic resonance spectroscopy in IDH-mutated patients with gliomas. Nature Medicine 2012; 18(4): 624–629.
118. Stenman, K., Stattin, P., Stenlund, H., Riklund, K., Gröbner, G., and Bergh, A. 1H HRMAS NMR derived bio-markers related to tumor grade, tumor cell fraction, and cell proliferation in prostate tissue samples. Biomarker Insights 2011; 6: 39–47.
119. Lin, J-K., Ho, Y: Hepatotoxicity and hepatocarcinogenicity in rats fed squid with or without exogenous nitrite. Food Chem Toxicol 1992; 30: 695–702.
120. Lin, J. K., Lee, Y. J., Chang, H. W. High Concentrations of Dimethylamine and methylamine in squid and octopus and their implications in tumour aetiology. Fd Chem. Toxic. 1983; 21: 143-149
121. Vissers, M. C. M., Kuiper, C., Dachs, G. U. Regulation of the 2-oxoglutarate-dependent dioxygenases and implications for cancer. Biochemical Society Transactions 2014; 42(4): 945–51.
122. Muncey, H. J., Jones, R., De Iorio, M. and Ebbels, T. M. D. MetAssimulo: simulation of realistic NMR metabolic profiles. BMC Bioinformatics 2010; 11: 496.
123. Lamblin, G., Rahmoune, H., Wieruszeski, J. M., Lhermitte, M., Strecker, G. and Roussel, P. Structure of two sulphated oligosaccharides from respiratory mucins of a patient suffering from cystic fibrosis. Biochem. J. 1991; 275: 199–206.
124. Klein, A., Lamblin, G., Vhermitte, M., Roussel, P., Breg, J., Van Halbeek, H., et al. Primary structure of neutral oligosaccharides derived from respiratory-mucus glycoproteins of a patient suffering from bronchiectasis, determined by combination of 500-MHz 1H-NMR spectroscopy and quantitative sugar analysis. European Journal of Biochemistry 1988; 171: 643–654.
125. Razzak, M., Karim, M. R., Hoq, R. and Mirza, A. H. New Schiff Bases from 6,6'-Diformyl-2,2'-Bipyridyl with amines containing O, S, N and F: Synthesis and Characterization. International journal of organic chemistry 2015; 5: 264–270.
126. Pore, Y. and Kuchekar, B. Synthesis of novel N1, 6- di-substituted 5-cyano-2-thiouracil derivatives as antinociceptive agents. Digest Journal of Nanomaterials and Biostructures 2008; 3(4): 293–298.
127. Grande, S., Palma, A., Luciani, A. M., Rosi, A., Guidoni, L. and Viti, V. Glycosidic intermediates identified in 1H MR spectra of intact tumour cells may contribute to the clarification of aspects of glycosylation pathways. NMR in Biomedicine 2011; 24(1): 68–79.
128. Odeh, F., Ismail, S. I., Abu-Dahab, R., Mahmoud, I. S., and Al Bawab, A. Thymoquinone in liposomes: a study of loading efficiency and biological activity

towards breast cancer. Drug Delivery 2012; 19: 1–7.

129. Kilonda, B. B., Lohohola, O., Toppet, S., and Compernolle, F. Acetylation products of pentacyclic triterpene glucosides from Combretum Psidioides. Arkivoc 2003;(iv): 3–21.
130. Hers, H. G. The control of glycogen metabolism in the liver. Annual Review of Biochemistry 1976; 45: 167–89.
131. Zois, C. E., Favaro, E., and Harris, A. L. Glycogen metabolism in cancer. Biochemical Pharmacology 2014; 92(1): 3–11.
132. Vliegenthart, J. F. G., Halbeek, H. Van, and Dorland, L. The applicability of 500-MHz high-resolution ^{1}H-NMR spectrometry for the structure determination of carbohydrates derived from glycoproteins. Pure and Appl. Chem., 1981; 53: 45-77.
133. Kojima, H., Tohsato, Y., Kabayama, K., Itonori, S., and Ito, M. Biochemical studies on sphingolipids of Artemia franciscana: Complex neutral glycosphingolipids. Glycoconjugate Journal 2013; 30(3): 257–268.
134. Teneberg, S., Ångström, J., and Ljungh, Å. Carbohydrate recognition by enterohemorrhagic Escherichia coli: Characterization of a novel glycosphingolipid from cat small intestine. Glycobiology 2004; 14(2): 187–196.
135. Hong, Y., Duda, K., Cunneen, M. M., Holst, O., and Reeves, P. R. The WbaK acetyltransferase of Salmonella enterica group E gives insights into O antigen evolution. Microbiology 2013; 159(PART11): 2316–2322.
136. Alonso, A. P., Piasecki, R. J., Wang, Y., LaClair, R. W., and Shachar-Hill, Y. Quantifying the Labeling and the Levels of Plant Cell Wall Precursors Using Ion Chromatography Tandem Mass Spectrometry. Plant Physiology 2010; 153(3): 915–924.
137. Steindl, C., Schäffer, C., Smrecki, V., Messner, P., and Müller, N. The secondary cell wall polymer of Geobacillus tepidamans GS5-97T: structure of different glycoforms. Carbohydrate Research 2005; 340(14): 2290–2296.
138. Ting Y., Liron B., Lindsay G., Sung G. L. and Maor Bar-Peled. Identification of galacturonic acid-1-P kinase: a new member of the GHMP kinase super family in plants and comparison with galactose-1-P kinase. Journal of Biological Chemistry 2009; 284(32): 21526-21535.
139. Yu, G., Guan, H., Ioanoviciu, A. S., Sikkander, S. A., Thanawiroon, C., Tobacman, J. K., et al. Structural studies on kappa-carrageenan derived oligosaccharides. Carbohydrate Research 2002; 337(5): 433–440.
140. Karnjanapratum, S., Tabarsa, M., Cho, M., and You, S. Characterization and immunomodulatory activities of sulfated polysaccharides from Capsosiphon fulvescens. International Journal of Biological Macromolecules 2012; 51(5): 720–729.
141. Hamilton, G., Yokoo, T., Bydder, M., Cruite, I., Schroeder, M. E., Sirlin, C. B., et al. In vivo characterization of the liver fat 1H MR spectrum. NMR in Biomedicine 2011; 24(7): 784–790.
142. Bondock, S., Rabie, R., Etman, H., and Fadda, A. Synthesis and antimicrobial activity of some new heterocycles incorporating antipyrine moiety. European Journal of Medicinal Chemistry 2008; 43(10): 2122–2129.

143. Sowers, L. C., Eritja, R., Kaplan, B., Goodman, M. F., and Fazakerly, G. V. Equilibrium between a wobble and ionized base pair formed between fluorouracil and guanine in DNA as studied by proton and fluorine NMR. Journal of Biological Chemistry 1988; 263(29): 14794–14801.
144. Bianchi, E., Djerassi, C., Budzikiewicz, H., and Sato, Y. Structure of tomatillidine. The Journal of Organic Chemistry 1965; 30(3):754–760.
145. Kennedy, J. P., and Makowski, H. S. (1967). Carbonium Ion Polymerization of Norbornene and Its Derivatives. Journal of Macromolecular Science: Part A – Chemistry 1967, 1(3), 345–370.
146. Luca, A. C., Mersch, S., Deenen, R., Schmidt, S., Messner, I., Schafer, K. L., et al. Impact of 3D microenvironment on genotype, gene expression and EGFR inhibition of colorectal cancer cell lines. PloS one 2013; 8(3): e59689.
147. Bellis, A. D., Bernabe, B. P., Weiss, M. S., Shin, S., Weng, S., Broadbelt, L. J. et al. Dynamic transcription factor activity profiling in 2D and 3D cell cultures. Biotechnology and bioengineering 2013; 110(2): 563-572.
148. Zimmermann, D., Hartmann, M., Moyer, M. P., Nolte, J. & Baumbach, J. I. Determination of volatile products of human colon cell line metabolism by GC/MS analysis. Metabolomics 2007; 3: 13–17.
149. Sponring, A., Filipiak, W., Mikoviny, T., Ager, C., Schubert, J., Miekisch, W. Troppmair, J. et al. Release of volatile organic compounds from the lung cancer cell line NCI-H2087 in vitro. Anticancer 2009; 29(1): 419–426.
150. Abaffy, T. et al. Differential volatile signatures from skin, naevi and melanoma: a novel approach to detect a pathological process. PloS one 2010; 5: e13813.
151. Hanai, Y. et al. Analysis of volatile organic compounds released from human lung cancer cells and from the urine of tumor-bearing mice. Cancer cell international 2012;12: 7.
152. Mochalski, P., Sponring, A., King, J., Unterkofler, K., Troppmair, J., & Amann, A. Release and uptake of volatile organic compounds by human hepatocellular carcinoma cells (HepG2) *in vitro*. Cancer Cell International 2013; 13(1):1.
153. Lavra, L., Catini, A., Ulivieri, A., Capuano, R., Baghernajad Salehi, L., Sciacchitano, S., … Di Natale, C. Investigation of VOCs associated with different characteristics of breast cancer cells. Scientific Reports 2015; 5: 13246.
154. Schallschmidt, K., Becker, R., Jung, C., Rolff, J., Fichtner, I., & Nehls, I. Investigation of cell culture volatilomes using solid phase microextraction: Options and pitfalls exemplified with adenocarcinoma cell lines. Journal of Chromatography B: Analytical Technologies in the Biomedical and Life Sciences 2015; 1006: 158–166.
155. Van Den Dool, H., & Kratz, P. D. A generalization of the retention index system including linear temperature programmed gas—liquid partition chromatography. Journal of Chromatography A 1063; 11(3): 463–471.
156. Sanz, G., Leray, I., Dewaele, A., Sobilo, J., Lerondel, S., Bouet, S., … Mir, L. M. Promotion of cancer cell invasiveness and metastasis emergence caused by olfactory receptor stimulation. PLoS ONE 2014; 9(1).
157. Croute, F., Poinsot, J., Gaubin, Y., Beau, B., Simon, V., Murat, J. C., & Soleilhavoup, J. P. Volatile organic compounds cytotoxicity and expression of HSP72, HSP90 and GRP78 stress proteins in cultured human cells. Biochimica et Biophysica Acta - Molecular Cell Research 2002; 1591(1–3): 147–155.

158. Nealson, K.H. Autoinduction of bacterial luciferase Occurrence, mechanism and significance. Arch. Microbiol. 1997; 112:73–79.
159. Waters CM, Bassler BL. Quorum sensing: cell-to-cell communication in bacteria. Annu. Rev. Cell Dev. Biol. 2005; 21:319–46.
160. Lee J, Jayaraman A, Wood TK. Indole is an interspecies biofilm signal mediated by SdiA. BMC Microbiol. 2007; 7:42.
161. Saghi, H., Moradi, F., Mohseni, R., Abadi, A. H., Ataee, R. A., Zadeh, P. B. et al. Quorum Sensing in Bacterial Pathogenesis. Global Journal of Infectious Diseases and Clinical Research 2015; 1(1): 004–009.
162. Muhammad Kamran Taj, Wei Yunlin, Zohra Samreen, Imran Taj, Taj Muhammad Hassani, & Ji Xiu Ling. Quorum Sensing and Its Different Signals Systems in Bacteria. IMPACT: International Journal of Research in Applied, Natural, and Social Sciences 2014; 2(2): 117–124.
163. Barriuso, J. Quorum sensing mechanisms in fungi. AIMS Microbiology 2015; 1(1): 37–47.
164. Hornby JM, Jensen EC, Lisec AD, et al. Quorum sensing in the dimorphic fungus Candida albicans is mediated by farnesol. App Environ Microbiol 2001; 67: 2982–2992.
165. Geiger J, Wessels D, Lockhart SR, et al. Release of a potent polymorphonuclear leukocyte chemoattractant is regulated by white-opaque switching in Candida albicans. Infect Immun 2004;72: 667–677.
166. Chen, C. C., Wang, L., Plikus, M. V., Jiang, T. X., Murray, P. J., Ramos, R. et al. (2015). Organ-level quorum sensing directs regeneration in hair stem cell populations. Cell 2015; 161(2): 277–290.
167. Sethi, S., Nanda, R., & Chakraborty, T. Clinical application of volatile organic compound analysis for detecting infectious diseases. Clinical Microbiology Reviews 2013; 26(3): 462–475.
168. Hryniuk, A. & Ross, B. M. A preliminary investigation of exhaled breath from patients with celiac disease using selected ion flow tube mass spectrometry. Journal of Gastrointestinal and Liver Diseases 2010; 19(1): 15–20.
169. Spooner, A. D., Bessant, C., Turner, C., Knobloch, H., & Chambers, M. Evaluation of a combination of SIFT-MS and multivariate data analysis for the diagnosis of Mycobacterium bovis in wild badgers. The Analyst 2009; 134(9): 1922.
170. Smith, D., Španěl, P., Selected ion flow tube mass spectrometry (SIFT-MS) for on-line trace gas analysis Mass Spectrom Rev., 2005; 24: 661–700.
171. Filipiak, W., Sponring, A., Filipiak, A., Ager, C., Schubert, J., Miekisch, W., … Troppmair, J. TD-GC-MS Analysis of Volatile Metabolites of Human Lung Cancer and Normal Cells *In vitro*. Cancer Epidemiology Biomarkers & Prevention 2010; 19(1): 182–195.
172. Ulanowska, A., Trawiańska, E., Sawrycki, P., & Buszewski, B. Chemotherapy control by breath profile with application of SPME-GC/MS method. Journal of Separation Science 2012; 35(21): 2908–2913.
173. Chen, X., Xu, F., Wang, Y., Pan, Y., Lu, D., Wang, P., … Zhang, W. A study of the volatile organic compounds exhaled by lung cancer cells *in vitro* for breath diagnosis. Cancer 2007; 110(4): 835–844.

174. Peng, G., Track, E., & Haick, H. Detecting simulated patterns of lung cancer biomarkers by random network of single-walled carbon nanotubes coated with nonpolymeric organic materials. Nano Letters 2008; 8(11): 3631–3635.
175. Bailly, A., and Weisskopf, L. The modulating effect of bacterial volatiles on plant growth: Current knowledge and future challenges. Plant Signal Behav 2012; 7: 79–85.
176. Meldau, D.G., Long, H.H., and Baldwin, I.T. A native plant growth promoting bacterium, Bacillus sp. B55, rescues growth performance of an ethylene-insensitive plant genotype in nature. Front Plant Sci 2012; 3: 112.
177. Meldau, D.G., Meldau, S., Hoang, L.H., Underberg, S., Wu¨nsche, H., and Baldwin, I.T. Dimethyl disulfide produced by the naturally associated bacterium Bacillus sp. B55 pro- motes Nicotiana attenuata growth by enhancing sulfur nutrition. Plant Cell 2013; 25: 2731–2747.
178. Kiuchi F, Goto Y, Sugimoto N, Akao N, Kondo K, Tsuda Y. Nematocidal activity of turmeric: synergistic action of curcumi- noids. Chem Pharm Bull (Tokyo). 1993;41:1640–3.
179. Aggarwal BB, Sethi G, Baladandayuthapani V, Krishnan S, Shishodia S. Targeting cell signaling pathways for drug discovery: an old lock needs a new key. J Cell Biochem. 2007; 102:580–92.
180. Ravindran, J., Prasad, S., and Aggarwal, B. B. Curcumin and Cancer Cells: How Many Ways Can Curry Kill Tumor Cells Selectively. American Association of Pharmaceutical Scientists Journal 2009; Vol. 11, No. 3: 495- 510.
181. Fuchs, P., Loeseken, C., Schubert, J. K., & Miekisch, W. Breath gas aldehydes as biomarkers of lung cancer. International Journal of Cancer 2010; 126(11), 2663–2670. http://doi.org/10.1002/ijc.24970.
182. Crowell, P. L., Kennan, W. S., Haag, J. D., Ahmad, S., Vedejs, E., & Gould, M. N. Chemoprevention of mammary carcinogenesis by hydroxylated derivatives of d-limonene. Carcinogenesis 1992; 13(7): 1261–1264.
183. Nam, J. H., Choi, I. J., Cho, S.-J., Kim, C. G., Jun, J. K., Choi, K. S., … Kim, Y.-W. (2012). Association of the interval between endoscopies with gastric cancer stage at diagnosis in a region of high prevalence. Cancer, 118(20), 4953–60. http://doi.org/10.1002/cncr.27495.
184. Braun, P. X., Gmachl, C. F., & Dweik, R. A. (2012). Bridging the collaborative gap: Realizing the clinical potential of breath analysis for disease diagnosis and monitoring-tutorial. IEEE Sensors Journal, 12(11), 3258–3270. http://doi.org/10.1109/JSEN.2012.2210403.
185. Gordon SM, Szidon JP, Krotoszynski BK, et al. Volatile organic compounds in exhaled air from patients with lung cancer. Clin Chem 1985;31:1278-82.
186. Phillips M, Cataneo RN, Cummin AR, et al. Detection of lung cancer with volatile markers in the breath. Chest 2003;123:2115-23.
187. Chen X, Xu F, Wang Y, et al. A study of the volatile organic compounds exhaled by lung cancer cells *in vitro* for breath diagnosis. Cancer 2007;110:835-44.
188. Bajtarevic, A., Ager, C., Pienz, M., Klieber, M., Schwarz, K. E., Ligor, M., … Amann, A. Noninvasive detection of lung cancer by analysis of exhaled breath. BMC Cancer 2009; 9(1), 348. http://doi.org/10.1186/1471-2407-9-348.

189. Wang, C., Dong, R., Wang, X., Lian, A., Chi, C., Ke, C., … Li, E. Exhaled volatile organic compounds as lung cancer biomarkers during one-lung ventilation. Scientific Reports 2014; 4, 7312. http://doi.org/10.1038/srep07312.
190. Filipiak, W., Filipiak, A., Sponring, A., Schmid, T., Zelger, B., Ager, C., … Troppmair, J. Comparative analyses of volatile organic compounds (VOCs) from patients, tumors and transformed cell lines for the validation of lung cancer-derived breath markers. Cancer Epidemiology, Biomarkers & Prevention 2013; 8(0), 22. http://doi.org/10.1088/1752-7155/8/2/027111.
191. Kumar, S., Huang, J., Abbassi-Ghadi, N., Španěl, P., Smith, D., & Hanna, G. B. Selected ion flow tube mass spectrometry analysis of exhaled breath for volatile organic compound profiling of esophago-gastric cancer. Analytical Chemistry 2013; 85(12), 6121–6128. http://doi.org/10.1021/ac4010309.
192. Kumar, S., Huang, J., Abbassi-Ghadi, N., Mackenzie, H. a., Veselkov, K. a., Hoare, J. M., … Hanna, G. B. Mass Spectrometric Analysis of Exhaled Breath for the Identification of Volatile Organic Compound Biomarkers in Esophageal and Gastric Adenocarcinoma. Annals of Surgery 2015, 0(0), 1. http://doi.org/10.1097/SLA.0000000000001101.
193. Pennazza, G., Santonico, M., Martinelli, E., D'Amico, A. & Di Natale, C. Interpretation of exhaled volatile organic compounds. Eur Respir Mon 2010; 49, 115–129.
194. Israeli, E; Ilan, Y; Meir, SB; Buenavida, C; Goldin, E. "A novel 13C-urea breath test device for the diagnosis of Helicobacter pylori infection: continuous online measurements allow for faster test results with high accuracy". J Clin Gastroenterol. 2003; 37 (2): 139–41.
195. Phillips M. Breath tests in medicine. Sci. Am 1992; 7:74 –79.
196. Silva, C. L., Passos, M., & Câmara, J. S. Investigation of urinary volatile organic metabolites as potential cancer biomarkers by solid-phase microextraction in combination with gas chromatography-mass spectrometry. British Journal of Cancer 2011; 105(12): 1894–904. http://doi.org/10.1038/bjc.2011.437.
197. Mochalski, P. P., King, J., Haas, M., Unterkofler, K., Amann, A., & Mayer, G. Blood and breath profiles of volatile organic compounds in patients with end-stage renal disease. Bmc Nephrology 2014; 15: 43. http://doi.org/10.1186/1471-2369-15-43.
198. Kalluri, U., Naiker, M., & Myers, M. A. Cell culture metabolomics in the diagnosis of lung cancer-the influence of cell culture conditions. Journal of Breath Research 2014; 8(2), 27109. http://doi.org/10.1088/1752-7155/8/2/027109.
199. Abaffy, T., Möller, M. G., Riemer, D. D., Milikowski, C., & DeFazio, R. A. Comparative analysis of volatile metabolomics signals from melanoma and benign skin: A pilot study. Metabolomics 2013, 9(5), 998–1008. http://doi.org/10.1007/s11306-013-0523-z.
200. John Toedt; Darrell Koza; Kathleen Van Cleef-Toedt . Chemical composition of everyday products, illustrated ed Greenwood Publishing Group 2005, pp. 48–49, ISBN 9780313325793.
201. 266. US 20140286880 A1
202. https://focusonfoodsafety.wordpress.com/tag/mouthwash.
203. EFSA Committee. Scientific Opinion on the safety assessment of carvone , considering all sources of exposure. European Food Safety Authority 2014, 12(7), 1–74.

204. Veeresha KL, Bansal M, Bansal V. Halitosis: A frequently ignored social condition. Journal of International Society of Preventive & Community Dentistry. 2011;1(1):9-13. doi:10.4103/2231-0762.86374.
205. Itoh, T., Miwa, T., Tsuruta, A., Akamatsu, T., Izu, N., Shin, W., … Setoguchi, Y. Development of an exhaled breath monitoring system with semiconductive gas sensors, a gas condenser unit, and gas chromatograph columns. Sensors (Switzerland 2016); 16(11). http://doi.org/10.3390/s16111891.
206. Beauchamp, J., Kirsch, F., & Buettner, A. Real-time breath gas analysis for pharmacokinetics: monitoring exhaled breath by on-line proton-transfer-reaction mass spectrometry after ingestion of eucalyptol-containing capsules. Journal of Breath Research 2010; 4(2): 26006. http://doi.org/10.1088/1752-7155/4/2/026006.
207. Klenk, Herbert; Gotz, Peter; Siegmeier, Rainer; Mayr, W. Phenol derivatives. Ullman's Encyclopedia of Industrial Chemistry 2012; 325–360. http://doi.org/10.1002/14356007.a19.
208. (US 20150233895 A1).
209. Deng K, Lin S, Zhou L, et al. High levels of aromatic amino acids in gastric juice during the early stages of gastric cancer progression. PLoS One. 2012;7: 49434.30.
210. Amal, H., Leja, M., Funka, K., Skapars, R., Sivins, A., Ancans, G., … Haick, H. Detection of precancerous gastric lesions and gastric cancer through exhaled breath. Gut 2016; 65(3), 400–7. http://doi.org/10.1136/gutjnl-2014-308536.
211. N.E. Rawson, Human olfaction, in: T.E. Finger, W.L. Silver, D. Restrepo (Eds.), The Neurobiology of Taste and Smell, Wiley, New York, 2000.
212. R. Axel, The molecular logic of smell, Sci. Am. 1995; 273: 154–159.
213. B. Malnic, J. Hirono, T. Sato, L.B. Buck, Combinatorial receptor codes for odors, Cell 1999; 96: 713–723.
214. Lei, H., Pitt, W. G., McGrath, L. K., & Ho, C. K. Resistivity measurements of carbon-polymer composites in chemical sensors: Impact of carbon concentration and geometry. Sensors and Actuators, B: Chemical 2004, 101(1–2), 122–132.
215. Chalovich, J. M., & Eisenberg, E. NIH Public Access. Biophysical Chemistry 2005; 257(5), 2432–2437. http://doi.org/10.1016/j.immuni.2010.12.017.Two-stage
216. Munoz, B.C., Steinthal, G. and Sunshine, S., "Conductive polymer-carbon black composites-based sensor arrays for use in an electronic nose", Sensor review 1999, Vol. 19 No. 4, pp. 300-5.
217. Arshak, K., Moore, E., Lyons, G. M., Harris, J., & Clifford, S. (2004). A review of gas sensors employed in electronic nose applications. Sensor Review, 24(2), 181–198.
218. Pearce, T.C., Schiffman, S.S., Nagle, H.T. and Gardner, J.W. (2003), Handbook of Machine Olfaction, Wiley-VCH, Weinheim.
219. Albert, K.J. and Lewis, N.S., "Cross reactive chemical sensor arrays", Chem. Rev 2000. Vol. 100, pp. 2595-626.
220. Freund, M.S. and Lewis, N.S., "A chemically diverse conducting polymer based electronic nose", Proc. Natl. Acad. Sci. USA 1995, Vol.92, pp. 2652-6.
221. Y. Dan, Y. Lu, N. J. Kybert, Z. Luo, A. T. C. Johnson, Nano Lett. 2009, 1472.
222. Raguse, B., Barton, C. S., Müller, K. H., Chow, E., & Wieczorek, L. Gold nanoparticle chemiresistor sensors in aqueous solution: Comparison of hydrophobic and hydrophilic nanoparticle films. Journal of Physical Chemistry C 2009, 113(34), 15390–15397. http://doi.org/10.1021/jp9034453.

223. J. T. Robinson, F. K. Perkins, E. S. Snow, Z. Wei, P. E. Sheehan, Nano Lett. 2008, 8, 3137.
224. R. K. Joshi, H. Gomez, F. Alvi, A. Kumar, J. Phys. Chem. C 2010, 114, 6610.
225. Salehi-Khojin, A., Estrada, D., Lin, K. Y., Bae, M. H., Xiong, F., Pop, E., & Masel, R. I. (2012). Polycrystalline graphene ribbons as chemiresistors. Advanced Materials, 24(1), 53–57.
226. L. Ye, B. R. Goldsmith, N. J. Kybert, A. T. C. Johnson, Appl. Phys. Lett. 2010, 97, 083107.
227. Rhoades DF. 1983. Responses of alder and willow to attack by tent caterpillars and webworms: evidence for phenomenal sensitivity of willows. In: Hedin PA, ed. Plant resistance to insects. Washington, DC: American Chemical Society, 55–68.
228. Baldwin IT, Schultz JC. Rapid changes in tree leaf chemistry induced by damage: evidence for communication between plants. Science 1983; 221, 277–279.
229. Mescher, M. C., & De Moraes, C. M. Role of plant sensory perception in plant-animal interactions. Journal of Experimental Botany 2015, 66(2), 425–433.
230. Frost, C. J., Mescher, M. C., Dervinis, C., Davis, J. M., Carlson, J. E., & De Moraes, C. M. Priming defense genes and metabolites in hybrid poplar by the green leaf volatile cis-3-hexenyl acetate. New Phytologist 2008, 180(3), 722–734.
231. Frost, C. J., Appel, H. M., Carlson, J. E., De Moraes, C. M., Mescher, M. C., & Schultz, J. C. Within-plant signalling via volatiles overcomes vascular constraints on systemic signalling and primes responses against herbivores. Ecology Letters 2007, 10(6), 490–498.
232. Runyon, J. B. Volatile Chemical Cues Guide Host Location and Host Selection by Parasitic Plants. Science 2006, 313(5795), 1964–1967. http://doi.org/10.1126/science.1131371.
233. Karban R, Baldwin IT, Baxter KJ, Laue G, Felton GW. Communication between plants: induced resistance in wild tobacco plants following clipping of neighboring sagebrush. Oecologia 2000; 125, 66–71.
234. Karban R, Maron J, Felton GW, Ervin G, Eichenseer H. Herbivore damage to sagebrush induces resistance in wild tobacco: evidence for eavesdropping between plants. Oikos 2003 100, 325–332.
235. Karban R, Maron J. The fitness consequences of interspecies eavesdropping between plants. Ecology 2002; 83, 1209–1213.
236. Heil M, Silva Bueno JC. Within-plant signaling by volatiles leads to induction and priming of an indirect plant defense in nature. Proceedings of the National Academy of Sciences, USA 2007; 104, 5467–5472.
237. Chen, G., Paronyan, T. M., Pigos, E. M., & Harutyunyan, A. R. Enhanced gas sensing in pristine carbon nanotubes under continuous ultraviolet light illumination. Scientific Reports 2012; 2, 343.
238. Shaik, M., Rao, V. K., Gupta, M., Murthy, K. S. R. C., & Jain, R. Chemiresistive gas sensor for the sensitive detection of nitrogen dioxide based on nitrogen doped graphene nanosheets. RSC Adv. 2016; 6(2), 1527–1534.

Appendix 1

Publications:

1. **Ramachandran, G. K**., & Yeow, C. H. Proton NMR characterization of intact primary and metastatic melanoma cells in 2d & 3d cultures (Accepted – Journal of Biological Research).
2. **Ramachandran, G. K**., Yong, W. P., & Yeow, C. H. Identification of Gastric Cancer Biomarkers Using 1H Nuclear Magnetic Resonance Spectrometry. *Plos One* 2016; ***11***(9), e0162222.
3. L.C. Hernandez-Barraza, **G. K. Ramachandran,** J.H. Low, and C.H. Yeow. "The biomechanics of ACL injury: progresses toward prophylactic strategies." Critical Reviews in Biomedical Engineering 2013. 41(4-5), 309-321.

Manuscripts under peer review:

1. **Ramachandran, G. K**., & Yeow, C. H. Comparison of the volatile signatures of primary melanoma cells (WM 115) in 2D cultures and 3D cultures (Journal of Breath Research).
2. **Ramachandran, G. K**., & Yeow, C. H. Cellular level quorum sensing is manifested by release of Volatile organic compounds in human metastatic melanoma cells (WM266) (Scientific Reports).
3. **Ramachandran, G. K**., Yong, W. P., & Yeow, C. H. Volatile Biomarkers and Curcumin Induced Volatile Signatures of Multicellular Gastric Cancer Tumor Spheroids (Scientific Reports).

Manuscripts under preparation:

1. **Ramachandran, G. K**., Yong, W. P., So, B.Y., & Yeow, C. H. Identification of Non-Invasive Breath Biomarkers for the Diagnosis of Gastric Cancer- A Clinical Study.
2. **Ramachandran, G. K**., & Yeow, C. H. Florisensors: A novel flower based chemiresistive gas sensors.

Awards:

- IFBME Young investigator award, awarded at the 16th International conference on Biomedical Engineering 2016 held on 7-10 December 2016 at Singapore.

- Finalist in the BES Design Award competition at the Biomedical Engineering Society 10th Scientific Meeting 2016 held on 14th may 2016 at Singapore.

Appendix 2:

Conference Presentations:

- Presented a paper at the 16th International conference on Biomedical Engineering 2016 held on 7-10 December 2016 at Singapore.
  - Topic: Volatile biomarkers and curcuminoid incuded cell death associated volatile signatures of multicellular gastric cancer tumor spheroids.
- Presented a poster at Sydney cancer conference 2016 held on 22 and 23 september 2016 at Sydney.
  - Topic: Gastric cancer detection using Proton Nuclear Magnetic Resonance Spectrometry
- Presented a flex sensor deign in the BES Design Award competition at the Biomedical Engineering Society 10th Scientific Meeting 2016 held on 14th may 2016 at Singapore.
  - Topic: BI-DIRECTIONAL SMART (BEST) flex sensors for rehabilitation
- Presented a poster at 7th WACBE World Congress on Bioengineering held on 6 – 8 July 2015 at Singapore.
  - Topic: Magnetic Resonance Based Cancer Biomarkers
- Presented a paper at 9th International Conference of Anticancer Research 2014 held on 6-10 October 2014 at Sithonia, Greece.
  - Topic: Comparative Metabolomics Of Primary And Metastatic Melanoma Cells - Towards Novel Diagnostic Method.
- Presented a paper at Biomedical Engineering Society 7th Scientific Meeting 2014 held on 17th may 2014 at Singapore.
  - Topic: Comparative Metabolomics Of Melanoma Cells lines
- Presented a paper at The 15th International Conference on Biomedical Engineering 2013 held on 4-7 December 2013 at Singapore.
  - Topic: Holistic cell-line metabolome profiling strategy for biomarker identification.
- Presented a poster at IEEE Grand Challenges in Life Sciences Conference held on 2-3 December 2013 at Singapore.
  - Topic: Holistic cell line metabolomics profiling strategy for biomarker identification

Appendix 3:

DSRB Approval Letter:

National Healthcare Group
Adding years of healthy life

3 Fusionopolis Link
#03-08 Nexus@one-north
Singapore 138543
Tel: 6496 6600 Fax:6486 6870
www.nhg.com.sg
RCB No. 200002150H

NHG DSRB Ref: **2014/01231**

02 November 2016

Dr Yong Wei Peng
Department of Haematology-Oncology
National University Hospital

Dear Dr Yong

RENEWAL OF NHG DOMAIN SPECIFIC REVIEW BOARD (DSRB) APPROVAL

STUDY TITLE: Identification of the volatile breath biomarkers for gastric cancer.

We are pleased to inform you that the NHG DSRB has renewed the approval for the application as titled above, being conducted in **National University Hospital** and **Ng Teng Fong General Hospital**. The approval period is from **02 November 2016** to **01 November 2017**.

The documents reviewed are:

a) NHG DSRB Study Status Report Form ID: **2014/01231-SRF0002**
b) NHG DSRB Application Form: **Version No. 3**
c) Study Protocol: Version 03 dated 23 March 2016
d) Main Informed Consent Form (NUH): Version 03 dated 23 March 2016
e) Main Informed Consent Form (NTFGH): Version 01 dated 13 April 2016
f) Case Report Form: Version 02 dated 16 August 2016

The documents acknowledged are:

a) Informed Consent Form Version 1 with Short Consent Form (Malay): Version dated 19 July

2016
b) Informed Consent Form Version 1 with Short Consent Form (Simplified Chinese): Version dated 19 July 2016

Continued approval is conditional upon your compliance with the following requirements:

1. Only the approved Informed Consent Form should be used. It must be signed by each subject prior to initiation of any protocol procedures. In addition, each subject should be given a copy of the signed consent form.

2. No deviation from, or changes of the protocol should be implemented without documented approval from the NHG DSRB, except where necessary to eliminate apparent immediate hazard(s) to the study subjects.

3. Any deviation from, or a change of, the protocol to eliminate an immediate hazard should be promptly reported to the NHG DSRB within seven calendar days.

4. Please note that for studies requiring Clinical Trial Certificate, apart from the approval from NHG DSRB, no deviation from, or changes of the Research Protocol and Informed Consent Form should be implemented without documented approval from the Health Sciences Authority unless otherwise advised by the Health Sciences Authority.

5. Please submit the following to the NHG DSRB:

a. All Unanticipated Problems Involving Risk To Subjects Or Others (UPIRTSOs) must be reported to the NHG DSRB. For more than minimal risk studies, all problems involving local deaths must be reported immediately within 24 hours after first knowledge by the Investigator, regardless of the causality and expectedness of the death. For no more than minimal risk studies, only problems involving local deaths that are related or possibly related to the study must be reported immediately within 24 hours after first knowledge by the Investigator. All other problems that fulfil the UPIRTSOs reporting criteria must be reported as soon as possible but not later than seven calendar days after first knowledge by the Investigator.

b. Report(s) on any new information that may adversely affect the safety of the subject or the conduct of the study.

c. NHG DSRB Study Status Report Form – this is to be submitted 4 to 6 weeks prior to expiry of the approval period. The study cannot continue beyond **01 November 2017** until approval is renewed by the NHG DSRB.

d. Study completion – this is to be submitted using the NHG DSRB Study Status Report Form within 4 to 6 weeks of study completion or termination.

Established since May 2006, the NHG Research Quality Management (RQM) Program seeks to

promote the responsible conduct of research in a research culture with high ethical standards, identify potential systemic weaknesses and make recommendations for continual improvement. Hence, this research study may be randomly selected for a review by the Research Quality Management (RQM) team. For more information, please visit www.research.nhg.com.sg.

The NHG DSRB operates in accordance to the ICH GCP, Singapore Guideline for Good Clinical Practice and all applicable laws and regulations.

Yours Sincerely

Dr Ross Soo
Chairman
NHG Domain Specific Review Board B2

Cc: Institutional Representative, NUH
c/o Research Office, NUH
Departmental Representative of Haematology-Oncology, NUH

Cc: Institutional Representative, NTFGH
Departmental Representative of Surgery, NTFGH

(This is an electronic-generated letter. No signature is required.)